

General Disclaimer

One or more of the Following Statements may affect this Document

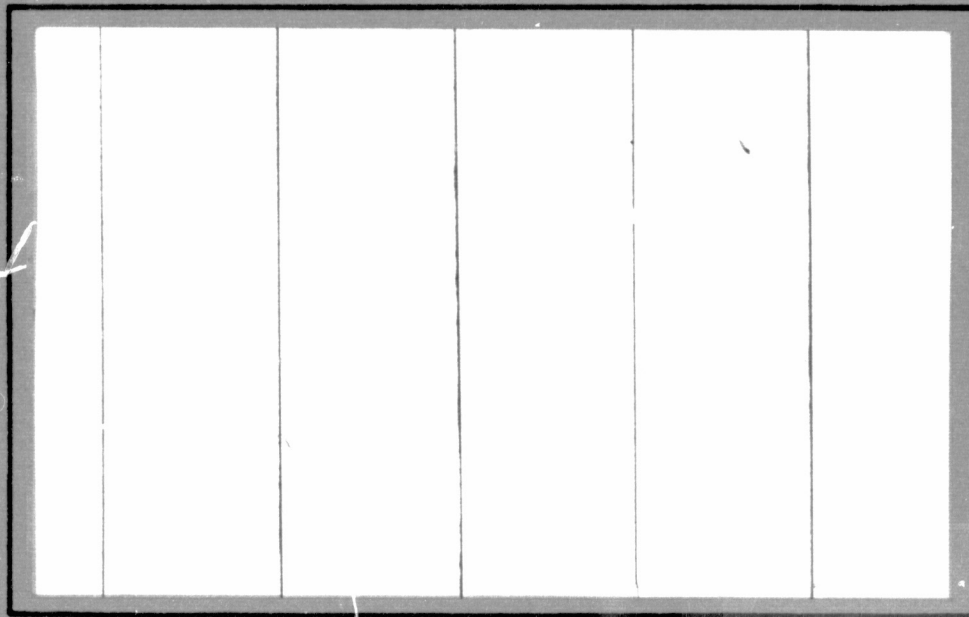
- This document has been reproduced from the best copy furnished by the organizational source. It is being released in the interest of making available as much information as possible.
- This document may contain data, which exceeds the sheet parameters. It was furnished in this condition by the organizational source and is the best copy available.
- This document may contain tone-on-tone or color graphs, charts and/or pictures, which have been reproduced in black and white.
- This document is paginated as submitted by the original source.
- Portions of this document are not fully legible due to the historical nature of some of the material. However, it is the best reproduction available from the original submission.

(NASA-CR-146135) AN INVESTIGATION OF THE
FAILURE AND FRACTURE BEHAVIOR OF
GRAPHITE/EPOXY LAMINATES Final Report, 1
Oct. 1974 - 30 Sep. 1975 (Virginia
Polytechnic Inst. and State Univ.) 115 p HC G3/24

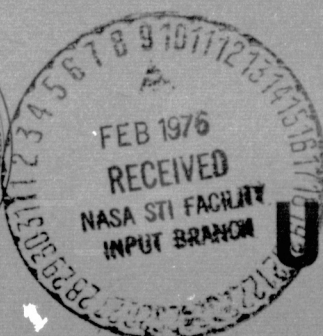
N76-16180
HC \$5.50

Unclas
09958

OF
**COLLEGE
ENGINEERING**



**VIRGINIA
POLYTECHNIC
INSTITUTE
AND
STATE
UNIVERSITY**



**BLACKSBURG,
VIRGINIA**

College of Engineering
Virginia Polytechnic Institute and State University
Blacksburg, VA 24061

VPI-E-75-23

September 1975

An Investigation of the Failure and Fracture
Behavior of Graphite/Epoxy Laminates

H. F. Brinson, Professor
Y. T. Yeow, Research Associate

Department of Engineering Science and Mechanics

Prepared for:

National Aeronautics and Space Administration
Grant No. NASA-NSG 2038
Materials Science Branch
Ames Research Center
Moffett Field, CA. 94035

Approved for Public Release; distribution unlimited.

BIBLIOGRAPHIC DATA SHEET	1. Report No. VPI-E-75-23	2.	3. Recipient's Accession No.
4. Title and Subtitle AN INVESTIGATION OF THE FAILURE AND FRACTURE BEHAVIOR OF GRAPHITE/EPOXY LAMINATES			5. Report Date Sept. 1975
7. Author(s) H. F. Brinson, Y. T. Yeow			6.
9. Performing Organization Name and Address Engineering Science and Mechanics Virginia Polytechnic Inst. & State University Blacksburg, VA 24061			8. Performing Organization Rept. No. VPI-E-75-23
			10. Project/Task/Work Unit No.
			11. Contract/Grant No. NASA-NSG-2038
12. Sponsoring Organization Name and Address NASA Materials Science Branch Ames Research Center Moffett Field, CA 94035			13. Type of Report & Period Covered Final 10/1/74-9/30/75
			14.
15. Supplementary Notes See also Battelle Report FUNDAMENTAL ANALYSIS OF THE FAILURE OF POLYMER-BASED FIBER REINFORCED COMPOSITES (Sept. 30, 1975) M. F. Kanninen, E. F. Rybicki, W. I. Griffith, and D. Broek			
16. Abstracts See pg. ii			
17. Key Words and Document Analysis. 17a. Descriptors composites, failure, fracture			
17b. Identifiers/Open-Ended Terms			
17c. COSATI Field/Group			
18. Availability Statement Distribution unlimited			19. Security Class (This Report) UNCLASSIFIED
			20. Security Class (This Page) UNCLASSIFIED
			21. No. of Pages 114
			22. Price

INSTRUCTIONS FOR COMPLETING FORM NTIS-35

(Bibliographic Data Sheet based on COSATI

Guidelines to Format Standards for Scientific and Technical Reports Prepared by or for the Federal Government, PB-180 600).

1. **Report Number.** Each individually bound report shall carry a unique alphanumeric designation selected by the performing organization or provided by the sponsoring organization. Use uppercase letters and Arabic numerals only. Examples FASEB-NS-73-87 and FAA-RD-73-09.
2. **Leave blank.**
3. **Recipient's Accession Number.** Reserved for use by each report recipient.
4. **Title and Subtitle.** Title should indicate clearly and briefly the subject coverage of the report, subordinate subtitle to the main title. When a report is prepared in more than one volume, repeat the primary title, add volume number and include subtitle for the specific volume.
5. **Report Date.** Each report shall carry a date indicating at least month and year. Indicate the basis on which it was selected (e.g., date of issue, date of approval, date of preparation, date published).
6. **Performing Organization Code.** Leave blank.
7. **Author(s).** Give name(s) in conventional order (e.g., John R. Doe, or J. Robert Doe). List author's affiliation if it differs from the performing organization.
8. **Performing Organization Report Number.** Insert if performing organization wishes to assign this number.
9. **Performing Organization Name and Mailing Address.** Give name, street, city, state, and zip code. List no more than two levels of an organizational hierarchy. Display the name of the organization exactly as it should appear in Government indexes such as Government Reports Index (GRI).
10. **Project/Task/Work Unit Number.** Use the project, task and work unit numbers under which the report was prepared.
11. **Contract/Grant Number.** Insert contract or grant number under which report was prepared.
12. **Sponsoring Agency Name and Mailing Address.** Include zip code. Cite main sponsors.
13. **Type of Report and Period Covered.** State interim, final, etc., and, if applicable, inclusive dates.
14. **Sponsoring Agency Code.** Leave blank.
15. **Supplementary Notes.** Enter information not included elsewhere but useful, such as: Prepared in cooperation with . . . Translation of . . . Presented at conference of . . . To be published in . . . Supersedes . . . Supplements . . . Cite availability of related parts, volumes, phases, etc. with report number.
16. **Abstract.** Include a brief (200 words or less) factual summary of the most significant information contained in the report. If the report contains a significant bibliography or literature survey, mention it here.
17. **Key Words and Document Analysis.** (a). **Descriptors.** Select from the Thesaurus of Engineering and Scientific Terms the proper authorized terms that identify the major concept of the research and are sufficiently specific and precise to be used as index entries for cataloging.
(b). **Identifiers and Open-Ended Terms.** Use identifiers for project names, code names, equipment designators, etc. Use open-ended terms written in descriptor form for those subjects for which no descriptor exists.
(c). **COSATI Field/Group.** Field and Group assignments are to be taken from the 1964 COSATI Subject Category List. Since the majority of documents are multidisciplinary in nature, the primary Field/Group assignment(s) will be the specific discipline, area of human endeavor, or type of physical object. The application(s) will be cross-referenced with secondary Field/Group assignments that will follow the primary posting(s).
18. **Distribution Statement.** Denote public releasability, for example "Release unlimited", or limitation for reasons other than security. Cite any availability to the public, other than NTIS, with address, order number and price, if known.
- 19 & 20. **Security Classification.** Do not submit classified reports to the National Technical Information Service.
21. **Number of Pages.** Insert the total number of pages, including introductory pages, but excluding distribution list, if any.
22. **NTIS Price.** Leave blank.

ORIGINAL PAGE IS
OF POOR QUALITY

Abstract

A fundamental investigation of the fracture behavior of fiber reinforced composites is discussed. It is suggested that experimental and analytical investigations should compliment each other. Further, it is suggested that in order to understand and mathematically model composite fracture it is necessary to explore, understand and characterize the stress-strain behavior of each type of laminate tested from initial loading to incipient fracture. That is, it is not only necessary to perform fracture studies but it is necessary to perform stress-strain characterization and failure studies as well. For this reason a literature survey is presented in which these three elements are discussed.

An experimental program to determine tensile properties of unnotched and notched unidirectional and multi-directional laminates composed of Hercules AS Fiber and 3501 Resin is described. Experimental unnotched moduli and strengths are presented, discussed and compared to lamination theory predictions. It is shown that rate effects are small and that lamination theory gives good results for moduli but not for strengths. Further, photographs of unnotched fracture surfaces as well as SEM photographs of inherent flaws are presented.

Single edge notched, double edge notched and inclined single edge notched fracture studies are presented. It is shown that stable crack growth does occur and some evidence of notch sensitivity is given. Further, the results of tests on various size circular holes is presented and compared to the fracture theories of Waddoups, et al., and Whitney, et al. Differences between theory and experiment are discussed.

TABLE OF CONTENTS

	<u>Page</u>
LIST OF TABLES	iv
LIST OF FIGURES	vi
INTRODUCTION	1
LITERATURE SURVEY	3
Stress-Strain Characterization	3
Failure Characterization	9
Fracture Characterization	12
EXPERIMENTAL PROCEDURES AND RESULTS	17
Materials and Test Procedures	17
Unnotched Tensile Properties	19
Single Edge Notch (SEN) Data	22
Inclined Single Edge Notch (ISEN) Data	24
Double Edge Notch (DEN) Data	25
Circular Hole Data	27
ANALYSIS AND COMPARISON OF RESULTS	28
DISCUSSION	33
ACKNOWLEDGEMENTS	38
REFERENCES	39
TABLES	42
FIGURES	61

LIST OF TABLES

	<u>Page</u>
Table 1. Hercules AS-3501 Graphite/Epoxy [0] _{8S} Tensile Properties	42
Table 2. Hercules AS-3501 Graphite/Epoxy [45] _{8S} Tensile Properties	43
Table 3. Hercules AS-3501 Graphite/Epoxy [90] _{8S} Tensile Properties	44
Table 4. Hercules AS-3501 Graphite/Epoxy [0/±30/0] _{2S} Tensile Properties	45
Table 5. Hercules AS-3501 Graphite/Epoxy [45/15/75/45] _{2S} Tensile Properties	46
Table 6. Hercules AS-3501 Graphite/Epoxy [90°/±60°/90°] _{2S} Tensile Properties	47
Table 7. Single Edge Notch (SEN) Data for Hercules Graphite/Epoxy Unidirectional Laminates	48
Table 8. Single Edge Notch (SEN) Data for Hercules Graphite/Epoxy Multi-directional Laminates	49
Table 9. Inclined Single Edge Notch (ISEN) Data for Hercules Graphite/Epoxy Unidirectional Laminates	50
Table 10. Inclined Single Edge Notch (ISEN) Data for Hercules Graphite/Epoxy Multi-directional Laminates	51
Table 11. Double Edge Notch (DEN) Data for Hercules Graphite/Epoxy Unidirectional Laminates	52
Table 12. Double Edge Notch (DEN) Data for Hercules Graphite/Epoxy Multi-directional Laminates	53
Table 13. Hole Data for Hercules Graphite/Epoxy [0] _{8S} and [0/±30/0] _{2S} Laminates	54
Table 13 (cont.) Hole Data for Hercules Graphite/Epoxy [0] _{8S} and [0/±30/0] _{2S} Laminates	55
Table 14. Comparison of Lamination Theory Predictions of Moduli with Experimental Results	56
Table 15. Comparison of Orthotropic Equalities and Transformations for Hercules Graphite/Epoxy [0] _{8S}	57

	<u>Page</u>
Table 16. Comparison of Orthotropic Equalities and Transformations for Hercules Graphite/Epoxy $[0/\pm 30/0]_{2S}$	58
Table 17. Comparison of Orthotropic Equalities and Transformations for Various Laminates	59
Table 18. Comparison of Experimental and Predicted Failure Loads Using Lamination Theory with Various Failure Theories (Hercules Graphite/Epoxy Laminates)	60

LIST OF FIGURES

	<u>Page</u>
Figure 1. Inherent Flaws in Graphite Epoxy Laminates a) Left; [0] _{8S} material--diamond machined surface at ~ 45° to fibers, 950X b) Right; [0/±30/0] _{2S} material--ultrasonically machined surface at ~ 90° to 0° fibers, 200X	61
Figure 2. Inherent Flaws in [0] _{8S} Graphite/Epoxy Laminates a) Left; 300X b) Right; 600X	62
Figure 3. Typical [0] _{8S} Stress-strain Data	63
Figure 4. Typical [0] _{8S} Axial Strain - Transverse Strain Data . .	64
Figure 5. Typical [45] _{8S} Stress-Strain Data	65
Figure 6. Typical [45] _{8S} Axial Strain - Transverse Strain Data . .	66
Figure 7. Typical [90] _{8S} Stress-Strain Data	67
Figure 8. Typical [90] _{8S} Axial Strain - Transverse Strain Data . .	68
Figure 9. Typical [0/±30/0] _{2S} Stress-Strain Data	69
Figure 10. Typical [0/±30/0] _{2S} Axial Strain - Transverse Data . . .	70
Figure 11. Typical [45/15/75/45] _{2S} Stress-Strain Data	71
Figure 12. Typical [45/15/75/45] _{2S} Axial Strain - Transverse Strain Data	72
Figure 13. Typical [90/±60/90] _{2S} Stress-Strain Data	73
Figure 14. Typical [90/±60/90] _{2S} Axial Strain - Transverse Strain Data	74
Figure 15. Fracture Planes in Unnotched Laminates a) Upper; [0] _{8S} specimen showing axial splitting b) Lower; [0/±30/0] _{2S} specimen showing delamination . .	75
Figure 16. Fracture Planes in Unnotched Laminates a) - d) Top to Bottom; [45] _{8S} , [90] _{8S} , [45/15/75/45] _{2S} and [90/±60/90] _{2S}	76
Figure 17. SEM Micrographs of [0] _{8S} Fracture Surface a) Left; 35X b) Right, 2000X	77

	<u>Page</u>
Figure 36. Double Edge Notch (DEN) Gross Fracture Stresses	98
Figure 37. Double Edge Notch (DEN) Net Fracture Stresses	99
Figure 38. Fracture Planes for Specimen Containing a Circular Hole a) - c) Left to right; $[0]_{8S}$, $[45]_{8S}$ and $[90]_{8S}$	100
Figure 39. Fracture Planes for Specimen Containing a Circular Hole a) - c) Top to Bottom; $[0/\pm 30/0]_{2S}$, $[45/15/75/45]_{2S}$ and $[90/\pm 60/90]_{2S}$	101
Figure 40. Circular Hole Gross Fracture Stresses	102
Figure 41. Circular Hole Net Fracture Stresses	103
Figure 42. Comparison of Experimental and Theoretical Fracture Strengths	104
Figure 43. Comparison of Experimental and Theoretical Fracture Strengths	105
Figure 44. Comparison of Experimental and Theoretical Fracture Strengths	106
Figure 45. Comparison of Experimental and Theoretical Fracture Strengths	107

INTRODUCTION

Composite materials have the potential of being superior to ordinary engineering materials for a variety of reasons. Notably among these are their high strength to weight ratios and the possibility to "tailor" their strength properties to fit a particular structural situation. However, the very qualities which make composite materials attractive also serve as limitations. In contrast to normal isotropic and homogeneous engineering materials such as metals and polymers, little is known about the failure and fracture behavior of these generally anisotropic and inhomogeneous materials. Thus, designers do not have clearly defined and proven failure or fracture criteria at their disposal. These factors precipitated the current study into the failure and/or fracture strengths and mechanisms of polymer based fiber reinforced laminated composites.

The above mentioned uncertainties about composite behavior refer to both experimental procedures in obtaining data and to the analytical approaches necessary to explain observed laboratory behavior. It was felt that a "two-pronged" program of analysis and experiment should be initiated in which analysis would guide experiment and in which experiment would guide analysis. Generally, the analytical work was to be conducted at Battelle and the experimental work was to be conducted at V.P.I. & S.U. This report relates to the effort performed at V.P.I. & S.U. A separate report is concurrently being prepared by M. F. Kanninen, E. G. Rybicki, et al. of Battelle Columbus Laboratories.

The objectives of the current program were to survey the literature for experimental techniques and applicable results on polymer based fiber reinforced composites, to test and evaluate various mechanical properties

of uniaxially and multiaxially oriented graphite/epoxy laminates with and without flaws under various loading conditions and for various flaw geometries, and to critically compare results with existing data and existing theories. This effort was to be performed on production type composites, i.e., composites which a designer is likely to work with as opposed to composites which are produced under controlled laboratory conditions.

As mentioned earlier, in order to design structures utilizing composites it is necessary to have reliable data and analytical characterization procedures for constitutive (stress-strain) properties, failure behavior and fracture behavior. Perhaps at this point it would be appropriate to state explicitly what is meant by these three necessary items. Herein, constitutive properties is taken to mean the measured relationships between stress and strain and their analytical characterization from initial loading (zero stress and strain) until separation (fracture). Constitutive properties include moduli and Poisson's ratios which may vary with strain level and with strain rate. That is, linear elasticity is not necessarily assumed.

Failure properties refers to the measurement of critical strengths and their analytical quantification via a failure, yield or strength theory. Such properties refer to materials containing only natural flaws where the size of the flaws are insignificant when compared to other material or constituent dimensions. Fracture, on the other hand, refers to the identification of a measured critical strength associated with a measured critical size flaw, notch or crack together with an analytical relation between strength and flaw size.

With these definitions it is intended to indicate that when dealing with laminated composites, experiment and analysis must and should

go hand-in-hand. The fundamental idea is that if generic properties of the constituents of a laminate (i.e., the matrix and the fibers or a single ply) are available, then the properties of the laminate can be predicted by analytical techniques. This is in contrast to the usual design procedures where prediction of the behavior of a metallic alloy is rarely attempted knowing only the behavior of the ingredients.

In the following, an effort has been made to review the various methods currently being used to experimentally ascertain information relevant to constitutive, failure, and fracture properties together with the current methods available for the quantification or prediction of such measurements. A test program and test results are described related to the collection of these three types of properties. Further, measured data are compared to predictions based on some of the currently available procedures.

LITERATURE SURVEY

In order to develop proper failure and/or fracture design guides for laminated composite materials it is necessary to thoroughly understand their stress-strain behavior and how this behavior is related to both failure and fracture. As a result, it is appropriate to review some of the more pertinent analytical and experimental procedures which are currently used in evaluating composite behavior.

Stress-Strain Characterization

Polymer based fiber reinforced composites are, in general, anisotropic and inhomogeneous materials. Except possibly for the rule of mixtures approach to stiffness, inhomogeneity is seldom accounted for. Most analytical techniques for the stress-strain characterization of laminated

composites is based upon linear anisotropic elasticity. Such a constitutive equation can be written as,

$$\underline{\epsilon} = \underline{S} \underline{\sigma} \quad (1)$$

where $\underline{\epsilon}$, \underline{S} , and $\underline{\sigma}$ are the strain, compliance and stress tensors, respectively. Alternately equation (1) could be written as,

$$\underline{\sigma} = \underline{Q} \underline{\epsilon} \quad (2)$$

where \underline{Q} is the stiffness tensor. The quantities \underline{S} and \underline{Q} must be experimentally determined and represent a minimum of 21 independent elastic constants for general anisotropy. Obviously, if general laminates were considered to be anisotropic, extensive test programs would have to be performed to obtain only these necessary constants. Further, obvious difficulties would exist if heterogeneity were included.

Often, linear orthotropic elastic constitutive equations are used to describe the behavior of individual plies or laminae or, sometimes, the entire laminate. The former is the foundation of lamination theory.^[1-4] The latter can be used for unidirectional laminates and as a first approximation to balanced symmetric general laminates.

For orthotropic materials the number of necessary constants is reduced from 21 to six.^[5] For the case of plane stress the number of constants is further reduced to four. Thus, equation (1) can be written as,

$$\begin{aligned}
 \epsilon_x &= \frac{1}{E_x} \sigma_x - \frac{\nu_{yx}}{E_y} \sigma_y \\
 \epsilon_y &= \frac{\nu_{xy}}{E_x} \sigma_x + \frac{1}{E_y} \sigma_y \\
 \epsilon_z &= \frac{\nu_{xz}}{E_x} \sigma_x - \frac{\nu_{yz}}{E_y} \sigma_y \\
 \gamma_{xy} &= \frac{1}{G_{xy}} \tau_{xy}
 \end{aligned} \tag{3}$$

where $\sigma_z = \tau_{xz} = \tau_{yz} = 0$, the principal material directions are x and y , the longitudinal and transverse moduli are E_x and E_y respectively, the longitudinal and transverse Poisson's ratios are ν_{xy} and ν_{yx} respectively, and the shear modulus is G_{xy} . Furthermore, $E_x \nu_{yx} = E_y \nu_{xy}$ and the number of independent constants to be experimentally determined is only four.

For unidirectional or balanced general laminates, the constants E_x , E_y , and ν_{xy} can easily be determined from separate specimens tested in uniaxial tension in each of the two in-plane principal directions. However, the determination of G_{xy} is not nearly so easy and numerous tests have been suggested for this purpose.^[4,6] Some of these are: the rail shear test, the short beam shear test, the picture frame test, and the torsion test. Another method is simply to use the orthotropic transformation equations together with a tension test on a specimen loaded in a direction other than a principal material direction. For example, the modulus at an angle θ to principal direction is given by,

$$\frac{1}{E_{x'}} = \frac{\cos^4 \theta}{E_x} + \left[\frac{1}{G_{xy}} - \frac{2\nu_{xy}}{E_x} \right] \sin^2 \theta \cos^2 \theta + \frac{\sin^4 \theta}{E_y} \tag{4}$$

where x , y and z are principal directions and x' is contained in the x - y plane. Given E_x , ν_{xy} , E_y and by measuring $E_{x'}$, then G_{xy} can be found

from eq. 4.

The use of eq. 4 to determine G_{xy} , in many respects, represents a better approach than the use of the rail shear or other tests. That is, it is easier to insure the existence of a state of uniaxial tension than a state of pure shear.

Another possible method of determining the shear modulus is through the use of special interrelations among the elastic constants. Two such cases due to St. Venant were reported by Lekhnitskii^[5] and can be written as,

$$\frac{1}{G_{xy}} - \frac{2\nu_{xy}}{E_x} = \frac{1}{E_x} + \frac{1}{E_y} \quad (5)$$

$$\frac{1}{G_{xy}} - \frac{2\nu_{xy}}{E_x} = \frac{2}{\sqrt{E_x E_y}} \quad (6)$$

where x and y are principal material directions. Obviously, if equations (5) and (6) are valid, only two tensile tests are necessary to determine E_x , E_y , ν_{xy} , and G_{xy} .

Because of the possibility of unbalanced and/or unsymmetric layups, most analyses use the properties of a single ply, lamina or orthotropic layer together with the necessary orthotropic transformation equations to "build up" or calculate the necessary elastic compliances or stiffnesses for either a symmetric or unsymmetric multi-layered laminate. As this laminated plate (lamination) theory can be found in a variety of references [1-4] only an outline of the procedures will be given here.

Consider a unidirectional orthotropic lamina under a state of plane stress in which the principal material directions coincide with the coordinate directions x and y , i.e., the x and y are parallel and perpendicular

to the fiber direction. Such lamina are called specially orthotropic and for this case the compliances and stiffnesses of equations (1) and (2) can be written as,

$$\underline{S} = \begin{bmatrix} S_{11} & S_{12} & 0 \\ S_{21} & S_{22} & 0 \\ 0 & 0 & S_{66} \end{bmatrix} = \underline{Q}^{-1} \quad (7)$$

or

$$\underline{Q} = \begin{bmatrix} Q_{11} & Q_{12} & 0 \\ Q_{21} & Q_{22} & 0 \\ 0 & 0 & Q_{66} \end{bmatrix} = \underline{S}^{-1} \quad (8)$$

Substitution of (7) into (1) yields equation (3). Relations between \underline{S} , \underline{Q} , and the quantities E_x , E_y , ν_{xy} in equations (3) are given in reference [4]. Note also that only four of the quantities \underline{S} and \underline{Q} in equations (7) and (8) are independent.

If the principal material directions do not coincide with the coordinate axes x and y , equations (7) and (8) are no longer valid, i.e., the axes x and y are not parallel and perpendicular to the fiber directions. This is always the case for an arbitrary lamina or ply of an angle laminate. For such a lamina equations (1) and (2) are valid and,

$$\bar{\underline{S}} = \begin{bmatrix} \bar{S}_{11} & \bar{S}_{12} & \bar{S}_{13} \\ \bar{S}_{21} & \bar{S}_{22} & \bar{S}_{23} \\ \bar{S}_{31} & \bar{S}_{32} & \bar{S}_{33} \end{bmatrix} = \bar{\underline{Q}}^{-1} \quad (9)$$

or

$$\bar{\underline{Q}} = \begin{bmatrix} \bar{Q}_{11} & \bar{Q}_{12} & \bar{Q}_{13} \\ \bar{Q}_{21} & \bar{Q}_{22} & \bar{Q}_{23} \\ \bar{Q}_{31} & \bar{Q}_{32} & \bar{Q}_{33} \end{bmatrix} = \bar{\underline{S}}^{-1} \quad (10)$$

where the quantities \bar{S} and \bar{Q} are the transformed compliances and stiffnesses. That is, relations analogous to equation (4) have been used to calculate \bar{S} from S . For example,

$$\bar{S}_{11} = S_{11} \cos^4 \theta + (2S_{12} + S_{66}) \sin^2 \theta \cos^2 \theta + S_{22} \sin^4 \theta \quad (11)$$

A complete set of the appropriate transformation equations are given in references [4,5].

The laminate stiffnesses are calculated from the transformed laminae stiffnesses, eq. (10), by

$$\bar{A} = \sum_{k=1}^n (\bar{Q})_k (Z_k - Z_{k-1}) \quad (12)$$

where Z_k represents the distance from the middle surface of the k^{th} layer and $(\bar{Q})_k$ represents the transformed lamina stiffnesses of the k^{th} layer. The laminate compliances are given by,

$$\bar{a} = \bar{A}^{-1} h \quad (13)$$

where h is the total thickness of the laminate. In other words, the laminate constitutive equation is,

$$\bar{\epsilon} = \bar{a} \bar{\sigma} \quad (14)$$

The six constants, \bar{a} , necessary to define the behavior of a general laminate can be obtained knowing only the behavior of a single ply. Therefore, using lamination theory, only the properties of a single unidirectional ply need to be determined experimentally. As single plies are quite thin (~ 0.005 in.), properties are usually determined by testing a multi-layered unidirectional laminate. These are taken as the assumed properties of a

single ply and the properties of general laminates are then calculated for each configuration being considered. Obviously, if the properties of the unidirectional laminate do not represent the properties of a single ply or if different defects are present in the manufacture of the general laminate as opposed to the unidirectional laminate, the "calculated" properties are likely to be in error.

Much experimental work has been reported on the stress-strain behavior of composites.[7-13] However, often only longitudinal and transverse moduli are reported and not the additionally required Poisson's ratios and moduli at various angles to the load direction. As a result, assumptions of behavior must often be made to calculate laminate properties with lamination theory.

Failure Characterization

The characterization of failure properties of laminated composites implies that unnotched failure stresses or strains can be calculated from a postulated strength, failure or yield criterion. For isotropic and homogeneous materials, such criteria as the maximum normal stress (Rankine), maximum shear stress (Tresca), maximum distortional energy (von-Mises), etc., are well established. For anisotropic inhomogeneous materials, similar failure theories are not well established. A large number of failure theories have been suggested for composite materials all of which are, at least partially, based upon modifying isotropic theories to include material anisotropy. Heterogeneity and nonlinear stress-strain behavior is largely ignored. A well documented and complete survey of more than 16 failure theories has been given by Sandhu with some experimental verification.[14-16]

The definition of failure must be decided before a failure criteria is of any value. Usually, an ultimate strength (maximum stress at separation) or the first departure from linear elastic behavior (or some similar definition of yielding) is used. The former works well for brittle behavior and the latter for ductile behavior for the case of isotropic materials. The precise definition to use for the failure of laminated composites is as yet unclear. However, as the macroscopic stress-strain behavior is usually nearly linear to separation, most analyses use an ultimate strength approach as opposed to a yield approach. In either event no information is yet available regarding the direction of failure or yielding such as that given by the "flow rule" in plasticity treatments of isotropic material.

Only two failure criteria will be treated herein. These are referred to as the Tsai-Hill^[4] (Azzi-Tsai^[14]) and Ashkenazi^[14] failure theories. A brief description of each follows.

The Tsai-Hill theory is based upon a yield criterion proposed for anisotropic materials by Hill which was later modified by Azzi and Tsai for an orthotropic or unidirectional lamina. For a complete description of each, see reference [14]. The governing equation for a state of plane stress can be written as,

$$\frac{\sigma_1^2}{X^2} - \frac{\sigma_1\sigma_2}{Y^2} + \frac{\sigma_2^2}{Y^2} + \frac{\tau_{12}^2}{S^2} = 1 \quad (15)$$

where σ_1 , σ_2 and τ_{12} are the stresses on an element whose sides are parallel and perpendicular to the fiber direction. Also, X , Y and S are the strengths from uniaxial tension and shear tests performed in the principal material directions. It has been shown that (15) conforms much closer to

experimental data for lamina than do simple extension of the maximum stress and strain theories to unidirectional composites^[4].

The application of the Tsai-Hill theory to general laminates may be accomplished using lamination theory. The in-plane stress resultants can be calculated using (12) with,

$$\underline{\epsilon}^{\circ} = \underline{A}^{-1} \underline{N} = \underline{A}' \underline{N} \quad (16)$$

where $\underline{\epsilon}^{\circ}$ represents the in-plane laminate strains ϵ_x° , ϵ_y° and γ_{xy}° , $\underline{A}' = \underline{A}^{-1}$ represent the compliances (per unit length, i.e., in/lb), and \underline{N} represents the stress resultants (per unit length, i.e., lb/in). For uniaxial tension, $N_x = N_1$, $N_y = N_{xy} = 0$ and

$$\epsilon_x^{\circ} = A'_{11} N_1, \epsilon_y^{\circ} = A'_{12} N_1, \gamma_{xy}^{\circ} = A'_{16} N_1 \quad (17)$$

The stresses in each layer are

$$\begin{aligned} \sigma_x &= (\bar{Q}_{11} A'_{11} + \bar{Q}_{12} A'_{12} + \bar{Q}_{16} A'_{16}) N_1 \\ \sigma_y &= (\bar{Q}_{12} A'_{11} + \bar{Q}_{22} A'_{12} + \bar{Q}_{26} A'_{16}) N_1 \\ \tau_{xy} &= (\bar{Q}_{16} A'_{11} + \bar{Q}_{26} A'_{12} + \bar{Q}_{66} A'_{16}) N_1 \end{aligned} \quad (18)$$

These stresses can be transformed to principal directions (parallel and normal to the fibers) for each ply and substituted into equation (15). Then the maximum applied failure load, N_1 , for uniaxial tension can be determined. It might be noted that by this procedure failure of a single lamina does not necessarily constitute failure of the entire laminate. Also, the procedure described does not include the "free edge" effect or address the problem of failure due to interlaminar normal or shear stresses.

The Ashkenazi theory for orthotropic composites also assumes that strength properties are tensorial. For plane stress this failure criterion may be written as, [14]

$$\frac{1}{\sigma_x} = \frac{\cos^4 \theta}{X} + \left(\frac{4}{X^{45}} - \frac{1}{X} - \frac{1}{Y} \right) \sin^2 \theta \cos^2 \theta + \frac{\sin^4 \theta}{Y} \quad (19)$$

$$\frac{1}{\tau_{xy}} = \frac{\cos^2 2\theta}{S} + \frac{4 \sin^2 \theta \cos^2 \theta}{S^{45}}$$

where σ_x and τ_{xy} are normal and shear stresses on an element making an angle θ with the principal material directions, X , Y and S are the strengths from uniaxial and shear tests performed in the principal material direction, and X^{45} and S^{45} are the strengths at 45° to the principal material directions. While it is unclear from reference [14], presumably equations (19) are for unidirectional lamina and extension to general laminates can be achieved by use of lamination theory as outlined by equations (16) - (18). Note, however, that equations (19) are valid only for uniaxial tension or pure shear only and not for a complex stress state.

In order to use the above failure theories or others, it is necessary to know not only tensile strengths in the principal material direction but the shear strength as well. As with shear moduli, various tests have been proposed for the purpose of determining shear strengths such as rail shear, short beam shear, picture frame, torsion, etc. At this point it is difficult to assess the validity of such tests as opposed to using tensorial transformations to determine shear strengths from a tension test.

Fracture Characterization

The mathematical theory of linear elastic fracture mechanics (LEFM) is well established for homogeneous isotropic and anisotropic materials. [17,18]

However, there remain many fundamental questions in regard to the experimental determination of stress intensity factors (K) or strain energy release rates (G) for particular crack geometries. For example, LEFM assumes perfect cracks of zero width and zero crack root radius. Obviously, such perfection is not possible in the laboratory. As a result, there is still some concern for isotropic materials as to what effects finite crack tip radii have on G or K and especially how close to the finite crack tip data can be collected and still be correlated to LEFM. Even if near perfect crack tip geometries are generated using fatigue to grow or enlarge a small crack, a small region near the crack tip cannot be modeled well by LEFM because of finite deformation and plasticity effects. Thus for isotropic as well as anisotropic but homogeneous materials, a core region adjacent to the crack tip on the order of the size of the crack root radius must be excluded in any analysis using LEFM.

In composite materials, the picture is much more complex. These materials are inhomogeneous as well as anisotropic and various fracture mechanisms with separate but perhaps coupled fracture energies must be accounted for. However, perhaps the single most complicating feature of composite fracture is that self-similar crack growth is not likely to occur even for unidirectional or symmetric angle ply laminates. Without self-similar growth LEFM is, in general, not applicable to any material.

The early fracture theories of Waddoups, et al.,^[19] Cruse^[20], and Whitney, et al.,^[21] consider only self-similar crack growth. Each of these investigators found that in order to use various fracture solutions for either holes or cracks that the crack length had to be adjusted to include an intense energy region at each crack tip. The size of the intense energy region had to be found by experiment.

The more recent theories of Wu^[22,23] and Sih^[24,25] not only can be used to predict critical load levels for crack growth, but will also predict the direction of crack propagation. Wu's technique performs this function by locating the intersection of the stress vector surface and the failure surface (determined from unnotched biaxial tests). This calculation must be made at a distance r_0 away from the crack tip to avoid singular stress fields. Sih's technique employs a strain energy density concept. The strain energy density and its derivative must be found at a distance r_0 away from the crack tip to avoid singular stress fields. Thus, while each of these theories give non-self-similar crack growth predictions, the size of the intense region must be known a priori or found by experiment.

The approaches discussed to this point represent models with two arbitrary parameters as opposed to the usual model of LEFM with only one arbitrary parameter.

A more recent approach due to Kulkarni and Rosen^[26] uses a materials science approach to model crack growth normal to the crack plane. Such crack growth has been observed for both unidirectional and general laminates.^[7] Without going into details, a critical intense energy region in the direction of the crack and normal to the crack must be found by experiment. That is, this technique is essentially a model with three arbitrary parameters.

Perhaps it is worth while to note here that each of the fracture theories mentioned require either information relevant to accurate stress strain properties or to failure stresses and strains as well as valid fracture data.

Obviously, all the questions regarding the size of actual crack tip geometries as opposed to the assumed ideal crack tip geometries used in

fracture analyses are even more important for composite materials. This is reinforced by the fact that a recent experimental investigation tended to show that unidirectional graphite/epoxy notched composites are not in general notch sensitive.[27] In fact, notch insensitivity is implicit in the early fracture models as little distinction is made between a through circular flaw and a through crack.[19-21] For this reason and for later reference, the theories of Waddoups, et al.[19] and Whitney, et al.[20] will be briefly outlined.

Waddoups, et al., in reference [19], modeled a circular flaw in a composite as having two slits or cracks emanating symmetrically from either side of the hole perpendicular to the load direction. Even though the slits were defined only as intense energy regions they were modeled mathematically as cracks using the Bowie crack solution.[28] The latter can be written as,

$$K_{IC} = \sigma_C \sqrt{\pi a} f(a/r) \quad (20)$$

where K_{IC} is the opening mode critical stress intensity factor, σ_C is the critical remote load, a is the length of the intense energy region (or crack) adjacent to the hole and $f(a/r)$ is a function of the hole radius r . A table for $f(a/r)$ values for an infinite plate for different hole sizes is given in reference [28]. For a specimen with no hole, $f(a/r) \equiv 1.0$. Therefore,

$$\frac{\sigma_0}{\sigma_C} = f(a/r) \quad (21)$$

where σ_0 is the critical remote load for an unnotched tensile specimen. Thus, given σ_0 and σ_C for one size hole, critical stress intensity factors

can be calculated for other size holes using equation (20) provided a/r values can be found. The a/r values were found using the elliptical hole analysis of Griffith^[29] which essentially determines the size of the intense energy region or the value a .

The fundamental idea is that using the results from one unnotched tensile test and from one notched tensile test, critical stresses for other size holes can be calculated assuming K_{IC} and a to remain constant. An identical procedure was used for slits. For either the case of holes or slits the size of the intense energy region was found to be $a \sim 0$ (0.04 in.).

Whitney and Nuismer^[21] used quite a different technique to explain the hole size effect in composites. Their argument was that, while different size holes in an infinite plate have the same stress concentration factor, the stress gradient is quite different for each. That is, large stresses are localized more closely to the edge of a small hole than a large hole. As a result, a critical defect is more likely to occur in a region of high stress for a large hole. Both a point stress and an average stress technique were used. The point stress criterion was given by,

$$\frac{\sigma_c}{\sigma_0} = \frac{2}{[2 + R^2 + 3R^4 + f(K_T^\infty, R)]} \quad (22)$$

where $R = r/r + d_0$, $2r$ is the hole diameter, d_0 is the size of the damage zone, and σ_c and σ_0 are the critical notched and unnotched stresses as defined earlier. The quantity $f(K_T^\infty, R)$ is a function of the hole size and the orthotropic stress concentration factor for an infinite sheet, K_T^∞ . The average stress criterion was given by,

$$\frac{\sigma_c}{\sigma_0} = \frac{2(1 - R)}{[2 - R^2 - R^4 + f(K_T^\infty, R)]} \quad (23)$$

where $\lambda = r/r + a_0$, a_0 is the size of the damage zone and σ_c , σ_0 , and $f(K_T, R)$ are as defined previously.

Identically the same technique was used for cracks except the stress state in front of a crack was used instead of the stress state in front of a hole. Good correlation between theory and experiment was shown for a variety of quasi-isotropic laminates. [21]

EXPERIMENTAL PROCEDURES AND RESULTS

It should be emphasized that the work reported in this section represents all the data which has been collected to date. Additional data is currently being collected the results of which will be reported at a later date.

Materials and Test Procedures

The materials studied in this investigation were manufactured by Lockheed (Sunnyvale, Calif.) from prepreg tapes composed of Hercules (Magna, Utah) graphite AS fibers and epoxy resin 3501. The fundamental properties of the fibers were: 380-400 ksi tensile strength, $30-40 \times 10^3$ ksi elastic modulus and 10,000 fibers/tow. The resin was a hot-melt 100% solids epoxy. No properties of the resin were available. The resulting $[0]_8$ s and $[0/\pm 30/0]_{2s}$ laminates were medium strength-medium modulus composite materials. Large 0.80 in thick plates were received from which individual specimens were machined.

Some effort was made to determine the best procedures for machining specimens. Diamond saws, tungsten carbide cutting tools, and ultrasonic machining techniques were attempted. Diamond saws were selected to give the best surface for the amount of machine time required. Surfaces machined by the various techniques were examined with a scanning electron

microscope (SEM) and various inherent flaws were found. Figures 1a) and 1b) are SEM photographs of a diamond and an ultrasonically machined surface respectively. Also shown in Figure 1 and in Figure 2 are examples of typical flaws which were found. Figure 1a) shows a near cylindrical void while Figure 1b) shows a flaw which appears to be in a single ply and extending at an angle to the interface between laminae. Additional flaws are shown in Figure 2 which gives an idea of the size and magnitude of the inherent flaws which were found.

Uniaxial tension tests were performed on specimens with and without flaws using an Instron testing machine. After machining, all specimens were stored in a desiccator until tested. Specimens were allowed to sit and stabilize to the test environment for at least 1 hr. prior to testing. Test temperatures were generally at room temperature of approximately 75°F and the relative humidity was generally less than 60%.

Unnotched specimens were 0.5 in. wide with ~ 4.5 in. between grips of the Instron tester. These specimens were instrumented with longitudinal and transverse strain gages and were tested at strain (head) rates from 0.002 in./min. to 2 in./min.

Specimens (1 in. wide with ~ 4.5 in. between grips) with single edge notches, double edge notches and circular cut-outs were also tested. Notched specimens were generally tested at a head rate of 0.01 in./min. under similar environmental conditions as the unnotched specimens. Edge notches were used as opposed to center notches because notch widths and notch tip geometries could be made much smaller using diamond saws as opposed to end mills.

All tests were conducted without tabs, using sandpaper between epoxy coated wedge grips to minimize penetration of grip serrations into the

graphite/epoxy materials. Data collected in this manner correlated well with data collected by NASA-Ames using tabs.

Unnotched Tensile Properties

Tensile tests were conducted on unnotched tensile specimens with nominal cross-sectional dimensions of 0.5 in. X 0.080 in. Both $[0]_{8S}$ and $[0/\pm 30/0]$ laminates were tested at various strain rates and with loads at 0° , 45° , and 90° to the principal material direction. A compilation of the test results is given in Tables 1-6. Because of the variability of stress-strain data, a statistical subroutine from the library of our IBM-370 computer was used to condition the data. Typical computer generated stress strain diagrams and axial strain-transverse strain diagrams for various strain rates together with actual data points are given in Figures 3-14. Note that the first number in the caption in each case refers to the direction of the load with respect to the principal fiber direction. That is, the notation $[45/15/75/45]$ indicates that the tensile load was applied to a strip cut at 45° to the 0° fiber direction of the $[0/\pm 30/0]_{2S}$ laminate.

It is apparent by examining Tables 1-6 that moduli, Poisson's ratios, and tensile strength do not appear to be significantly dependent upon strain rate, at least for the ranges examined. This is even true for cases where the load was at 90° to the principal fiber direction, i.e., where the material should be matrix dominated and hence viscoelastic.

As yield strength is often a more sensitive indicator of rate dependence than other variables, efforts were made to determine the yield point of the materials tested. As some stress-strain curves were concave rather than convex, offset methods of defining yielding were not appropriate. Each stress-strain curve could be approximated reasonably well by two

straight lines. The point of intersection of such a bilinear curve was taken as the yield point. Again, no definitive conclusion could be reached regarding rate dependence in general. For $[0]_{8S}$ and $[0/\pm 30/0]_{2S}$ tests, this definition indicates a decrease of yield stress with increased strain rate. This is likely to be the result of a scissoring effect of the fibers and not a normal yield mechanism. Tests for other load directions gave less indication of any variability of a yield stress as defined.

Generally, the instantaneous modulus, $d\sigma/d\epsilon = E_t$, and Poisson's Ratio changed throughout each test by as much as 25%. While decreases usually occurred, increases were noted for the $[0]_{8S}$ and $[0/\pm 30/0]_{2S}$ tests. Because of these facts it would seem inappropriate to use initial elastic properties in fracture analyses. Nor would it be appropriate to use tensorial transformations in failure analyses.

As indicated in Table 5, Poisson's ratios were negative for the $[45/15/75/45]$ tests.

Final fracture surfaces were in general perpendicular to the load direction for the $[0]_{8S}$ and $[0/\pm 30/0]_{2S}$ test (see Figure 15). As may be seen in Figure 15a), longitudinal splitting was always at least a secondary (and sometimes a primary) fracture mode for the $[0]_{8S}$ tests. All other fracture surfaces for the unnotched tests tended to follow the principal fiber direction. For example see Figure 16.

The fracture process for the $[0/\pm 30/0]_{2S}$ specimens was often quite explosive and in many cases fragmentation occurred, i.e., fragments would be expelled considerable distances from the test machine. Also, for this series of tests, post specimen examination did reveal some evidence of delamination. However, it is felt that this delamination occurred after separation due to rebound impact forces (see Figure 15b which shows a

specimen which fractured in two places simultaneously).

In many tests various factors indicated that fracture occurred first in inner plies. Figure 17a) is an SEM photograph of the central portion of a $[0]_{8S}$ specimen and gives the appearance that fracture first occurred on an inner ply near the middle of the specimen. Crack propagation then appears to move across the ply and through adjacent plies simultaneously.

Figure 17b) is a micrograph of another $[0]_{8S}$ specimen showing individual broken and pulled out fibers.

For the $[0/\pm 30/0]_{2S}$, $[45/15/75/45]_{2S}$, and $[90/\pm 60/90]_{2S}$ tests audible noise could be heard in nearly every case long before separation. Undoubtedly this audible noise was due to breakage of either individual fibers or individual plies and most likely was due to the latter.

Another indication that fracture occurred on inner plies first can be seen by examination of Figure 18 which shows the load-time and strain-time traces from one strain-rate test for a $[90/\pm 60/90]_{2S}$ specimen. As may be observed, small excursions in load occurred simultaneously with large excursions in strain. This was accompanied by large amounts of audible noise with no visible signs of failure on the surface of the specimen. A possible explanation for these observations is that fracture may have occurred first on an inner ply or plies near the location of the strain gage on a surface ply resulting in a transfer of strain from inner to outer plies with little loss in load carrying capacity. Such a process could cause a large increase in strain on an outer ply at the strain gage site and not affect the load carrying capacity appreciably.

It should be noted that the manufacturers specification for the tensile strength of the $[0]_{8S}$ material was 240 ksi. Our tests, substantiated by NASA-Ames, indicated a tensile strength of only 153 ksi.

This extreme difference seems to be a fault of the manufacturing technique. Also, as may be observed by examination of Tables 1-6, these graphite/epoxy materials contained extreme thickness variations, i.e., as much as 35%. Such variations in strength and thicknesses are obviously very important in attempts to understand the failure and fracture behavior of composite materials.

Single Edge Notch (SEN) Data

A series of tests were performed on single edge notched specimens with various notch lengths. The notches were made with a 0.006 in diamond saw with the resulting notch width of ~ 0.0075 in. The tip of the notch was reasonably flat but with rounded corners. One corner appears to consistently have a smaller radius than the other. Figure 19 shows the geometry of a typical notch. In all cases notches were normal to the applied load direction, but the tensile load was at various directions to the fiber angle(s).

Details of the specimen geometry and test results are shown in Tables 7 and 8. Fracture stresses were calculated using the net section average thickness. The fracture angle refers to the direction of initial crack propagation with respect to the direction of load. With the exception of the $[0/\pm 30/0]_{2S}$ tests, crack propagation was in the direction of, or nearly so, the principal fiber direction. Minor deviations are likely due to misalignment of loads or specimen geometries or minor perturbations during the fracture process.

Axial splitting was the predominant fracture mode for the $[0]_{8S}$ tests. That is, when the load was in the fiber direction of the zero fiber with the crack normal to the fiber direction, fracture occurred parallel to the

load in every case. This was likely due to thickness variations and gripping conditions and the fracture loads are not thought at this time to represent realistic material values. The photograph of Figure 20 shows such a fracture mode.

Only in the $[0/\pm 30/0]_{2S}$ tests did the crack propagate in a different direction than the principal fiber direction. In this case crack propagation was erratic but was generally normal to the load and principal fiber direction. Figure 21 gives visual evidence of these results. (Note that for the SEN specimens only a starter notch was made sometimes with a thick saw blade but the notch tip was always made using the 0.006 saw blade.)

In most cases fracture appeared to occur at the smallest notch tip radii. Also, in nearly all general laminate tests audible noise could be heard substantially before fracture. Also, in these cases and in some unidirectional tests, visible and stable crack growth was observed. That stable growth was observed is evident from examination of successive 35mm photographs taken during fracture shown in Figures 20, 22, and 23 for $[0]_{8S}$, $[45]_{8S}$ and $[90/\pm 60/90]_{2S}$ tests respectively. Similar observations were made in other tests.

The audible noise mentioned for the general ply tests appeared to occur in many cases in conjunction with a load reduction. That is, at some point prior to complete separation, load reduction would occur instantaneously. After a delay time, the load would again increase to its previous or a higher value. Repeated low reductions were observed in some cases as typified by Figure 24.

Plots of the gross stress and net section stress versus crack length for the SEN data given in Tables 7 and 8 are shown in Figures 25 and 26. With the exception of the $[0]_{8S}$ data, notch sensitivity does seem to be present.

Inclined Single Edge Notch (ISEN) Data

A series of tests were performed on single edge notched specimens with the notch at various angles to the applied load. Thus, both the load and notch were at various angles to the principal fiber direction. Details of specimen geometry and the results of the various tests are given in Tables 9 and 10. All angles are with respect to the load direction. Note that the crack lengths were always such that their projected length normal to the load was half the specimen width. This was done such that relevant comparisons between ISEN and other tests could be made.

In the ISEN tests a microscope was mounted directly on the test machine such that in situ observations could be made and photographed. Figure 27a) shows the longitudinal splitting at the tip of a 45° notch in a $[0]_{8S}$ specimen while still sustaining a tensile load in the $[0^\circ]$ direction. Figure 27b) shows the same results for a 75° notch in a $[90/\pm 60/90]_{2S}$ specimen.

Figure 28 represents a sequence of photographs taken for a $[45/15/75/45]_{2S}$ specimen with a notch at 40° to the load direction. Here it is graphically shown that stable growth occurs for this type of specimen while still sustaining additional load. The last photograph of Figure 28d) shows the specimen after separation and indicates that the fracture process is self-similar in the outer 45° ply, but is decidedly not self-similar in inner plies. That is, by noting the jagged appearance of the fracture surface of the inner plies, it is obvious that the total fracture process is extremely complicated.

Figure 29 shows the fracture planes of two $[45]_{8S}$ specimens after separation when the initial notch was inclined in the same general direction as the fibers (with respect to the load) and when the initial notch was

inclined generally at right angles to the fibers. Obviously, self-similar or non-self-similar crack growth can be controlled by the manner in which the crack is induced. That is, fracture occurs primarily in the matrix with little fiber breakage.

The fracture surfaces after separation of the six $[0/\pm 30/0]_{2S}$ specimens with different angles of inclination of the initial notch are shown in Figure 30. Here it is obvious that a variety of fracture modes from nearly self-similar to totally non-self-similar was observed. Note the generally jagged appearance of the fracture surfaces indicating different directions of crack growth in interior plies and exterior plies. Note also the photograph of Figure 30f) where almost perfect self-similar behavior from a macroscopic standpoint was observed. Of course at a local level, at any particular instant in the fracture process, the fracture process may not have been self-similar.

Gross stresses and net stresses are shown plotted versus the angle of inclination of the crack (with respect to the load direction) in Figures 31 and 32. With the exception of the tests for the $[0]_{8S}$ and $[45]_{8S}$ specimens, it appears that fracture stresses tend to increase, as expected, when the crack is aligned more closely with the load direction.

Again in nearly all tests of general laminate audible noise could be heard well before separation and repeated instantaneous load reductions followed by increases of loads to larger values were observed.

Double Edge Notch (DEN) Data

It is not clear that single edge notch (SEN) fracture data is as meaningful for a composite material as it is for a homogeneous isotropic material. That is, approximate solutions for SEN specimens are available

for quantifying data for isotropic materials. For composites there are no such solutions. Because of the above facts and because symmetry of loading is sometimes very important, a series of tests was performed on double edge notch specimens (DEN) with various lengths of notches normal to the load and at various angles to the principal fiber direction. Tables 11 and 12 give information relevant to the geometry of the specimens and the results of these tests.

In general, the same type of information was obtained from these tests as from SEN or ISEN tests. That is, for unidirectional laminates fracture always occurred in the matrix. In other words, fracture planes were always parallel to the fiber direction regardless of load or length of notch. For our general laminate, again audible noise was heard long before separation and frequently repeated instantaneous load reduction followed by gradual load recovery were observed. Stable crack growth was observed at one or both crack tips with a microscope as in the ISEN tests. Figure 33 is a sequence of photographs showing the stable crack growth for the $[0/\pm 30/0]_{2S}$ specimens. Note the additional cracks somewhat above and below the notch tip and the jagged appearance of the fracture surface in Figure 33. Again, apparently fracture occurs in inner and outer plies at different times and different directions. While the general appearance of fracture is self-similar in a gross sense and especially for the outer plies, self-similar behavior is not the fracture mode on a local level for the inner plies.

The $[90/\pm 60/90]_{2S}$ DEN specimen containing a .05 in. length notch on one side is shown in Figure 34. As may be observed fracture occurred at a considerable distance from the site of the machined notch. In this particular case the specimen thickness at the crack tip was 0.085 in. while its

minimum value was 0.075 in. at the fracture site. Thus the average areas at each location were about the same, i.e., $\sim 0.075 \text{ in.}^2$. Thus, it would appear that an inherent flaw existed at the minimum section which was more critical than the machined notch. One might infer from this case that the material is not notch insensitive. Obviously this is not necessarily the case as the material is not a continuum and as such the converse is likely to be true. The real question is only the size of critical inherent flaw if one existed.

Figure 35 shows the fracture plane of all six $[0/\pm 30/0]_{2S}$ specimens. As found earlier for SEN and ISEN specimens, some fracture planes tended to be self-similar while others did not. In fact, it seems that for these tests that initial separation of all layers (in contrast to separation only in an outer ply) tended to be in the 30° direction.

Gross stresses and net fracture stresses are given in Figures 36 and 37. Obviously, considerable differences were found between both gross and net fracture stresses of the SEN and DEN specimens. This is particularly apparent from examination of the net stresses of Figures 24 (SEN) and 37 (DEN). The DEN results for our general laminates tend to indicate less notch sensitivity than the SEN tests.

Circular Hole Data

Tests were performed on both types of laminated specimens containing circular holes of varying sizes. Details of geometry and the results of the various tests are given in Table 13.

For unidirectional laminates fracture originated at the edge of the hole and propagated in the direction of the fibers in each case. Figure 38 gives typical examples of fracture planes for the $[0]_{8S}$, $[45]_{8S}$ and $[90]_{8S}$.

For our general laminates fracture originated (in most cases) at the edge of the hole and propagated in various directions depending on the lay-up. Figure 39 gives typical examples of fracture planes for various $[0/\pm 30/0]_{2S}$, $[45/15/75/45]_{2S}$ and $[90/\pm 60/90]_{2S}$ specimens. Also note the $[90/\pm 60/90]_{2S}$ specimen which separated at a location other than the hole. In this case the thickness at the edge of the hole was 0.079 in. and was 0.074 in. at one location where fracture occurred. Thus, even though the net area was smallest at the minimum section, fracture occurred at the point where the specimen was the thinnest. Again, presumably an inherent flaw at the fracture site was more critical than the machined hole.

Gross and net fracture stresses are shown in Figures 40 and 41. With the exception of the data for the $[45]_{8S}$ and $[90]_{8S}$ specimens, the hole results are quite similar to the DEN results.

ANALYSIS AND COMPARISON OF RESULTS

As outlined in an earlier section, it is possible to predict the stiffness properties of laminates using lamination theory in conjunction with the properties of a single ply. In our case, the data for a unidirectional graphite/epoxy laminate was assumed to represent the properties of a single ply. Lamination theory was then used to predict the stiffness behavior of both our unidirectional laminate and our general laminate. The former was done only as a check on the computer program which was used. Table 14 shows the results of this effort for the Hercules graphite/epoxy tensile data contained herein. Also shown is the results of the same calculation for two other laminates whose properties are given in reference [8]. As may be observed, lamination theory gives excellent predictions for tensile moduli. The good agreement between theory and predictions gives

some confidence in both the use of lamination theory and in our experimental results.

Another means of evaluating data on composites is to assess the validity of anisotropic transformation equations, equalities, etc. For unidirectional laminates orthotropic theory should work reasonably well. That is, equations (3) and (4) should be valid and the equality $E_x \nu_{yx} = E_y \nu_{xy}$ should be maintained. Table 15 shows the comparisons for this equality and the calculations of the shear modulus using equation (4) and using the two special orthotropic relations (5) and (6) due to St. Venant. Note that the equality is not satisfied by nearly a factor of two and that the shear moduli calculated by the three different methods are not in agreement either. The value calculated by equation (4) does agree with the value from lamination theory given in Table 14 inasmuch as equation (4) is in fact used in lamination theory.

Table 16 shows the same calculations and comparisons for the Hercules multi-directional laminate data. The equality $E_x \nu_{yx} = E_y \nu_{xy}$ is more closely satisfied especially for the higher rates. This leads us to believe that some rate effect is present but is small and is not likely to be found by measurement of tensile properties alone. In other words, the viscoelastic effect, though small, is much larger for low rates than high rates. The same can be said for the data in Table 15.

The shear moduli calculated by the various equations are now in much closer agreement. This probably is an indication, as with the satisfaction of the equality, that the $[0/\pm 30/0]_{2S}$ laminate tends to be more nearly quasi-isotropic than the $[0]_{8S}$ laminate. In other words, the equality would obviously be satisfied for an isotropic material as would St. Venant's

special orthotropic equations.

Considerable disagreement between the shear modulus of the multi-directional material calculated by equation (4) and by lamination theory (Table 14) is shown. This could be a reflection on the experimental data, i.e., using unidirectional laminate data as input for the behavior of a single ply in the general laminate, a reflection on the use of lamination theory in general, or on the use of orthotropic transformations for balanced and symmetric laminates. It may very well be that the results of Tables 14, 15 and 16 indicate that balanced symmetric laminates can, as a first approximation, be considered to be orthotropic and that standard orthotropic transformation equations can be used with equal, if not more, confidence than lamination theory.

In an effort to quantify the above idea, comparisons of properties, the orthotropic equality, and St. Venant's orthotropic equations were made for data found in the literature on a variety of composites. While the results are not conclusive for lack of sufficient data, it does appear that both the equality and St. Venant's special equations are better suited or more nearly valid for quasi-isotropic materials. If such is the case, one would wonder at the need for lamination theory for such materials.

Lamination theory was used to predict the tensile loads at failure. These results are shown in Table 18. The procedures used to obtain the results by the Tsai and Azzi-Hill and the Ashkenazi theories were as outlined in an earlier section. As may be observed, the Ashkenazi theory consistently gives closer correlation to the experimental data than the Tsai and Azzi-Hill theory. As will be recalled, the fundamental difference in the two approaches is that in the former, the value σ_x from equation (18) substitutes directly into (19) while in the latter, the value σ_x , σ_y and

τ_{xy} must be transformed into the fiber directions before substitution into equation (15). Of course, it is possible to use the same procedure of Ashkenazi with the Tsai and Azzi-Hill theory of equation (15). That is, the value of σ_x from (18) can be taken as equivalent to σ_1 in equation (15). This is referred to as the modified Tsai and Azzi-Hill procedure in Table 18 and gives results comparable to the Ashkenazi theory. Additional work is currently underway in hopes of obtaining better correlation between theory and experiment.

Efforts were made to compare our experimental results for circular holes with the fracture theories of Waddoups, Eisenmann and Kaminski^[19] and Whitney and Nuismer^[21] which were described briefly in the literature review section. Inasmuch as these theories are for infinite plates, our results for finite width plates had to be modified in such a way that meaningful comparisons could be made. This was accomplished using the approach of Whitney and Nuismer which can be expressed as,

$$\sigma_c)_{\text{exp}}^{\infty} = \frac{K_{fw}}{K_T^{\infty}} \sigma_c^{fw})_{\text{exp}} \quad (24)$$

where $\sigma_c)_{\text{exp}}^{\infty}$ is the remote stress for an infinite plate, K_{fw} is a finite width isotropic correction factor, K_T^{∞} is an orthotropic stress concentration factor for an infinite plate, $\sigma_c^{fw})_{\text{exp}}$ is the measured critical remote stress. The precise formulations for K_{fw} and K_T^{∞} can be found in reference [21]. The experimental data was corrected by the above procedure and is shown together with the theories of Waddoups, et al., and Whitney, et al., in Figures 42 and 43. The analytical results are essentially a plot of equations (21), (22) and (23). (Note that the latter two include an orthotropic stress concentration factor, K_T^{∞} , to attempt to incorporate

material anisotropy. See reference [21].)

Interestingly enough, better correlation between theory and experiment seemed to occur for the unidirectional laminate than for the angle ply laminates. This is especially true as the experimental fracture stress values for the $[0]_{8S}$ specimen are felt to be somewhat on the low side due to longitudinal splitting.

Some of the differences observed in Figures 42 and 43 are undoubtedly due to the analytical methods used to effect a comparison. That is, the rather arbitrary use of an isotropic finite width correction factor together with an orthotropic stress concentration factor in equation (24) is likely to be at least partially responsible for the deviations between theory and experiment. It might be noted that an arbitrary damage zone size of 0.04 in. was used for the Waddoups, et al., theory and for the point stress criteria of Whitney, et al., while an arbitrary damage zone size of 0.15 in. was used for the average stress theory of Whitney, et al. These are the values given by the respective authors to represent the size of the damage zone for the laminates they investigated. It is possible that a different size damage zone is present in our materials at fracture. However, these effects are felt to be secondary to the possible errors in K_{fw} and K_T^∞ . The results of Figures 44 and 45 tend to confirm this observation. In Figures 44 and 45 the data was corrected by replacing the ortho-tropic stress concentration factor by an isotropic stress concentration factor, i.e., $K_T^\infty = 3.0$. Note that when this procedure was followed that the correlation with both theories was vastly improved.

As yet no correlation has been obtained between our notch data and the various fracture theories described earlier. The primary obstacle has been our inability of finding in the literature or obtaining directly a

correct fracture mechanics solution to a finite anisotropic strip containing single or double edge slits. Efforts are still underway in this area.

DISCUSSION

In this investigation an effort has been made to explore several aspects of laminated composites. Each was directly or indirectly related to the fracture behavior of composites. These were; the stress-strain characterization from tension tests up to and including failure, the failure or yield process itself, and finally the fracture behavior of laminated composites. All of these items are needed for fracture investigations as moduli, Poisson's ratio, etc., enter into all LEFM analyses; failure stresses and strains are often used as parameters in fracture studies; and, of course, information on fracture toughnesses of composites is of vital importance. The state of the art of these three areas was discussed at some length. From this discussion it is clear that much effort yet needs to be expended in order to analytically characterize each area as well as identify the most appropriate set of experiments to estimate the necessary parameters needed in a fracture analysis. For example, it is unclear whether it is best to determine shear properties from a tension test, torsion test, rail shear test, etc. Also, it is unclear if a flow rule can be used to predict failure planes as well as whether tensorial transformations are appropriate for failure analyses. That is, are nonlinearities large enough to cause linear analyses to be seriously in error? Further, similar questions can be raised about fracture testing in general, i.e., are nonlinearities important, etc.? Also, how does one measure the damage zones used in the various theories? What are the appropriate finite width correction factors for edge or center notches?

An experimental program to obtain the stress-strain, failure and fracture behavior of Hercules graphite/epoxy $[0]_{8S}$ and $[0/\pm 30/0]_{2S}$ laminates was conducted. Tension tests of unnotched specimens were performed where the load was at various inclinations to the fiber directions and different loading rates were used. Average properties were found at each strain rate tested. Generally, no rate effect was found over four orders of magnitude of strain rates. This was true even in cases where the load was at 90° to the principle fiber direction or when the composite was matrix dominated. Lamination theory was used to predict tensile moduli and stiffnesses with good success. Shear moduli were predicted both using orthotropic transformation equations and two special equations due to St. Venant as well as lamination theory. While the evidence is not conclusive, it does seem to show that the two former methods are at least as effective as the latter method for quasi-isotropic materials. Efforts were made to make similar comparisons with data found in the literature with similar results. Also, orthotropic equalities were tested for the data from our materials and the data found for other materials in the literature. It appears that these are more nearly satisfied for those materials which tend toward quasi-isotropy. That is, the equality was more closely satisfied for our $[0/\pm 30/0]_{2S}$ material than for our $[0]_{8S}$ material even though the latter should be closely approximated by orthotropic theory.

In our unnotched tests, audible noise was heard long before separation or fracture. Often, this was accompanied by a load reduction with subsequent load recovery as mentioned earlier. This plus other evidence indicated that first fracture often occurred in inner plies. In quite nonscientific terms, the two types of noise heard were reminiscent of that heard when a tension wire breaks and that heard when wood splits. The

former was generally heard only when the load was in the direction of the fibers. The latter was usually heard in all cases and might be likened to matrix failure with fibers pulling away from the matrix longitudinally.

The single most controlling factor related to unnotched fracture appeared to be the thickness at the fracture site. In other words, failure always seemed to occur at the thinnest point regardless of its location (i.e., in the grip or in the test section).

Lamination theory was used together with two separate failure theories to predict failure loads. Predictions were always quite inaccurate. Attempts are currently underway to modify the failure criteria. Preliminary indications are that considerable improvement can be made by not assuming that a ply is totally lost when only it has separated.

Various SEN, ISEN, DEN or hole fracture tests were performed. Considerable differences were noted among the various tests. SEN, DEN, and hole results disagreed by a considerable amount. It would appear that notch sensitivity of some type is present. On the other hand, ISEN test seemed to indicate a general trend toward notch insensitivity. That is, in some cases the fracture load actually decreased as the angle crack tended toward the load direction.

Longitudinal splitting was always the controlling fracture mode for unidirectional laminates with the load in the fiber direction. It was not clear that the fracture loads in these cases were representative of actual material behavior due to the gripping conditions. Fracture occurred generally normal to the 0° fiber in tests on $[0/-30/0]_{2S}$ specimens when the load was in the direction of the 0° fiber. In all other cases the fracture planes were aligned with the principal fiber. Thus, it appears that fracture first occurs in the matrix in all cases except possibly for symmetric

off-angle composite loaded in a principal fiber direction.

Probably the most important aspect of the fracture tests was that stable crack growth was observed. This stable growth was often accompanied by audible noise and a reduction in load with subsequent load recovery to even higher levels. Thus, fracture appeared to occur in stages on both inner and outer plies. Sometimes crack growth was self-similar and other times it was not depending primarily on the initial crack geometry, location and direction. Self-similarity was often produced in surface layers with obvious stages of non-self-similarity on interior layers.

Again, probably the most controlling factor in the fracture process seemed to be the thickness at the fracture site. In two cases fracture occurred at a site away from the notch where the material was thinnest ($90/\pm 60/90$ specimens). This does lead one to believe that the fracture process in nearly all composites is fiber dominated even when the material should be matrix controlled. That is, due to the manufacturing process, it is likely that the fibers per unit thickness is less where the laminate is the thinnest. If such is the case, then the thinnest section should be the most critical site.

The fracture results were compared to two of the earlier fracture theories which have been verified by others as being reasonable approaches to the fracture of laminated (quasi-isotropic) composites. In our case closer correlation was obtained between our unidirectional data and these theories than between our off-angle data and these theories. It is felt that much of the difficulty resides in the finite width correction factor which includes an orthotropic stress concentration factor. This correction factor is taken directly from isotropic theory and is modified for use with composites only by the inclusion of an orthotropic stress concentration

factor. When the orthotropic factor is disregarded, excellent agreement is obtained between the Waddoups, Eisenmann and Kaminski theory and the Whitney and Nuismer theory and our results. As of this writing, the reason for this latter fact is unknown.

In closing, it is appropriate to state again that laminated composites offer great promise as light weight but strong structural materials. However, before they can be used with confidence, more information about experimental and analytical characterization of their fracture behavior must be obtained. In fact, it is felt that one of the most serious disadvantages of composites today is their quality control and how this affects their performance in structural usage. Often thicknesses vary by significant amounts, warpages of varying degrees are present, residual thermal stresses are present, fiber densities vary by significant amounts, fiber directions are often in error, etc. All of these factors have serious effects on fracture behavior. With adequate quality control and with adequate testing and analytical studies, one aiding the other, perhaps some realistic fracture criteria can be developed to be valid for many different laminated composite systems.

ACKNOWLEDGEMENTS

The financial support provided for this work by NASA Grant NSG 2038 from the Materials Science Branch of Ames Research Center is gratefully acknowledged. Further, sincere appreciation is extended to D. P. Williams of NASA-Ames for his encouragement and many helpful suggestions. Also, the many helpful discussions with M. F. Kannenin, E. F. Rybicki and W. Griffith of Battelle Columbus Laboratories are acknowledged.

REFERENCES

1. Tsai, S. W., Halpin, J. C. and Pagano, N. J., Composite Materials Workshop, Technomic, 1968.
2. Ashton, J. E. and Whitney, J. M., Theory of Laminated Plates - Progress in Materials Science, Vol. 4, Technomic, Stanford, Conn., 1970.
3. Calcote, L. R., The Analysis of Laminated Composite Structures, Van Nostrand Reinhold, N. Y., 1969.
4. Jones, R. M., "Mechanics of Composite Materials," McGraw Hill, N. Y., 1975.
5. Lekhnitskii, G. S., Theory of Elasticity of an Anisotropic Elastic Body, Holden-Day, San Francisco, 1963.
6. Advanced Composites Design Guides, Vol's I-V, 3rd Edition, 1973.
7. Durchlaub, E. C., Freeman, R. B., "Design Data for Composite Structure Safelife Prediction," Boeing Vertol Co. Report, D210-10671-2, Vol. II, (AFML-TR-73-225), August 1973.
8. Hofer, K. E., et al., "Development of Engineering Data on the Mechanical and Physical Properties of Advanced Composite Materials," AFML-TR-72-205, Part 1, Sept. 1972.
9. Mullin, J. V., Mazzio, V. F., and Mehan, R. L., "Basic Failure Mechanisms in Advanced Composites," NASA CR-121000, 2420-N03, 1972.
10. McLaughlin, P. V., Jr., and Rosen, B. W., "Combined Stress Effects Upon Failure of Fiber Composites," Materials Science Corporation, TFR/7404/1112, April 1974.
11. Whiteside, J. B., Daniel, I. M. and Rowlands, R. E., "The Behavior of Advanced Filamentary Composite Plates with Cutouts," AFFDL-TR-73-48, June 1973.
12. McGary, F. J., Fracture of Graphite Fiber Reinforced Composites, AFML-TR-74-167, 1974.
13. Daniel, I. M., and Liber, T., "Lamination Residual Stresses in Fiber Composites," NASA CR-134 826, IITRI D 6073-I, March 1975.
14. Sandhu, R. S., "A Survey of Failure Theories of Isotropic and Anisotropic Materials," AFFDL-TR-72-71, Jan. 1972.
15. Sandhu, R. S., "Ultimate Strength Analysis of Symmetric Laminates," AFFDL-TR-73-137, Feb. 1974.

16. Sandhu, R. S., et al., "Laminate Tubular Specimens Subjected to Biaxial Stress States (Graphite/Epoxy), AFFDL-TR-73-7, Vol. II, March 1975.
17. Sih, G. C., "Handbook of Stress Intensity Factors," Institute of Fracture and Solid Mechanics, Lehigh University, Bethlehem, Pa., 1973.
18. Sih, G. C. and Paris, P. C., "Stress Analysis of Cracks," Fracture Toughness Testing and Its Applications, ASTM STP 381, April 1965, pp. 30-81.
19. Waddoups, M. E., Eisenmann, and Kaminski, "Macroscopic Fracture Mechanics of Advanced Composite Materials," Vol. 5, Oct. 1971, p. 446.
20. Cruse, T. A., "Tensile Strength of Notched Composites," J. Comp. Mat'ls., Vol. 7, April 1973, p. 218.
21. Whitney, J. M. and Nuismer, R. J., "Stress Fracture Criteria for Laminated Composites Containing Stress Concentrations," Journal of Composite Materials, Vol. 8, July 1974, pp. 253-265. See also "Uni-axial Failure of Composite Laminates Containing Stress Concentrations," ASTM Composite Materials Conference, Gaithersburg, Maryland, September 1974.
22. Wu, E. M., "Optimal Experimental Measurements of Anisotropic Failure Tensors," J. Comp. Mat'ls., Vol. 6, Oct. 1972, p. 472.
23. Wu, E. M., "Strength and Fracture of Composites," Composite Materials, Broutman, L. J. and Krock, R. H., Ed's., Vol. 5, Fracture and Fatigue, Broutman, L. J., Ed., Academic Press, N. Y., 1974.
24. Sih, G. C. and Chen, E. P., "Fracture Analysis of Unidirectional Composites," J. Comp. Mat'ls., Vol. 7, April 1973, p. 230.
25. Sih, G. C. and Chen, E. P., "Fracture Analysis of Unidirectional and Angle Ply Composites," NADC-TR-73-1, Lehigh University, Jan. 1973.
26. Kulkarni, S. V. and Rosen, B. W., "Design Data for Composite Structure Safelife Prediction: Analysis Evaluation," Materials Science Corporation TFR/2221, August 1973.
27. Williams, D. P. and Ramani, R., Private Communication, June, 1975.
28. Paris, P. C. and Sih, G. C., "Stress Analysis for Cracks," Fracture Toughness Testing and Its Application, STP-381, ASTM, Balt., Md., April 1955.
29. Griffith, A. A., "The Phenomena of Rupture and Flow of Solids," Philosophical Transactions of the Royal Society, Vol. 221A (1920).
30. Friend, C. A., Clyne, R. W. and Valentine, G. G., "Machining Graphite Composite Materials," Hercules, Inc., Magna, Utah.

31. Halpin, J. C., et al., "Characterization of Composites for the Purpose of Reliability Evaluation," Analysis of Test Methods for High Modulus Fibers and Composites, ASTM STP 521, ASTM, 1973.
32. Rowlands, R. E., et al., "Stress Analysis and Failure Analysis of a Glass-Epoxy Composite Plate with a Hole," presented at SESA Fall Meeting, Milwaukee, Wisconsin, Oct. 1971, SESA paper No. 1942.
33. Viswanathan, C. N., Davis, J. G., and Herakovich, C. T., "Tensile and Compressive Behavior of Borsic/Aluminum Composite Laminates," VPI-E-75-12, June 1975.

Head Rate	Strain Rate	Test No.	Modulus E _x	Poisson's Ratio	Yield Stress	Yield Strain	Fracture Stress	Fracture Strain
\dot{H} , in/min	$\dot{\epsilon}$, min ⁻¹		10 ⁶ psi	ν_{xy}	σ_Y^d , ksi	ϵ_Y , %	σ_f , ksi	ϵ_f , %
0.002	2.4X10 ⁻⁴	1 ^a	18.2	0.31	114.0	0.56	156.1	0.81
		2 ^a	18.7	0.32	125.0	0.62	146.9	0.79
		3	17.7	0.26	117.0	0.62	161.0	0.86
		av.	18.2	0.30	118.7	0.60	154.7	0.82
0.02	2.9X10 ⁻³	1 ^a	18.4	0.33	99.7	0.53	162.1	0.86
		2	17.2	0.31	94.3	0.54	136.5	0.77
		3	-	-	-	-	-	-
		av.	18.2	0.32	97.0	0.54	149.3	0.82
0.2	2.7X10 ⁻²	1	15.0	0.33	80.0	0.48	181.2	0.96
		2	18.4	0.41	87.5	0.44	124.3	0.69
		3	18.0	0.31	108.0	0.60	171.0	0.93
		av.	17.1	0.35	91.8	0.51	158.8	0.85
2.0	2.7X10 ⁻¹	1	18.7	0.33	33.0	0.23	138.0	0.75
		2 ^a	17.7	0.34	56.0	0.31	125.9	0.79
		3 ^a	17.4	0.28	64.0	0.36	180.7	0.95
		av.	17.9	0.32	51.0	0.30	148.2	0.83
Average for all tests			17.8	0.32	89.0	0.48	153.1	0.83

Remarks:

- a. Grip Failures
- b. Thickness variation, 0.070-0.087
- c. T = 70°F, R.H. = 45%
- d. Point of intersection of bilinear
 σ - ϵ curve.

Table 1. Hercules AS-3501 Graphite/Epoxy [0]₈₅ Tensile Properties.

Head Rate \dot{H} , in/min	Strain Rate $\dot{\epsilon}$, min ⁻¹	Test No.	Modulus E ₄₅ 10 ⁶ psi	Poisson's Ratio ν_{45°	Yield Stress σ_Y^d , ksi	Yield Strain ϵ_Y , %	Fracture Stress σ_f , ksi	Fracture Strain ϵ_f , %
0.002	2.9X10 ⁻⁴	1 ^a	2.5	0.33	6.2	0.24	15.4	0.74
		2	2.1	0.24	8.7	0.43	15.5	0.84
		3	2.2	0.40	9.0	0.41	15.8	0.92
		av.	2.3	0.32	8.0	0.36	15.6	0.83
0.02	2.8X10 ⁻³	1 ^a	2.4	0.22	9.9	0.44	15.8	0.85
		2	2.4	0.25	9.3	0.39	14.9	0.68
		3	2.5	0.21	8.1	0.33	16.0	0.80
		av.	2.4	0.23	9.1	0.39	15.6	0.78
0.2	2.7X10 ⁻²	1	2.0	0.36	9.0	0.45	15.6	0.95
		2	2.3	0.22	8.6	0.39	15.6	0.88
		3	2.2	0.33	9.9	0.46	17.6	0.91
		av.	2.2	0.30	9.2	0.43	16.3	0.91
2.0	2.8X10 ⁻¹	1	-	-	-	-	-	-
		2	1.8	0.27	10.0	0.35	13.7	0.84
		3	2.2	0.23	7.8	0.53	14.5	0.68
		av.	2.0	0.25	8.9	0.44	14.1	0.76
Average for all tests			2.2	0.28	8.8	0.40	15.5	0.90

Remarks:

- Grip Failure
- Thickness Variation, 0.070-0.076
- T = 70°F, R.H. = 47%
- Point of intersection of bilinear
 σ - ϵ curve.

Table 2. Hercules AS-3501 Graphite/Epoxy [45]_{8S} Tensile Properties.

Head Rate	Strain Rate	Test No.	Modulus E _y	Poisson's Ratio	Yield Stress	Yield Strain	Fracture Stress	Fracture Strain
\dot{H} , in/min	$\dot{\epsilon}$, min ⁻¹		10 ⁶ psi	ν_{yx}	σ_Y^d , ksi	ϵ_Y , %	σ_f , ksi	ϵ_f , %
0.002	2.9X10 ⁻⁴	1 ^a	1.4	0.017	3.5	0.24	6.7	0.50
		2	1.7	0.010	3.5	0.25	5.1	0.40
		3	2.0	0.020	3.5	0.18	6.6	0.42
		av.	1.7	0.016	3.5	0.22	6.1	0.44
0.02	3.1X10 ⁻³	1	-	-	-	-	-	-
		2	2.0	0.021	4.1	0.23	7.0	0.42
		3	2.0	0.018	3.3	0.16	6.9	0.41
		av.	2.0	0.020	3.7	0.20	7.0	0.42
0.2	2.7X10 ⁻²	1 ^a	1.8	0.014	4.2	0.23	8.2	0.48
		2	2.3	0.027	4.5	0.22	7.5	0.42
		3	2.0	0.019	4.0	0.21	7.2	0.43
		av.	2.1	0.020	4.2	0.22	7.6	0.44
2.0	2.7X10 ⁻¹	1	1.5	0.020	4.0	0.26	5.8	0.37
		2 ^a	2.2	0.019	4.6	0.21	9.6	0.49
		3	-	-	-	-	-	-
		av.	1.9	0.020	4.3	0.24	7.7	0.43
Average for all tests			1.9	0.019	3.9	0.22	7.1	0.43

Remarks:

- a. Grip Failure
- b. Thickness Variation, 0.050-0.085
- c. T = 70°F, R.H. = 40%
- d. Point of intersection of bilinear
 σ - ϵ curve.

Table 3. Hercules AS-3501 Graphite/Epoxy [90]_{8S} Tensile Properties.

Head Rate	Strain Rate	Test No.	Modulus E _x	Poisson's Ratio	Yield Stress	Yield Strain	Fracture Stress	Fracture Strain
\dot{H} , in/min	$\dot{\epsilon}$, min ⁻¹		10 ⁶ psi	ν_{xy}	σ_Y^d , ksi	ϵ_Y , %	σ_f , ksi	ϵ_f , %
0.002	1.9X10 ⁻⁴	1	12.8	0.89	82.5	0.64	130.7	1.00
		2 ^a	13.2	1.01	77.5	0.58	125.8	0.93
		3	11.9	0.92	70.0	0.58	128.6	1.04
		av.	12.6	0.94	76.7	0.60	128.3	0.99
0.02	1.9X10 ⁻³	1	12.7	0.93	-	-	135.1	1.06
		2 ^a	13.0	1.03	58.8	0.45	121.3	0.91
		3 ^a	11.9	0.97	81.3	0.68	110.6	0.94
		av.	12.5	0.98	70.1	0.57	122.3	0.97
0.2	1.9X10 ⁻²	1	12.2	0.89	72.5	0.60	118.3	0.96
		2 ^a	12.8	0.91	63.8	0.50	129.0	1.00
		3	13.4	0.94	82.3	0.61	151.1	1.10
		av.	12.8	0.91	72.9	0.57	132.8	1.02
2.0	2.6X10 ⁻¹	1 ^a	13.1	0.95	51.3	0.40	128.4	1.03
		2	13.8	0.81	50.6	0.36	122.7	1.00
		3 ^a	12.9	0.85	63.6	0.51	126.5	1.00
		av.	13.3	0.87	55.2	0.42	125.9	1.01
Average for all tests			12.8	0.93	68.6	0.54	127.3	1.00

Remarks:

- a. Grip Failure
- b. Thickness Variation, 0.074-0.085
- c. T = 65°F, R.H. = 56%
- d. Point of intersection of bilinear
 σ - ϵ curve.

Table 4. Hercules AS-3501 Graphite/Epoxy [0/±30/0]_{2S} Tensile Properties.

Head Rate	Strain Rate	Test No.	Modulus E ₄₅	Poisson's Ratio	Yield Stress	Yield Strain	Fracture Stress	Fracture Strain
\dot{H} , in/min	$\dot{\epsilon}$, min ⁻¹		10 ⁶ psi	ν_{45}°	σ_Y^d , ksi	ϵ_Y , %	σ_f , ksi	ϵ_f , %
0.002	2.6X10 ⁻⁴	1	3.7	-0.038	19.0	0.500	25.1	0.70
		2	3.8	-0.048	18.8	0.480	27.4	0.75
		3	3.9	-0.050	17.6	0.460	25.8	0.69
		av.	3.8	-0.045	18.4	0.480	26.1	0.71
0.02	2.8X10 ⁻³	1	4.2	-0.080	13.8	0.450	25.5	0.66
		2 ^a	4.2	-0.007	17.4	0.430	25.5	0.67
		3	-	-	-	-	-	-
		av.	4.2	-0.044	15.6	0.413	25.5	0.67
0.2	2.7X10 ⁻²	1 ^a	5.0	-	16.9	0.360	28.3	0.67
		2	3.7	-0.017	15.8	0.435	24.5	0.71
		3	4.2	-0.039	15.4	0.395	26.7	0.75
		av.	4.3	-0.027	16.0	0.397	26.5	0.71
2.0	2.7X10 ⁻¹	1	3.4	-0.060	17.0	0.485	25.4	0.71
		2	4.1	-0.074	16.5	0.425	27.8	0.68
		3	4.2	-0.043	17.5	0.410	28.9	0.71
		av.	3.9	-0.059	17.0	0.440	27.4	0.70
Average for all tests			4.0	-0.044	16.9	0.434	26.45	0.70

Remarks:

- Grip Failures [Adjacent to Grip only].
- Thickness Variation, 0.072-0.085
- T = 75°F, R.H. = 48%
- Point of intersection of bilinear σ - ϵ curve.
- Audible noise at 0.6 σ_f , first failure or inner ply.

Table 5. Hercules AS-3501 Graphite/Epoxy [45/15/75/45]_{2S} Tensile Properties.

	Head Rate \dot{H} , in/min	Strain Rate $\dot{\epsilon}$, min ⁻¹	Test No.	Modulus E_y 10 ⁶ psi	Poisson's Ratio ν_{yx}	Yield Stress σ_y^d , ksi	Yield Strain ϵ_y , %	Fracture Stress σ_f , ksi	Fracture Strain ϵ_f , %
			1	3.8	0.14	6.8	0.29	14.3	0.73
	0.002	2.7X10 ⁻⁴	2	3.1	0.16	8.3	0.38	13.5	0.88
			3	2.2	0.12	7.5	0.37	13.6	0.78
			av.	3.0	0.14	7.5	0.35	13.8	0.80
			1	2.3	0.14	5.8	0.26	13.1	0.78
	0.02	2.7X10 ⁻³	2	2.0	0.13	7.6	0.39	12.4	0.73
			3	2.0	0.12	9.3	0.49	13.2	0.81
			av.	2.1	0.13	7.6	0.38	12.9	0.77
			1	1.6	0.12	8.1	0.50	12.4	0.82
	0.2	2.9X10 ⁻²	2	2.0	0.14	6.5	0.29	13.9	0.70
			3	1.8	0.13	7.9	0.42	12.6	0.69
			av.	1.8	0.13	7.5	0.40	13.0	0.74
			1 ^a	1.4	0.12	8.3	0.48	12.7	0.85
	2.0	3.1X10 ⁻¹	2	1.9	0.11	7.9	0.45	10.6	0.56
			3	1.7	0.10	7.9	0.40	11.1	0.63
			av.	1.7	0.11	8.0	0.44	11.5	0.68
Average for all tests				2.2	0.13	7.6	0.40	12.8	0.75

Remarks:

- Grip Failure
- Thickness Variation, 0.072-0.080
- T = 78°F, R.H. = 30%
- Point of intersection of bilinear σ - ϵ curve.
- Audible noise @ 0.5 σ_f in all cases.
- Complete fracture of inner plies appeared to occur prior to gross fracture.

Table 6. Hercules AS-3501 Graphite/Epoxy [90°/±60°/90°]_{2S} Tensile Properties.

Specimen No.	Fiber Direction	Thickness Variation X10 ⁻³ in.	Net Section Av. Thickness X10 ⁻³ in.	Crack Tip Thick X10 ⁻³ in.	Crack Length in. (a)	Specimen Width in. (w)	Fracture Angle	Fracture Load (lb)	$\frac{a}{w}$	Gross Stress ksi	Net Stress ksi
I-1	[0°] _{8S}	77-84	81	84	0.199	0.983	0°	2600	0.20	32.9	41.2
I-2	"	79-83	81	83	0.299	0.984	0°	2390	0.30	30.0	43.1
I-3	"	77-81	79	80	0.396	0.986	0°	2690	0.40	34.6	57.8
I-4	"	77-78	78	75	0.500	0.986	0°	2100	0.51	27.5	55.7
I-5	"	73-77	75	--	0.601	0.984	0°	2410	0.61	32.7	83.9
I-6	"	76-78	77	79	0.697	0.980	0°	810	0.71	10.7	37.2
II-1	[45°] _{8S}	79-81	80	79	0.196	0.983	45°	148	0.20	1.9	2.4
II-2	"	72-79	76	79	0.297	0.983	"	105	0.30	1.4	2.0
II-3	"	84-86	85	84	0.399	0.984	"	88	0.41	1.1	1.8
II-4	"	80-82	81	82	0.496	0.982	47°	79	0.51	1.0	2.0
II-5	"	79-82	80	80	0.599	0.982	45°	35	0.61	0.4	1.1
II-6	"	80-83	82	83	0.701	0.983	47°	48	0.71	0.6	2.1
III-1	[90°] _{8S}	81-84	82	83	0.199	0.984	90°	121	0.20	1.5	1.9
III-2	"	82-84	83	82	0.301	0.988	"	66	0.31	0.8	1.2
III-3	"	84-87	85	86	0.399	0.987	"	50	0.40	0.6	1.0
III-4	"	82-83	83	83	0.502	0.986	"	37	0.51	0.5	0.9
III-5	"	81-82	82	81	0.601	0.984	"	20	0.61	0.2	0.6
III-6	"	--	--	--	0.705	--	--	--	--	--	--

Table 7. Single Edge Notch (SEN) Data for Hercules Graphite/Epoxy Unidirectional Laminates.

Specimen No.	Fiber Directions	Thickness Variation X10 ⁻³ in.	Net Section Av. Thickness X10 ⁻³ in.	Crack Tip Thick X10 ⁻³ in.	Crack Length in.(a)	Specimen Width in.(w)	Fracture Angle	Fracture Load (lb)	$\frac{a}{w}$	Gross Stress ksi	Net Stress ksi
IV-1	[90/±60/90] _{2S}	77-80	79	80	0.201	0.985	86°	600	0.21	7.8	9.8
IV-2	"	81-83	82	81	0.295	0.980	88°	446	0.30	5.6	8.0
IV-3	"	75-81	78	78	0.392	0.980	89°	295	0.40	3.9	6.4
IV-4	"	78-80	79	79	0.492	0.981	89°	230	0.50	3.0	6.0
IV-5	"	72-74	73	74	0.602	0.987	89°	125	0.61	1.7	4.5
IV-6	"	71-78	74	77	0.700	0.984	--	150	0.71	2.1	7.1
V-1	[45/15/75/45] _{2S}	72-80	76	79	0.201	0.989	48°	960	0.20	12.8	16.1
V-2	"	80-84	82	84	0.300	0.987	48°	650	0.30	8.1	11.6
V-3	"	79-81	80	81	0.396	0.984	50°	465	0.40	5.9	9.9
V-4	"	75-79	77	76	0.499	0.989	47°	345	0.51	4.5	9.2
V-5	"	75-78	77	78	0.599	0.982	50°	265	0.61	3.5	9.1
V-6	"	72-73	72	72	0.700	0.982	47°	178	0.71	2.5	8.7
VI-1	[0/±30/0] _{2S}	73-78	76	80	0.199	0.989	83°	2375	0.20	31.8	39.9
VI-2	"	71-81	76	81	0.298	0.989	29°	2080	0.30	27.9	39.9
VI-3	"	79-81	80	79	0.398	0.982	84°	1500	0.41	19.1	32.1
VI-4	"	80-88	74	76	0.498	0.986	70°	770	0.51	10.6	21.3
VI-5	"	72-81	77	80	0.599	0.984	69°	878	0.61	11.7	29.8
VI-6	"	74-82	78	76	0.704	0.986	72°	497	0.71	6.5	22.6

Table 8. Single Edge Notch (SEN) Data for Hercules Graphite/Epoxy Multi-directional Laminates.

Specimen No.	Fiber Direction	Thickness Variation X10 ⁻³ in.	Net Section Av. Thickness X10 ⁻³ in.	Crack Tip Thick X10 ⁻³ in.	Crack Length in. (a)	Specimen Width in. (w)	Angle of Inclined Notch	Fracture Load (lb)	$\frac{a}{w}$	Gross Stress ksi	Net Stress ksi
I-7	[0°] _{8S}	71-79	75	79	0.500	0.984	85°	1275	0.51	17.29	34.57
I-8	"	67-71	69	70	0.503	0.984	80°	1910	0.51	28.13	56.26
I-9	"	77-80	79	80	0.514	0.984	75°	2180	0.52	28.22	56.44
I-10	"	77-80	79	80	0.560	0.983	60°	1545	0.57	20.02	40.04
I-11	"	77-79	78	79	0.680	0.983	45°	1770	0.69	23.08	46.17
I-12	"	76-78	77	78	0.745	0.985	40°	1780	0.76	23.66	47.12
II-7	[45°] _{8S}	74-77	76	75	0.500	0.989	85°	50	0.51	0.67	0.87
II-8	"	79-83	81	83	0.502	0.984	80°	41	0.51	0.52	1.03
II-9	"	68-72	70	72	0.513	0.983	75°	45	0.52	0.65	1.31
II-10	"	77-79	78	79	0.560	0.987	60°	64	0.57	0.83	1.66
II-11	"	67-70	69	70	0.681	0.989	45°	69	0.69	1.02	2.04
II-12	"	79-84	82	84	0.763	0.991	40°	75	0.77	0.93	1.86
III-7	[90°] _{8S}	81-83	82	83	0.498	0.988	85°	50	0.5	0.61	1.22
III-8	"	81-83	82	81	0.504	0.983	80°	42	0.51	0.52	1.03
III-9	"	83-84	83	83	0.512	0.984	75°	41	0.52	0.50	0.99
III-10	"	81-83	82	83	0.565	0.988	60°	52	0.57	0.64	1.28
III-11	"	82-84	83	84	0.672	0.988	45°	46	0.68	0.58	1.16
III-12	"	81-83	82	81	0.752	0.985	40°	39	0.76	0.48	0.97

Table 9. Inclined Single Edge Notch (ISEN) Data for Hercules Graphite/Epoxy Unidirectional Laminates.

Specimen No.	Fiber Directions	Thickness Variation X10 ⁻³ in.	Net Section Av. Thickness X10 ⁻³ in.	Crack Tip Thick X10 ⁻³ in.	Crack Length in.(a)	Specimen Width in.(w)	Angle of Inclined Notch	Fracture Load (lb)	$\frac{a}{w}$	Gross Stress ksi	Net Stress ksi
IV-7	[0/±30/0] _{2S}	81-83	82	81	0.500	0.983	85°	900	0.51	11.2	22.3
IV-8	"	79-81	80	81	0.496	0.983	80°	1270	0.51	16.2	32.4
IV-9	"	79-83	81	83	0.506	0.986	75°	1222	0.51	15.3	30.6
IV-10	"	71-74	73	73	0.556	0.984	60°	1020	0.57	14.3	28.6
IV-11	"	80-83	82	80	0.675	0.984	45°	1065	0.69	13.3	26.6
IV-12	"	75-78	77	76	0.766	0.982	40°	945	0.78	12.6	25.2
V-7	[45/15/75/45] _{2S}	79-83	81	79	0.497	0.982	85°	420	0.51	5.3	10.6
V-8	"	79-84	82	83	0.503	0.985	80°	487	0.51	6.1	12.1
V-9	"	75-79	77	79	0.510	0.984	75°	429	0.52	5.7	11.3
V-10	"	76-78	77	76	0.559	0.985	60°	440	0.57	5.8	11.6
V-11	"	75-79	77	79	0.693	0.986	45°	434	0.70	5.7	11.4
V-12	"	79-80	80	80	0.762	0.981	40°	405	0.78	5.2	10.4
VI-7	[90/±60/90] _{2S}	78-79	79	78	0.492	0.980	85°	287	0.50	3.7	7.5
VI-8	"	78-80	79	78	0.506	0.983	80°	283	0.52	3.7	7.3
VI-9	"	75-77	76	77	0.517	0.986	75°	283	0.53	3.8	7.5
VI-10	"	77-82	80	80	0.561	0.986	60°	282	0.57	3.6	7.2
VI-11	"	73-81	77	74	0.701	0.985	45°	227	0.71	3.0	6.0
VI-12	"	81-83	80	81	0.775	0.988	40°	307	0.79	3.9	7.8

Table 10. Inclined Single Edge Notch (ISEN) Data for Hercules Graphite/Epoxy Multi-directional Laminates.

Specimen No.	Fiber Direction	Thickness Variation $\times 10^{-3}$ in.	Net Section Av. Thickness $\times 10^{-3}$ in.	Crack Tip Thick $\times 10^{-3}$ in.		Specimen Width in. (w)	Net Section Width in.	Fracture Load (lb)	$\frac{2a}{w}$	Gross Stress ksi	Net Stress ksi
A-1	$[0^\circ]_{8S}$	75-79	77	78	76	0.983	0.879	5380	0.11	71.1	79.5
A-2	"	83-85	84	83	85	0.984	0.778	5300	0.21	64.3	81.3
A-3	"	78-83	81	83	78	0.984	0.677	3150	0.31	39.8	55.6
A-4	"	77-83	80	78	83	0.982	0.576	2990	0.41	38.2	65.2
A-5	"	80-83	81	83	80	0.983	0.478	2450	0.51	30.7	63.0
A-6	"	67-70	69	70	70	0.984	0.282	1050	0.71	15.6	54.3
B-1	$[45^\circ]_{8S}$	73-76	75	73	76	0.984	0.877	295	0.11	4.0	4.5
B-2	"	71-75	73	75	71	0.982	0.779	205	0.21	2.9	3.6
B-3	"	77-81	79	77	78	0.982	0.680	123	0.31	1.6	2.3
B-4	"	57-69	63	57	68	0.987	0.574	90	0.42	1.5	2.5
B-5	"	61-71	66	61	71	0.988	0.478	92	0.52	1.4	2.9
B-6	"	83-86	85	86	83	0.982	0.282	58	0.71	0.7	2.4
C-1	$[90^\circ]_{8S}$	84-86	85	84	86	0.987	0.879	258	0.11	3.1	3.5
C-2	"	81-83	82	83	81	0.987	0.778	182	0.21	2.3	2.9
C-3	"	81-83	82	82	81	0.983	0.681	143	0.31	1.8	2.6
C-4	"	86-89	88	86	89	0.986	0.583	120	0.41	1.4	2.4
C-5	"	83-84	84	83	84	0.982	0.480	97	0.51	1.2	2.4
C-6	"	--	--	--	--	--	--	--	--	--	--

Table 11. Double Edge Notch (DEN) Data for Hercules Graphite/Epoxy Unidirectional Laminates.

Specimen No.	Fiber Direction	Thickness Variation $\times 10^{-3}$ in.	Net Section Av. Thickness $\times 10^{-3}$ in.	Crack Tip Thick $\times 10^{-3}$ in.		Specimen Width in. (w)	Net Section Width in.	Fracture Load (lb)	$\frac{2a}{w}$	Gross Stress ksi	Net Stress ksi
D-1	[0/ \pm 30/0] _{2S}	80-87	83	80	81	0.983	0.879	4390	0.11	53.6	60.0
D-2	"	77-85	81	79	83	0.982	0.776	3350	0.21	42.1	53.3
D-3	"	74-80	77	79	74	0.983	0.681	2760	0.31	36.5	52.6
D-4	"	71-80	76	80	71	0.986	0.576	2090	0.42	25.5	48.1
D-5	"	74-80	77	74	78	0.984	0.482	2190	0.51	29.0	59.3
D-6	"	79	79	79	79	0.987	0.278	1490	0.72	19.1	68.0
E-1	[45/15/75/45] _{2S}	79-83	81	80	79	0.984	0.877	1900	0.11	23.8	26.8
E-2	"	82-85	84	83	82	0.983	0.777	1380	0.21	16.8	21.3
E-3	"	82-85	84	82	83	0.983	0.681	1255	0.31	15.3	22.1
E-4	"	70-73	72	73	70	0.984	0.580	830	0.41	11.8	20.0
E-5	"	78-81	80	81	79	0.987	0.482	812	0.51	10.4	21.2
E-6	"	76-78	79	78	78	0.982	0.283	520	0.71	6.7	23.3
F-1	[90/ \pm 60/90] _{2S}	71-82	80	80	79	0.982	0.880	867	0.10	11.0	12.3
F-2	"	78-83	81	79	82	0.982	0.781	952	0.21	12.1	15.2
F-3	"	72-76	74	72	75	0.991	0.675	615	0.32	8.4	12.4
F-4	"	82-84	83	83	82	0.984	0.579	770	0.42	9.5	16.1
F-5	"	78-81	80	78	79	0.981	0.482	618	0.51	7.9	16.1
F-6	"	76-79	78	76	78	0.981	0.284	385	0.71	5.1	17.5

Table 12. Double Edge Notch (DEN) Data for Hercules Graphite/Epoxy Multi-directional Laminates.

Specimen No.	Fiber Directions	Thickness Variation X10 ⁻³ in.	Net Section Av. Thickness X10 ⁻³ in.	Hole Dia.	Specimen Width in.	Left Width in.	Side Thick X10 ⁻³ in.	Right Width in.	Side Thick X10 ⁻³ in.	Fracture Load (lb)	$\frac{d}{w}$	Gross Stress ksi	Net Stress ksi
G-1	[0°] _{8S}	81-84	83	0.122	0.984	0.431	83	0.432	83	8340	0.12	102.7	117.3
G-2	"	70-80	75	0.249	0.984	0.361	75	0.371	73	4830	0.25	65.4	87.6
G-3	"	72-80	76	0.491	0.984	0.243	73	0.247	78	2700	0.50	36.1	72.1
G-4	"	84-86	85	0.753	0.985	0.122	85	0.113	85	2000	0.77	23.9	101.6
H-1	[45°] _{8S}	77-80	78	0.123	0.985	0.428	77	0.431	78	650	0.13	8.4	9.6
H-2	"	73-76	75	0.249	0.989	0.370	75	0.365	73	500	0.25	6.8	9.1
H-3	"	78-81	80	0.498	0.981	0.242	78	0.249	79	344	0.51	4.4	9.0
H-4	"	73-78	76	0.751	0.983	0.121	76	0.114	78	133	0.76	1.8	7.6
J-1	[90°] _{8S}	81-83	82	0.122	0.986	0.427	82	0.434	81	408	0.12	5.0	5.8
J-2	"	81-83	82	0.249	0.984	0.366	81	0.369	82	353	0.25	4.4	5.9
J-3	"	81-83	82	0.498	0.983	0.246	82	0.241	81	150	0.51	1.9	3.8
J-4	"	81-84	83	0.752	0.984	0.114	82	0.119	81	85	0.76	1.1	4.4
K-1	[0/±30/0] _{2S}	77-81	79	0.123	0.984	0.431	81	0.426	79	4850	0.13	57.1	71.3
K-2	"	73-81	77	0.249	0.984	0.370	76	0.367	81	3880	0.25	51.2	68.6
K-3	"	79-82	81	0.499	0.984	0.245	79	0.238	81	2340	0.51	29.6	60.0
K-4	"	76-79	78	0.753	0.984	0.113	78	0.120	79	1400	0.77	18.4	78.2

Table 13. Hole Data for Hercules Graphite/Epoxy [0]_{8S} and [0/±30/0]_{2S} Laminates.

Specimen No.	Fiber Directions	Thickness Variation $\times 10^{-3}$ in.	Net Section Av. Thick $\times 10^{-3}$ in.	Hole Dia.	Specimen Width in.	Left Width in.	Side Thick $\times 10^{-3}$ in.	Right Width in.	Side Thick $\times 10^{-3}$ in.	Fracture Load (lb)	$\frac{d}{w}$	Gross Stress ksi	Net Stress ksi
L-1	[45/15/75/45] _{2S}	80-86	83	0.123	0.985	0.427	82	0.431	82	2060	0.13	25.3	28.9
L-2	"	74-79	77	0.249	0.985	0.365	78	0.371	77	1170	0.25	15.5	20.8
L-3	"	77-84	81	0.500	0.984	0.244	81	0.241	77	722	0.51	9.2	18.6
L-4	"	71-76	74	0.753	0.986	0.113	75	0.124	71	320	0.76	4.4	18.7
M-1	[90/ \pm 60/90] _{2S}	70-77	74	0.123	0.990	0.426	70	0.437	70	830	0.12	11.4	13.0
M-2	"	71-76	74	0.249	0.984	0.364	73	0.368	72	650	0.25	9.0	12.0
M-3	"	77-80	78	0.498	0.979	0.240	79	0.240	78	495	0.51	6.5	13.2
M-4	"	76-78	77	0.753	0.989	0.124	78	0.114	77	176	0.761	2.3	9.7

Table 13 (continued). Hole Data for Hercules Graphite/Epoxy [0]_{8S} and [0/ \pm 30/0]_{2S} Laminates.

Material	Lay-up	Theory		Experimental
		Tensile Mod.	Shear Mod.	Tensile Mod.
		$\times 10^6 \text{ psi}$	$\times 10^6 \text{ psi}$	$\times 10^6 \text{ psi}$
Hercules AS Fiber-3501 Resin	0°	17.7	0.8	17.8
	45°	2.2	1.6	2.2
	90°	1.9	0.8	1.9
	$[0/\pm 30/0]_{2S}$	12.8	2.3	12.8
	$[45/15/75/45]_{2S}$	4.7	1.5	4.0
	$[90/\pm 60/90]_{2S}$	2.2	2.3	2.2
AVCO-5505 Boron Comp. Ref. [8].	$[0/45/135/0/90]_S$	16.1	4.0	14.9
NARMCO-5206 Graphite-Epoxy [8].	$[0/45/135/0/90]_S$	12.2	3.0	11.1

Table 14. Comparison of Lamination Theory Predictions of Moduli with Experimental Results.

Head Rate \dot{H} in/in	Experimental				Analytical				
	E_x (10^6 psi)	E_y (10^6 psi)	ν_{xy}	ν_{yx}	$E_x \nu_{yx}$ (psi)	$E_y \nu_{xy}$ (psi)	G_{xy}^* (10^6 psi) Eq. (5)	G_{xy}^{**} (10^6 psi) Eq. (6)	G_{xy}^{***} (10^6 psi) Eq. (4)
0.002	18.2	1.70	0.30	0.016	.291	.510	1.48	2.54	.886
0.02	18.2	2.03	0.32	0.020	.364	.650	1.71	2.75	.868
0.2	17.1	2.05	0.35	0.020	.342	.718	1.70	2.64	.765
2.0	17.9	1.86	0.32	0.020	.358	.595	1.59	2.62	.693
Avg.	17.8	1.91	0.32	0.019	.339	.618	1.62	2.64	.803

Table 15. Comparison of Orthotropic Equalities and Transformations
for Hercules Graphite/Epoxy $[0]_{8S}$.

Head Rate H in/in	Experimental				Analytical				
	E_x (10^6 psi)	E_y (10^6 psi)	ν_{xy}	ν_{yx}	$E_x \nu_{yx}$ (psi)	$E_y \nu_{xy}$ (psi)	G_{xy}^* (10^6 psi) Eq. (5)	G_{xy}^{**} (10^6 psi) Eq. (6)	G_{xy}^{***} (10^6 psi) Eq. (4)
0.002	12.6	3.01	0.94	0.141	1.78	2.83	1.79	2.11	1.25
0.02	12.5	2.08	0.98	0.130	1.63	2.04	1.39	1.82	1.83
0.2	12.8	1.83	0.91	0.133	1.70	1.66	1.30	1.80	2.20
2.0	13.3	1.67	0.87	0.112	1.49	1.45	1.24	1.80	2.07
Avg.	12.8	2.15	0.93	0.129	1.65	1.99	1.43	1.88	1.84

Table 16. Comparison of Orthotropic Equalities and Transformations
for Hercules Graphite/Epoxy $[0/\pm 30/0]_{2S}$.

Ref.	Material & Layup	Experimental				Analytical				
		E_x (10^6 psi)	E_y (10^6 psi)	ν_{xy}	ν_{yx}	G_{xy} (10^6 psi)	$E_x \nu_{yx}$ (psi)	$E_y \nu_{xy}$ (psi)	G_{xy}^* (10^6 psi) Eq. (5)	G_{xy}^{**} (10^6 psi) Eq. (6)
8	Graphite/Epoxy [0] ₆	22.5	1.3	.30	.05	0.72	1.13	.38	1.17	2.50
29	Glass/Epoxy Single ply?	5.6	1.2	.26	-	0.60	-	-	0.82	1.01
29	Graphite/Epoxy Single ply?	21.0	1.7	.28	-	0.65	-	-	1.50	2.77
29	Boron/Epoxy Single ply?	30.0	2.7	.21	-	0.65	-	-	2.39	4.23
29	Boron/Aluminum Single ply?	33.0	21.0	.23	-	7.00	-	-	10.80	11.12
30	Glass/Epoxy [0/±45/0/90] _S	3.8	2.8	.36	.27	1.29	1.01	1.02	1.23	1.24
13	Boron/AVCO 5505 [0]	29.2	3.2	.17	.02	0.78	.58	.54	2.75	4.54
13	Boron/WRD 9371 [0]	32.1	2.1	.16	.02	1.11	.64	.34	1.93	3.90
13	Modmor I/ERLA 4289, [0]	27.3	0.6	.20	.04	0.70	1.09	.12	0.58	1.96
13	Modmor/ERLA 4617, [0]	27.5	1.0	.10	-	0.90	-	-	0.99	2.61
13	Modmor/WRD 9371, [0]	31.3	0.7	.25	.02	0.65	.63	.18	0.70	2.29
13	Scotch ply 1009- 26-5901, [0]	8.8	3.6	.23	.09	1.74	.79	.83	2.25	2.45
31	Borsic/Aluminum [0] ₈	33.7	14.3	.23	.11	-	3.71	3.29	8.83	9.55

Table 17. Comparison of Orthotropic Equalities and Transformations
for Various Laminates.

Lay-up	Experimental (lbs)	TSAI & AZZI-Hill (lbs)	ASHKENAZI (lbs)	Modified TSAI & AZZI-Hill (lbs)
45°	574	564	574	564
[0/±30/0] _{2S}	5093	3062	3064	3062
[45/15/75/45] _{2S}	1058	400	930	854
[90/±60/90] _{2S}	511	203	344	343

Table 18. Comparison of Experimental and Predicted Failure Loads Using Lamination Theory with Various Failure Theories (Hercules Graphite/Epoxy Laminates).

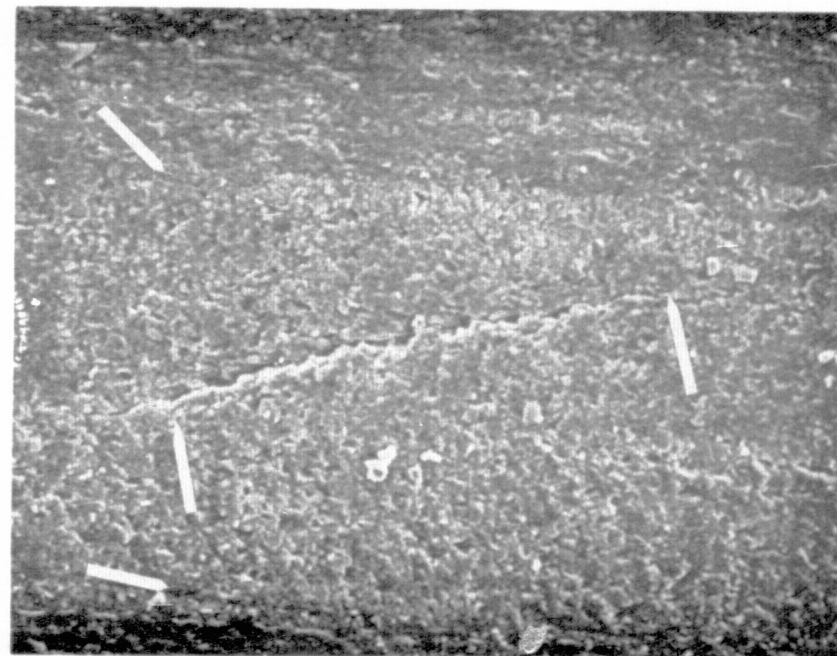
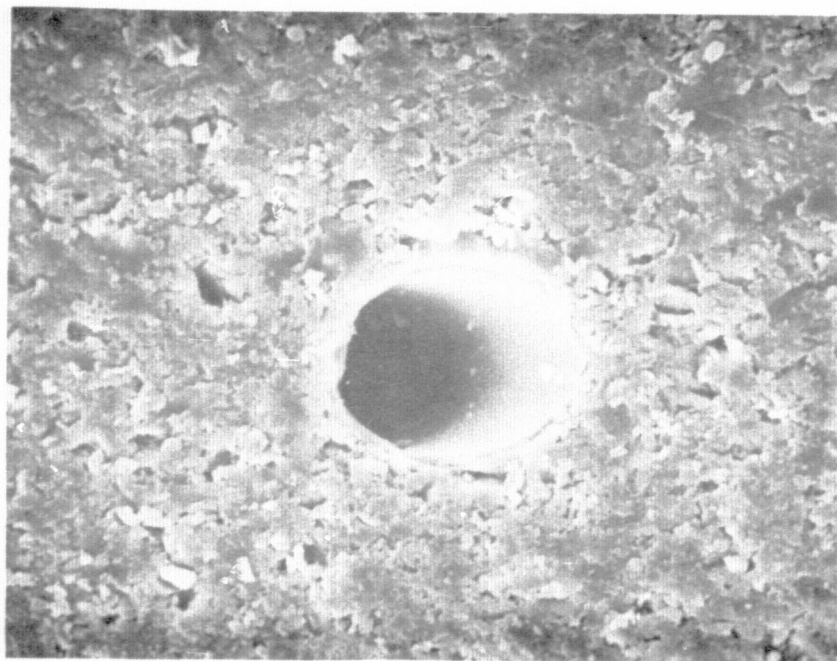


Figure 1. Inherent Flaws in Graphite Epoxy Laminates.

a) Left; $[0]_{8S}$ material--diamond machined surface at $\sim 45^\circ$ to fibers, 950X.

b) Right; $[0/\pm 30/0]_{2S}$ material--ultrasonically machined surface at $\sim 90^\circ$ to 0° fibers, 200X.
(Arrows denote flaw tips and laminae interfaces.)

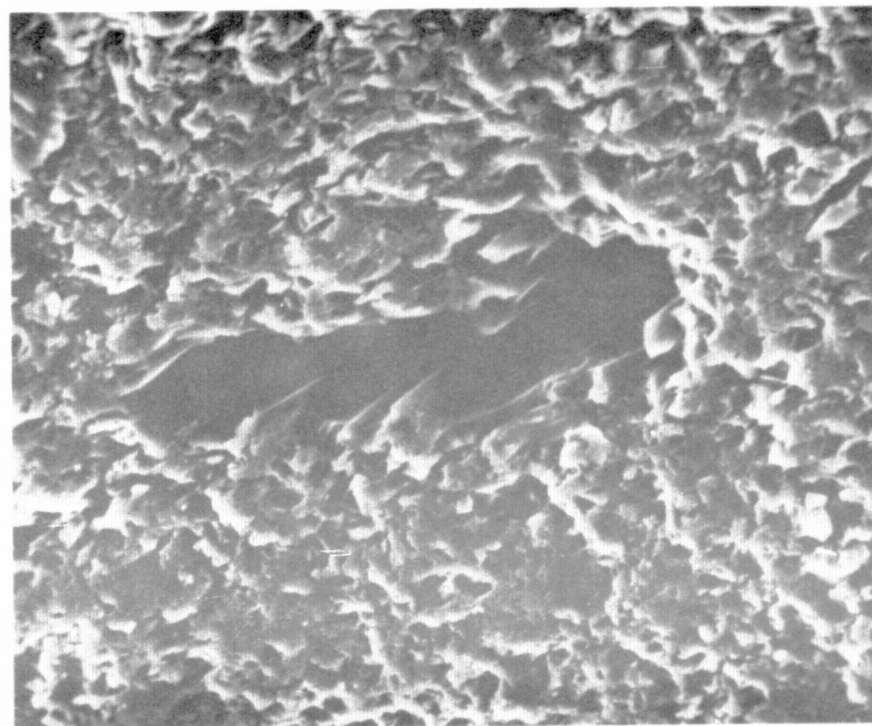
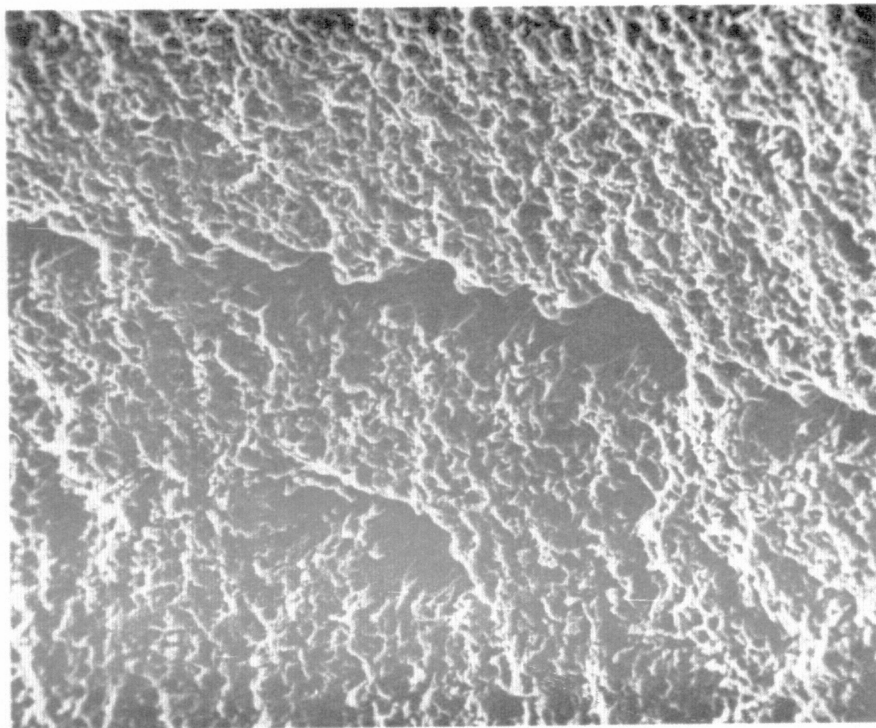


Figure 2. Inherent Flaws in $[0]_{8S}$ Graphite/Epoxy Laminates.
a) Left; 300X b) Right; 600X

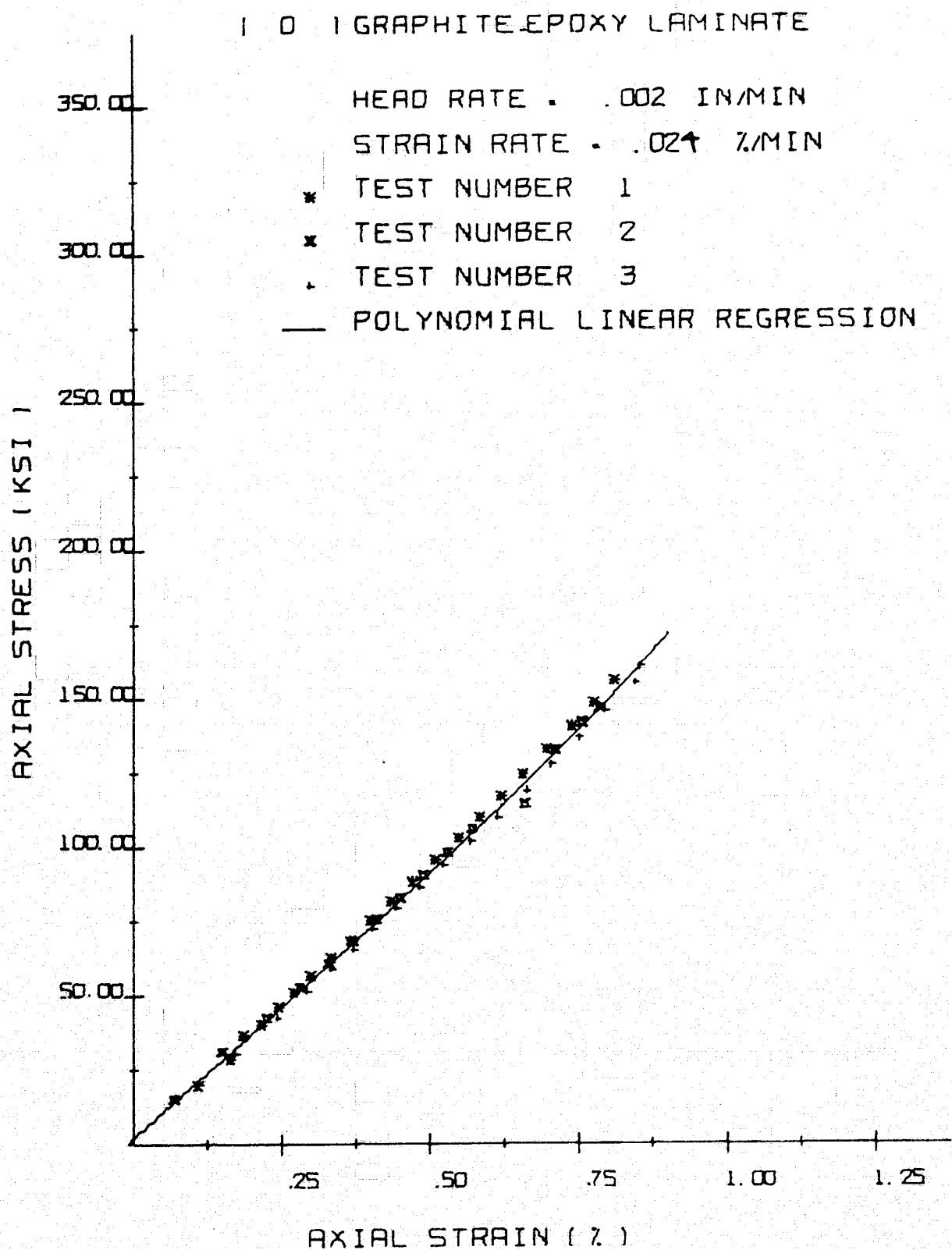


Figure 3. Typical $[0]_{85}$ Stress - Strain Data.

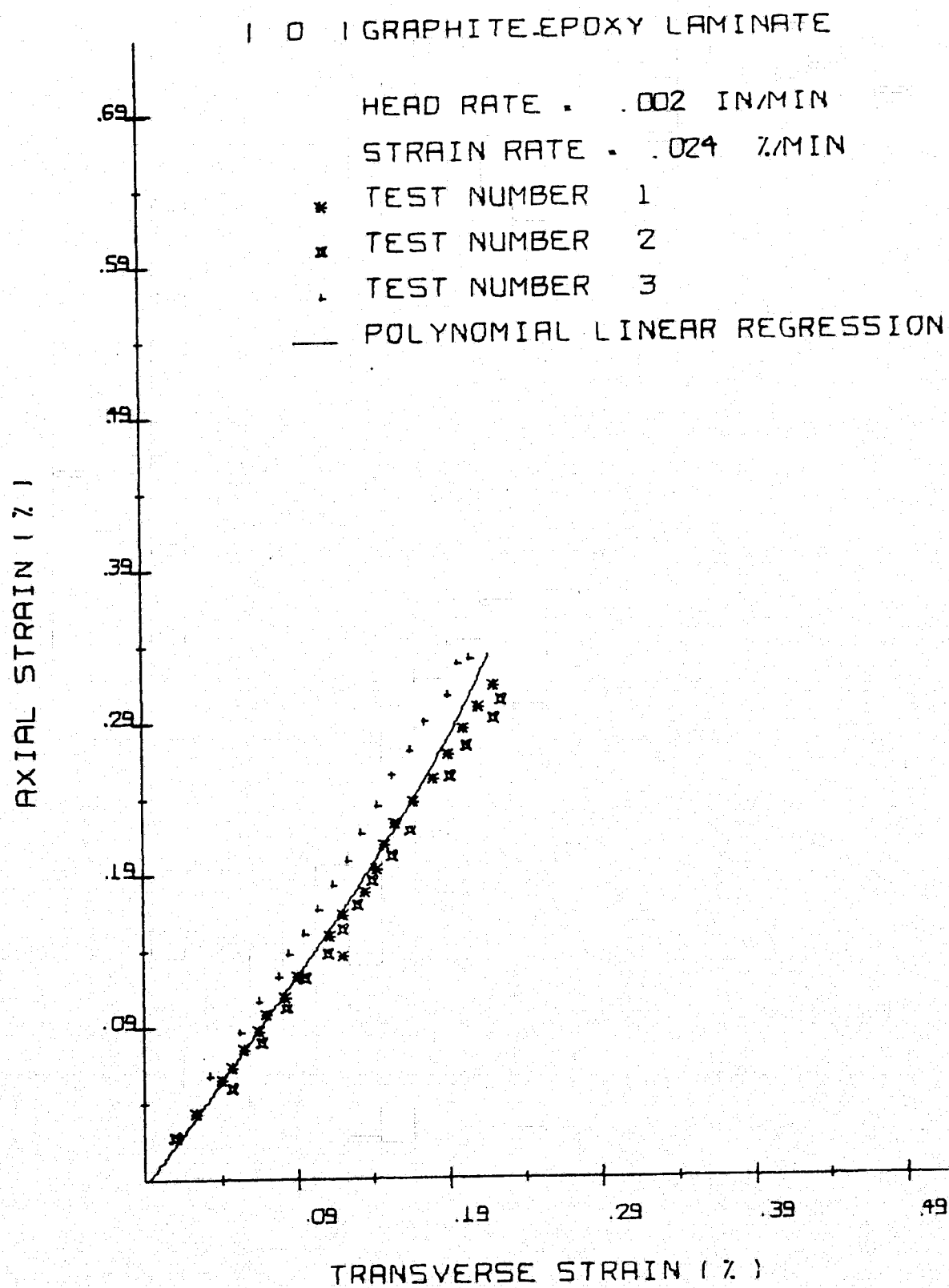
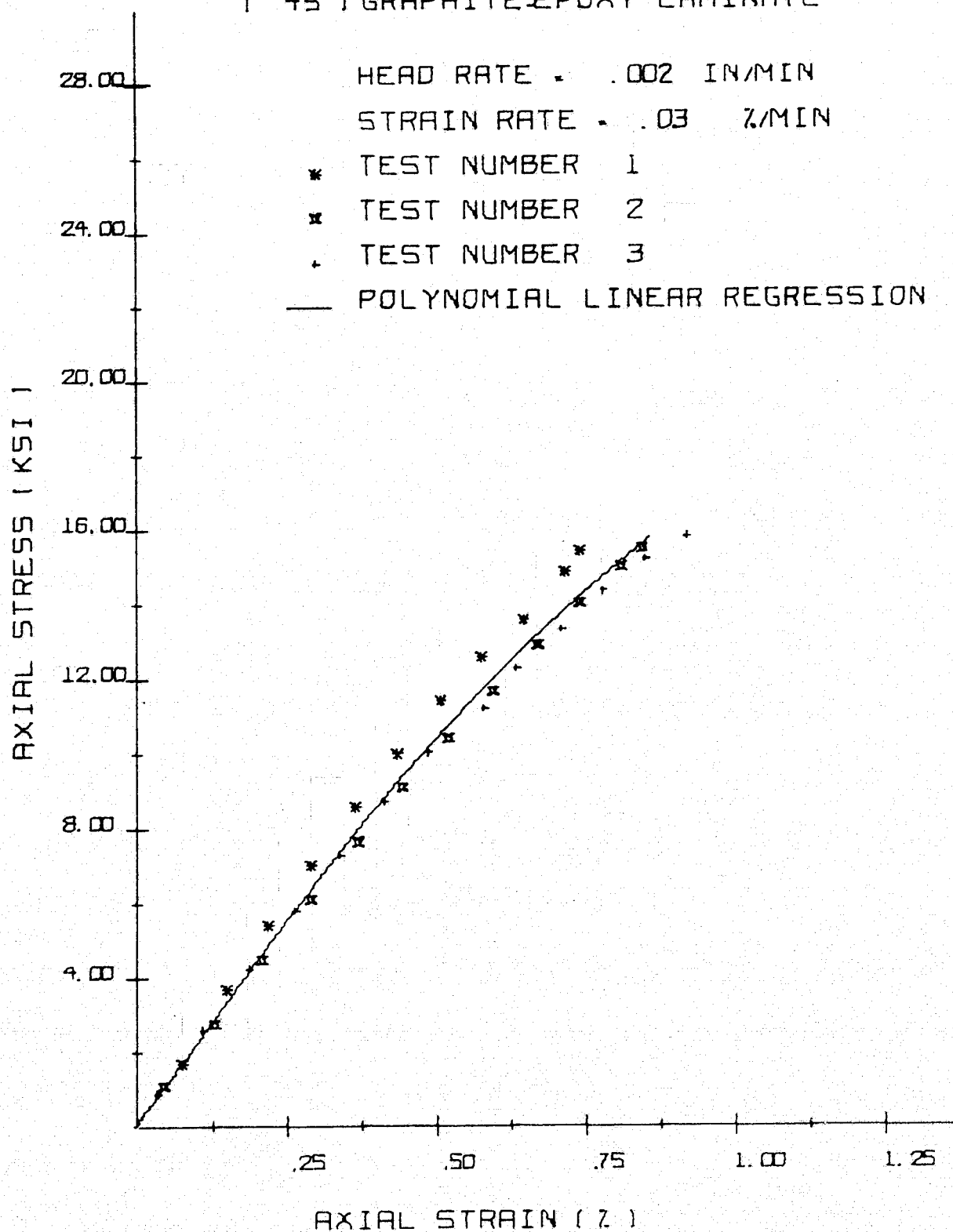


Figure 4. Typical $[0]_{85}$ Axial Strain - Transverse Strain Data.

[45] GRAPHITE EPOXY LAMINATE

Figure 5. Typical $[45]_{8S}$ Stress - Strain Data.

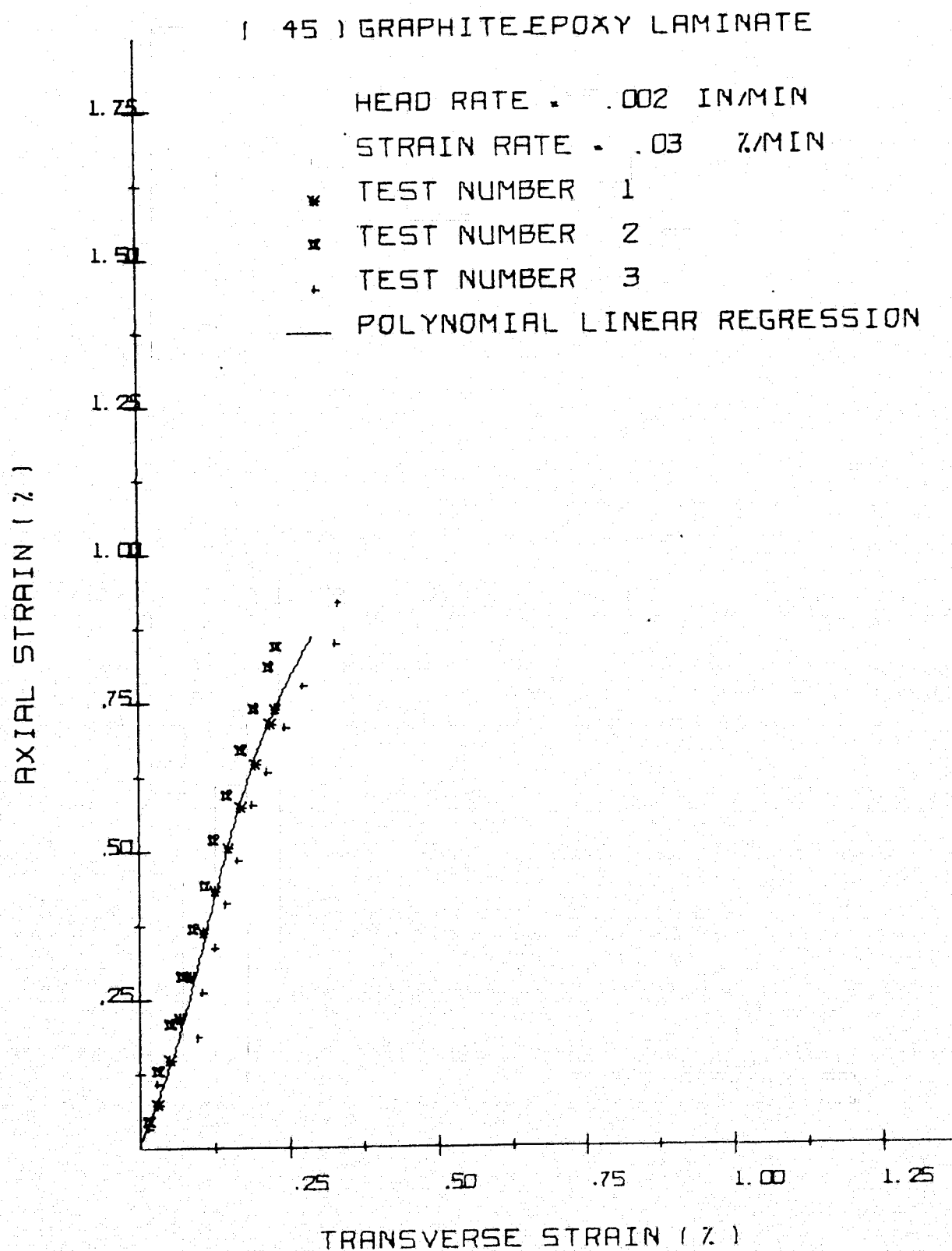


Figure 6. Typical [45]_{8S} Axial Strain - Transverse Strain Data.

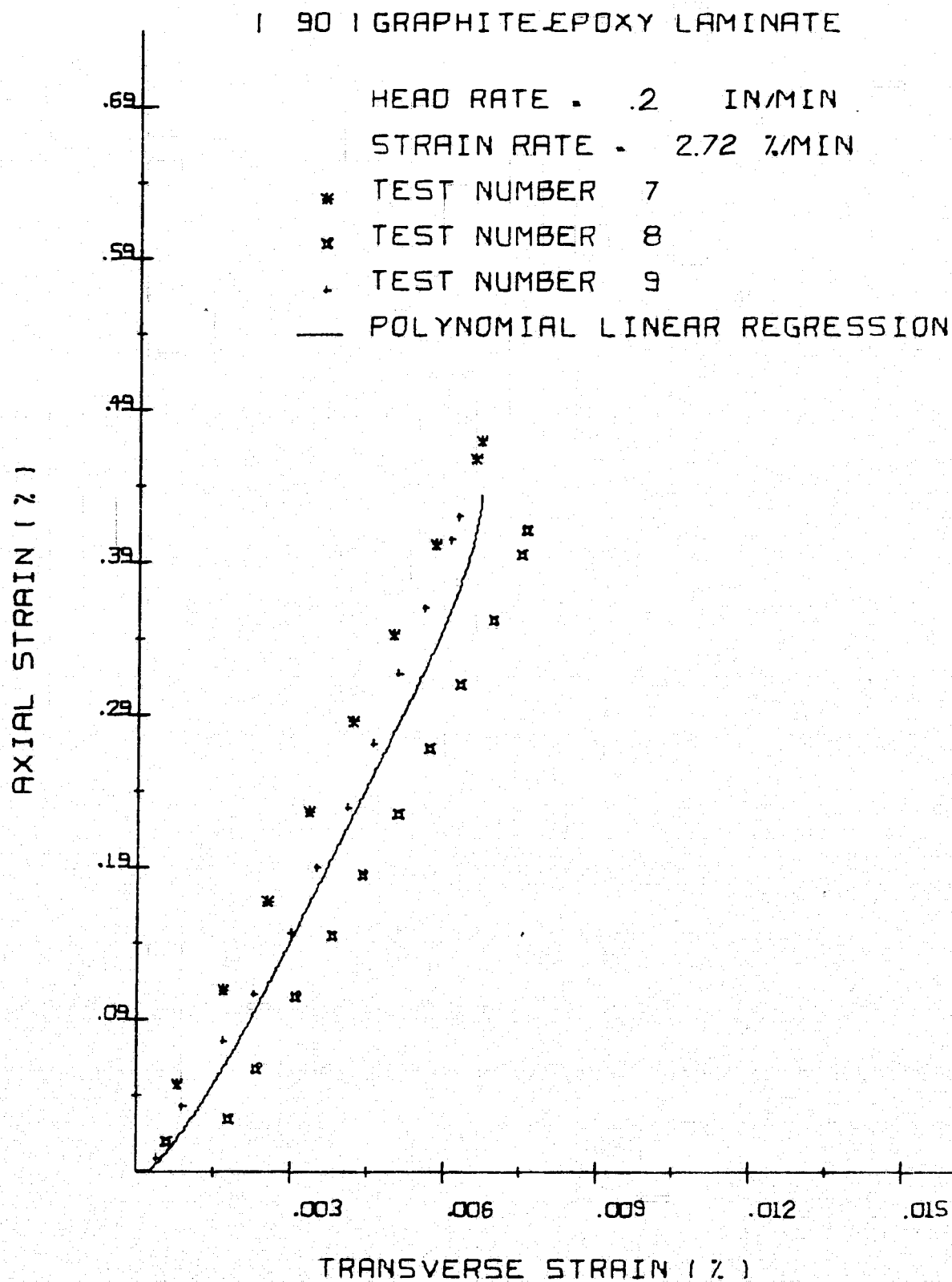


Figure 8. Typical $[90]_{8S}$ Axial Strain - Transverse Strain Data.

PRECEDING PAGE BLANK NOT FILMED

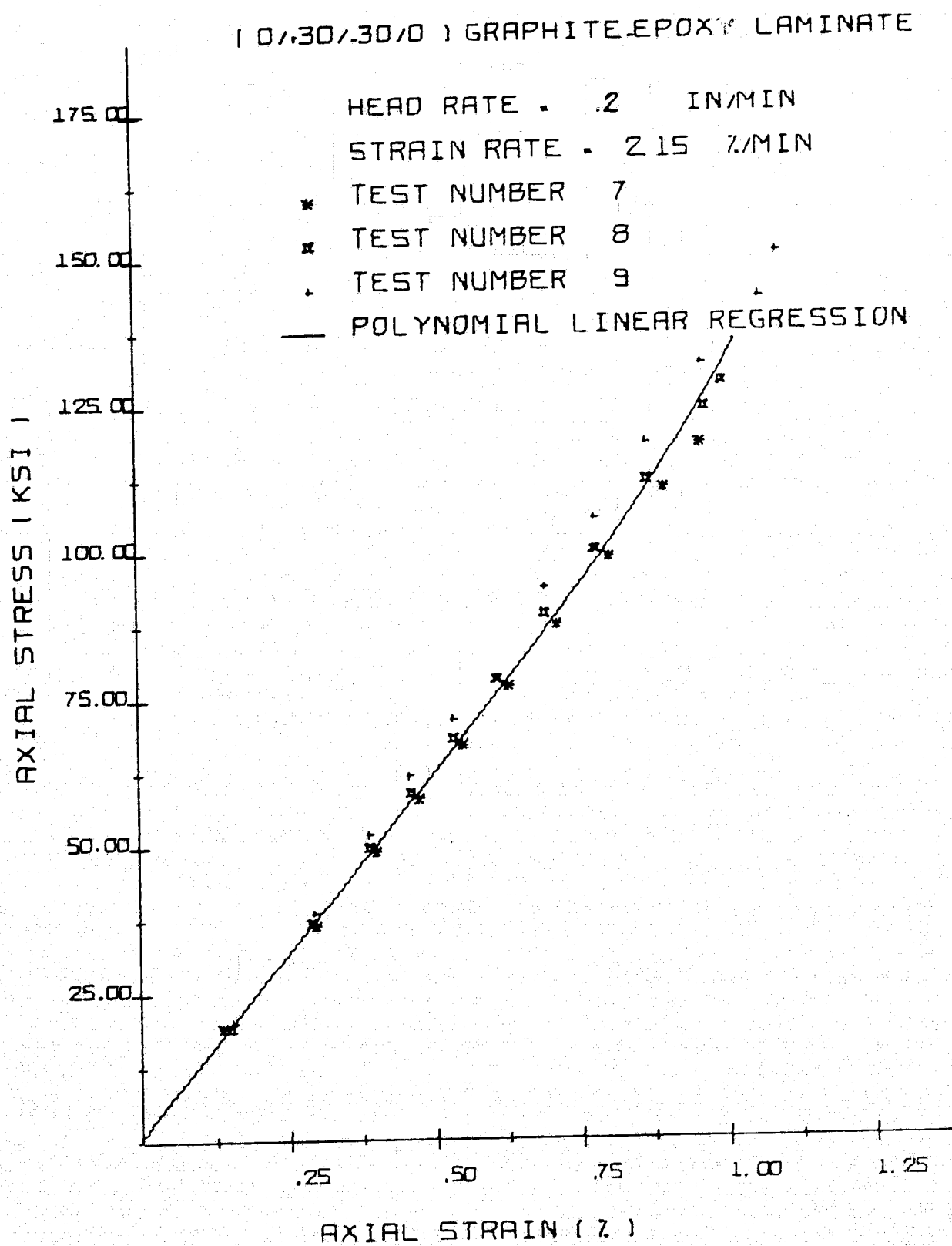


Figure 9. Typical $[0/\pm 30/0]_{2S}$ Stress - Strain Data.

(0/±30/±30/0) GRAPHITE EPOXY LAMINATE

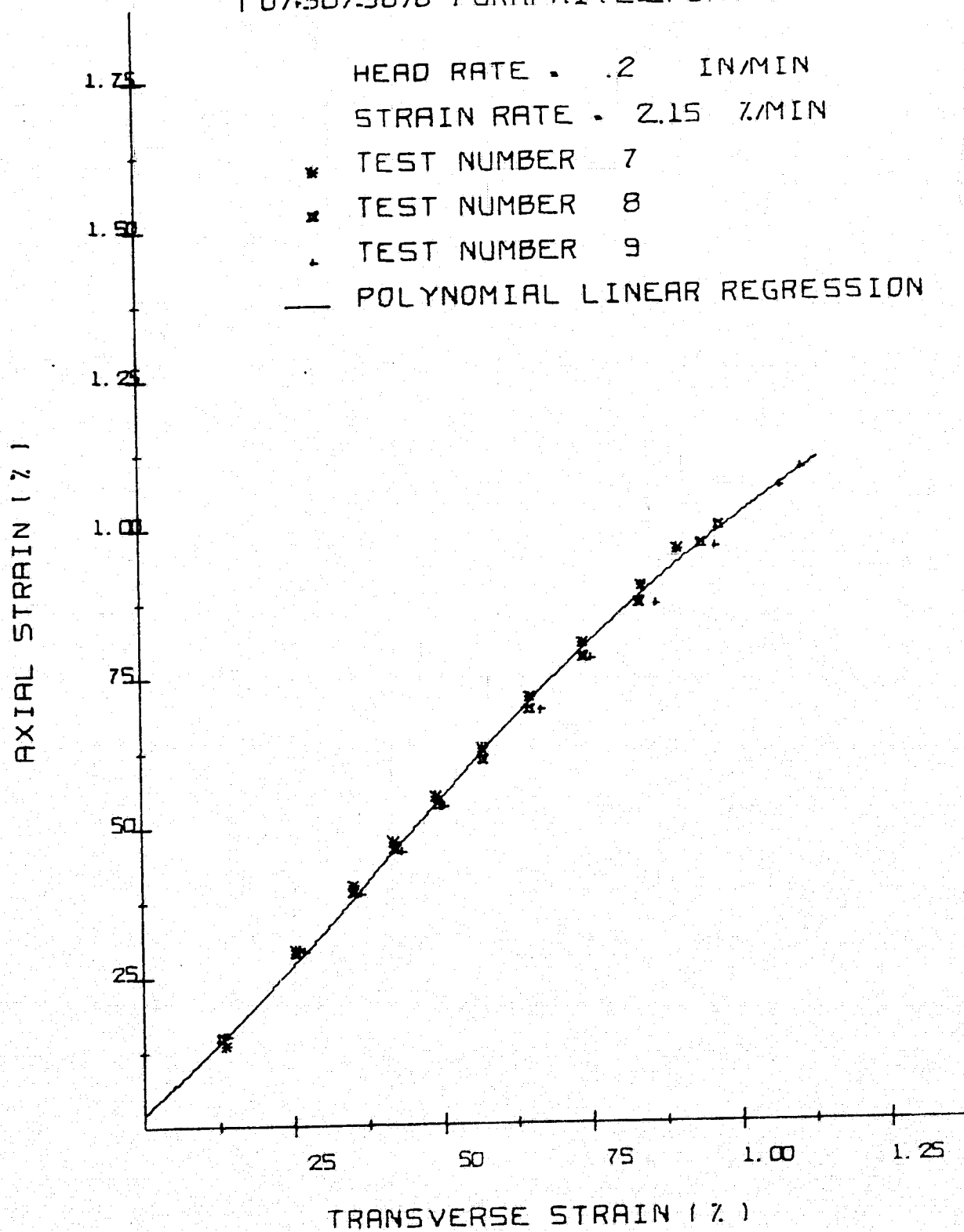
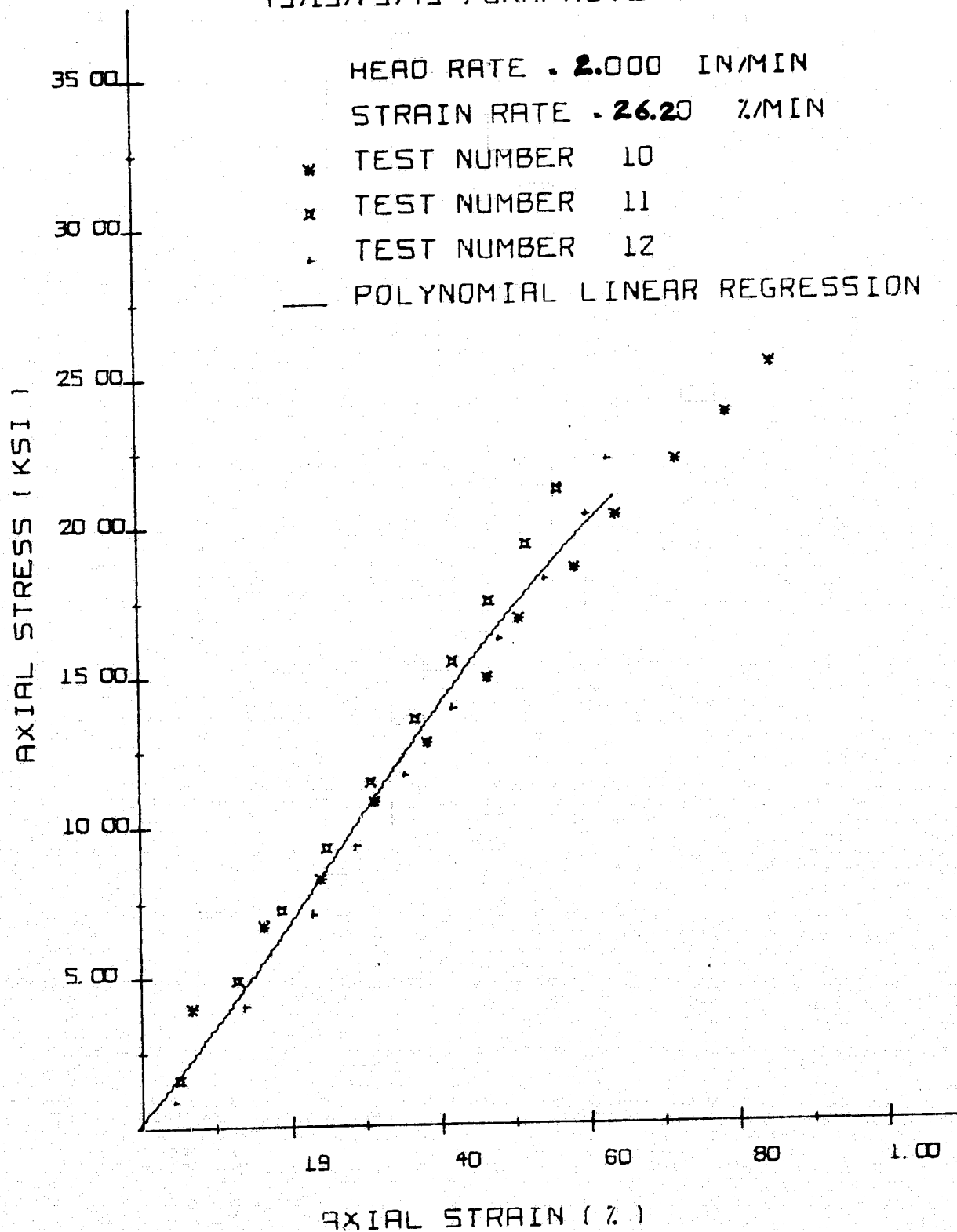


Figure 10. Typical $[0/\pm 30/0]_{2S}$ Axial Strain - Transverse Data.

[45/15/75/45] GRAPHITE EPOXY LAMINATE

Figure 11. Typical [45/15/75/45]_{2S} Stress-Strain Data

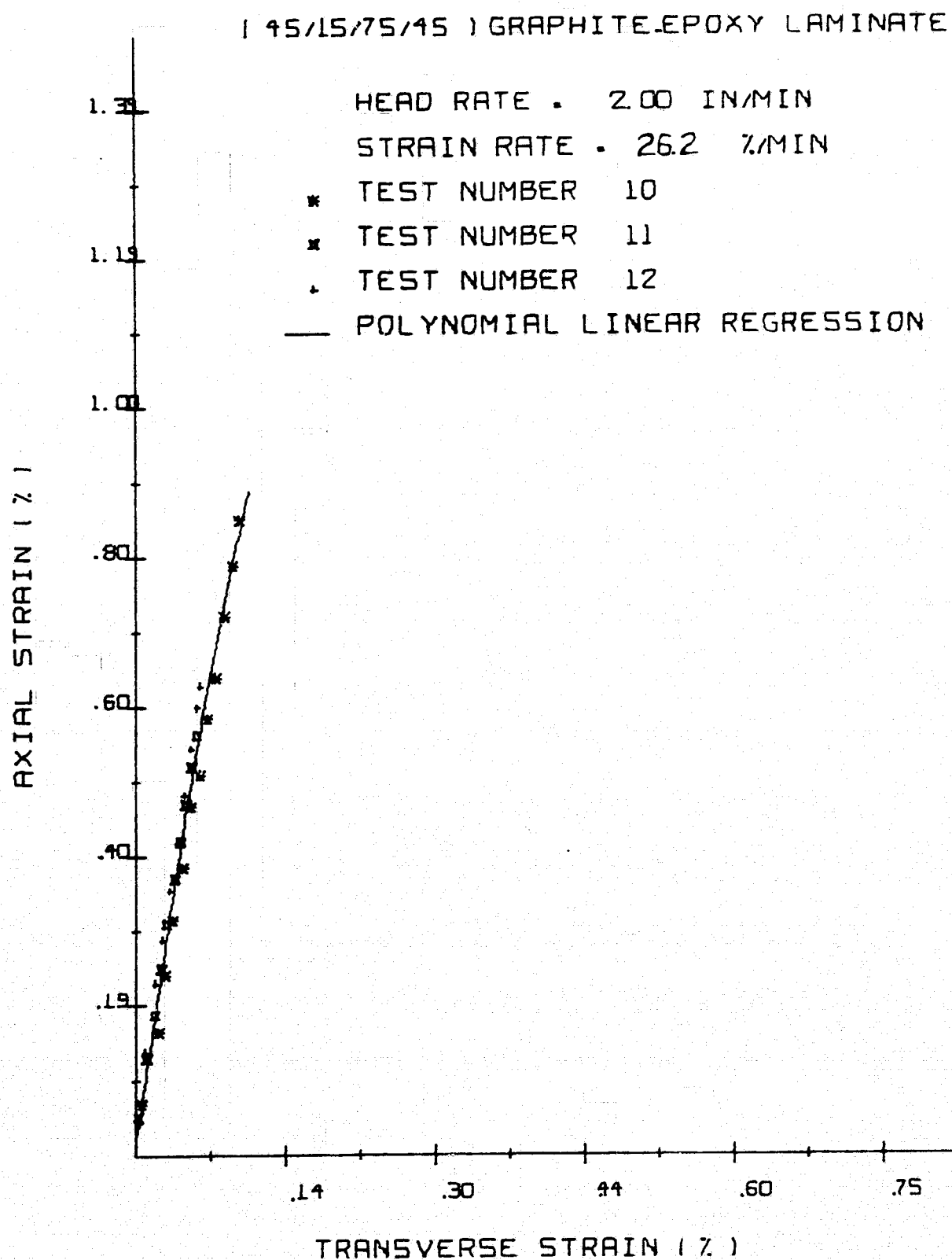


Figure 12. Typical [45/15/75/45]_{2S} Axial Strain - Transverse Strain Data.

(90/+60/-60/90) GRAPHITE EPOXY LAMINATE

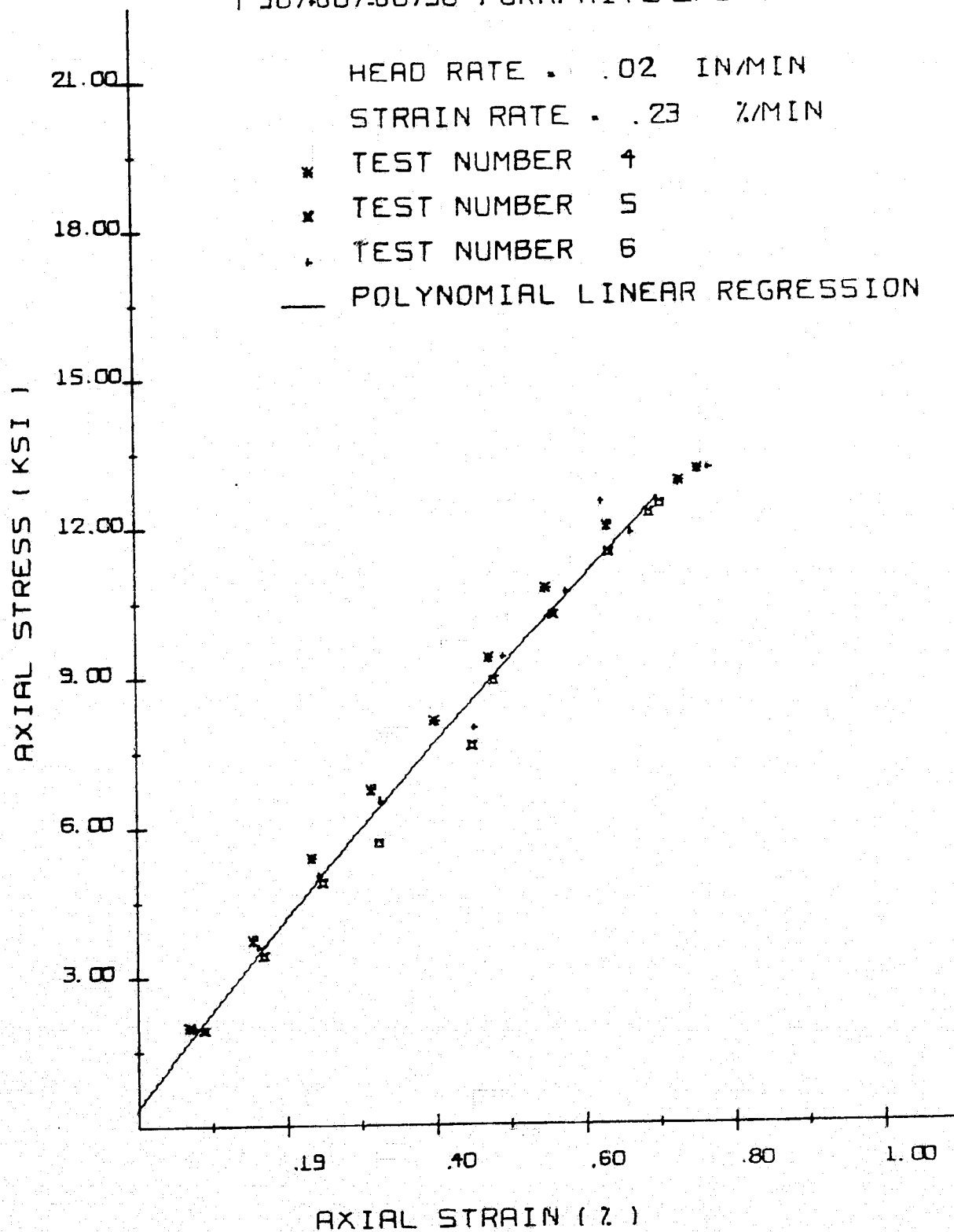


Figure 13. Typical $[90/\pm 60/90]_{2S}$ Stress - Strain Data.

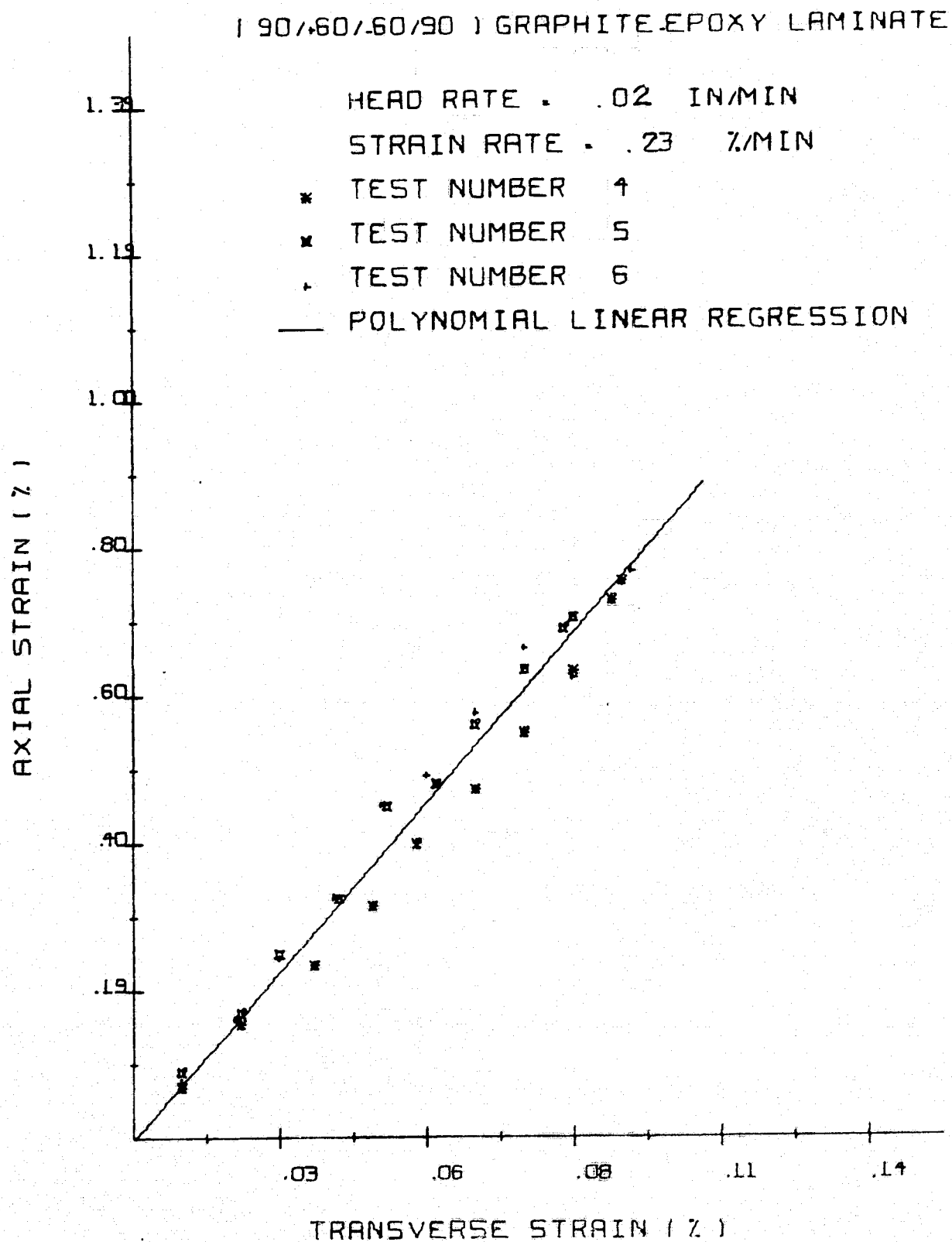


Figure 14. Typical $[90/\pm 60/90]_{2S}$ Axial Strain - Transverse Strain Data.

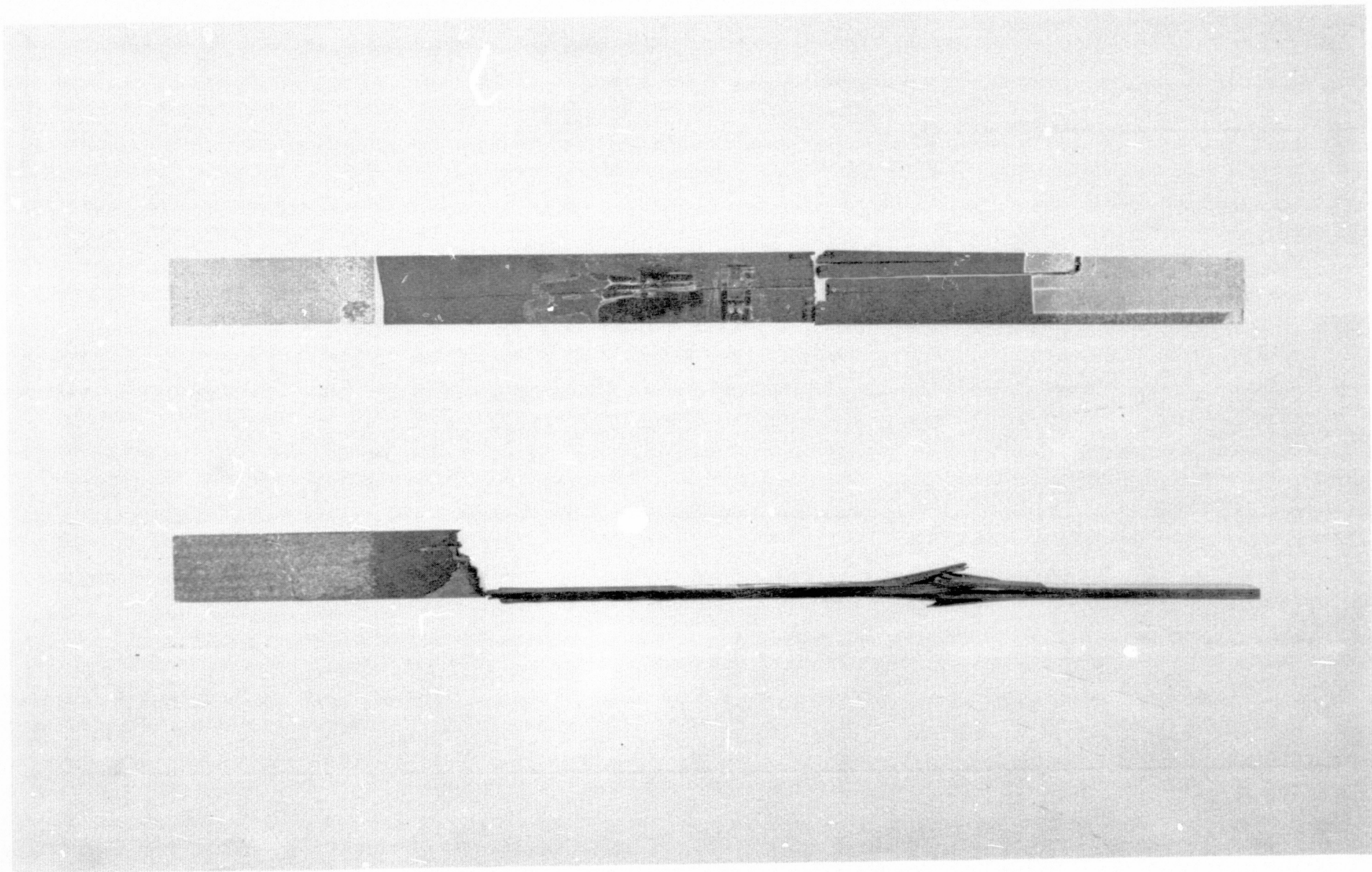


Figure 15. Fracture Planes in Unnotched Laminates.
a) Upper; $[0]_{8S}$ specimen showing axial splitting.
b) Lower; $[0/\pm 30/0]_{2S}$ specimen showing delamination.

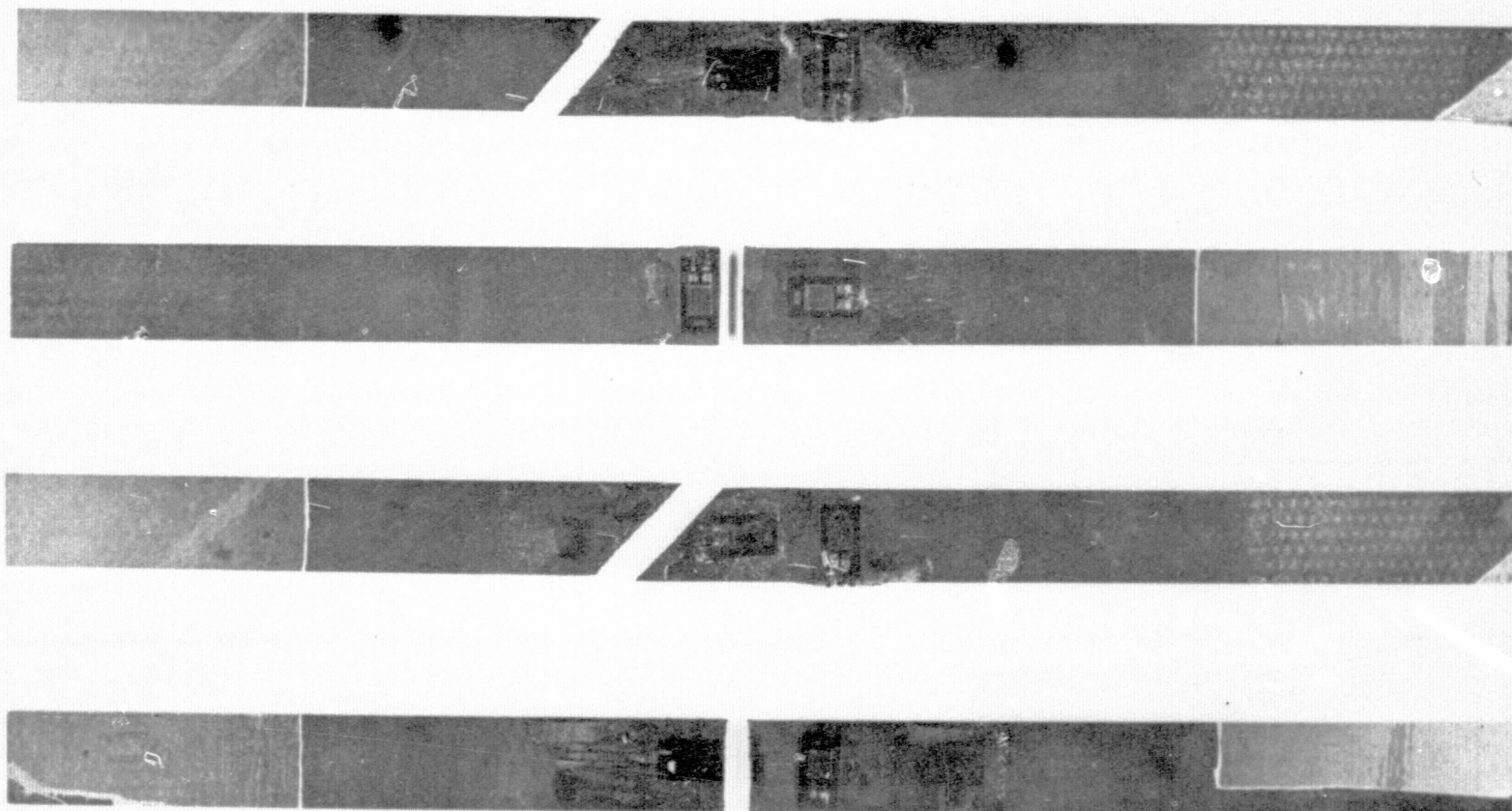


Figure 16. Fracture Planes in Unnotched Laminates.
a) - d) Top to bottom; $[45]_{8S}$, $[90]_{8S}$, $[45/15/75/45]_{2S}$ and $[90/\pm 60/90]_{2S}$.

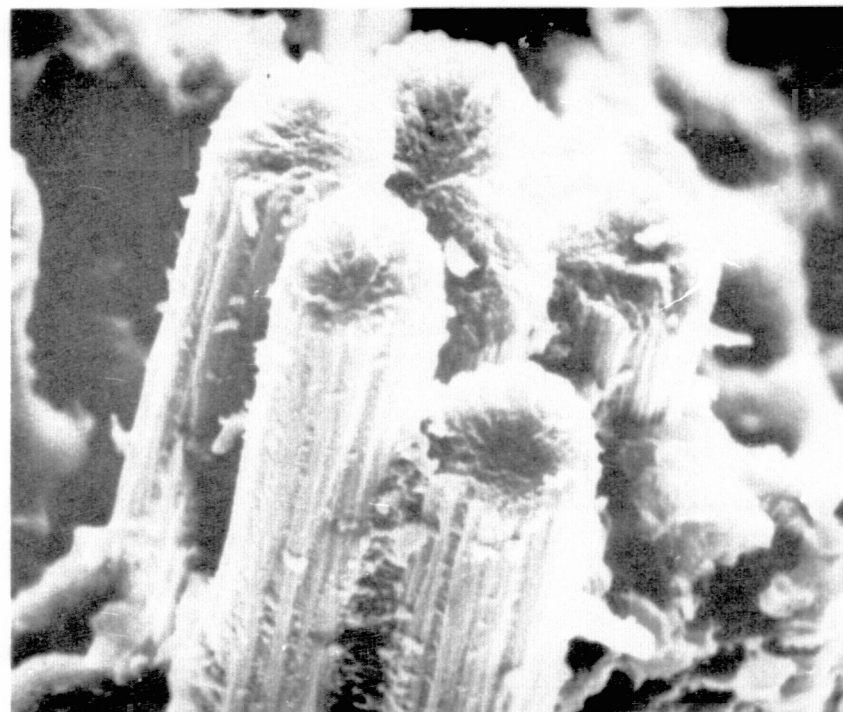
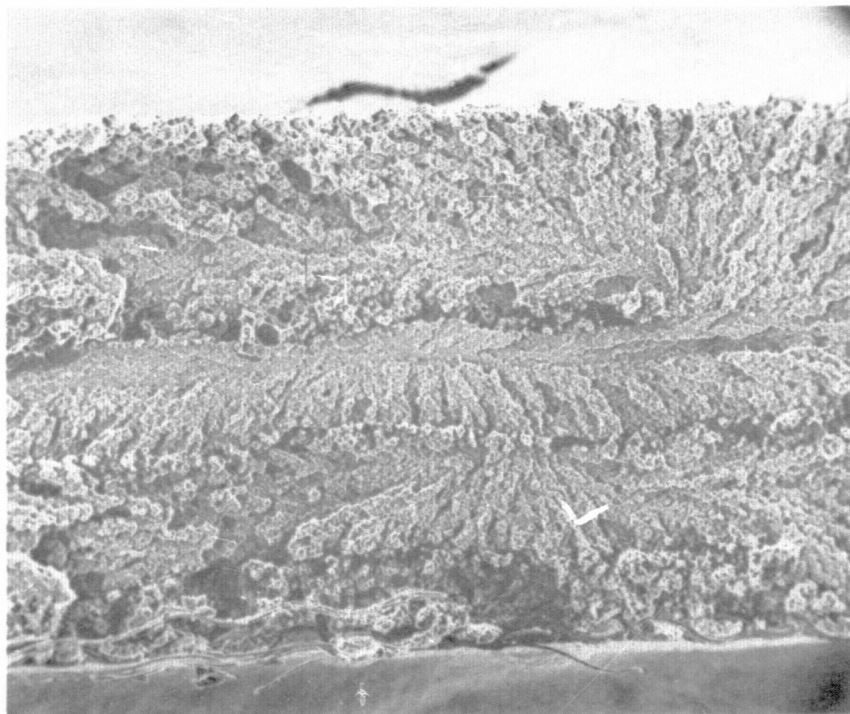


Figure 17. SEM Micrographs of $[0]_{8S}$ Fracture Surface.
a) Left; 35X b) Right; 2000X

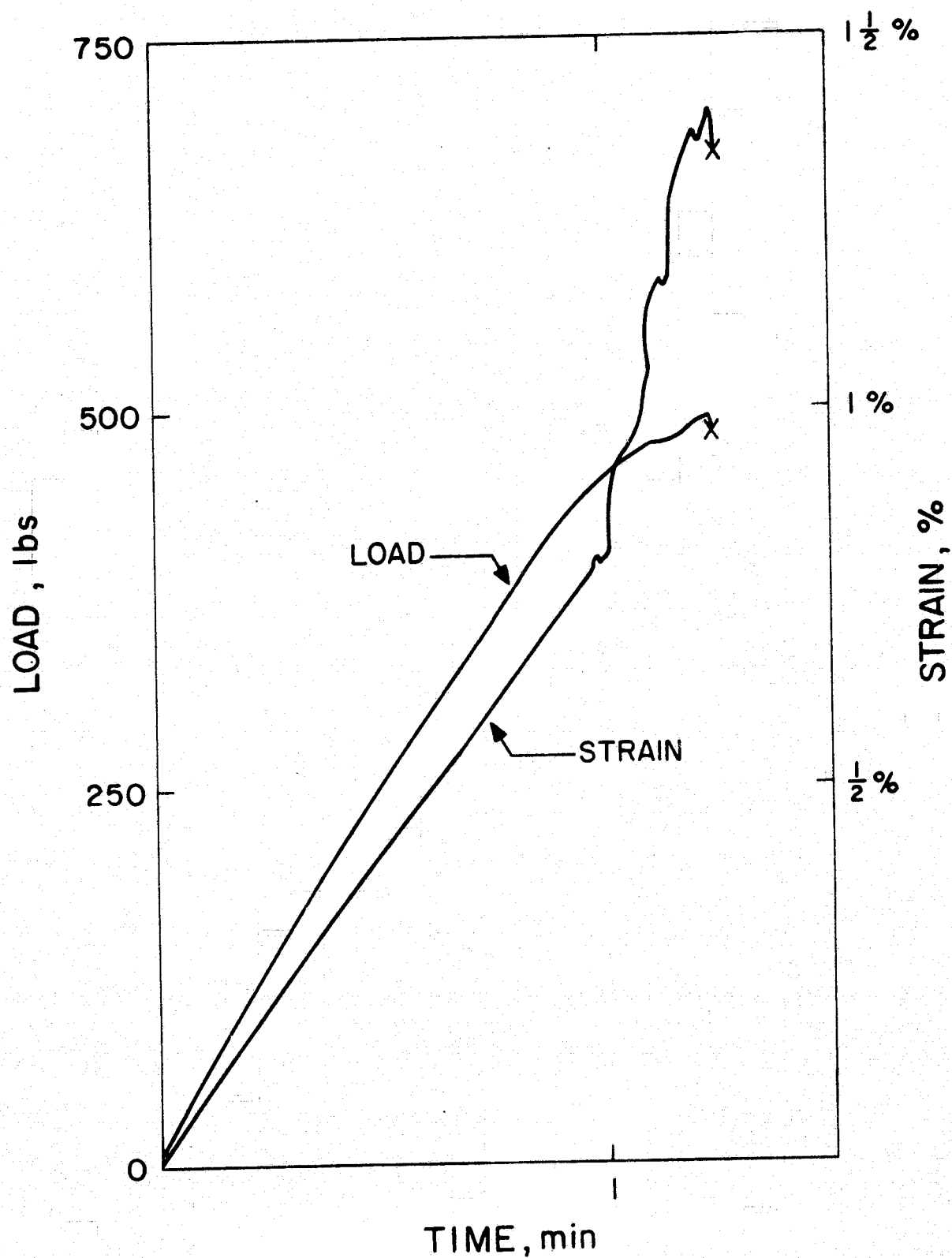


FIG. 18

LOAD-TIME AND STRAIN-TIME TRACE FOR
[90°±60°/90°]_{2S} SPECIMEN.

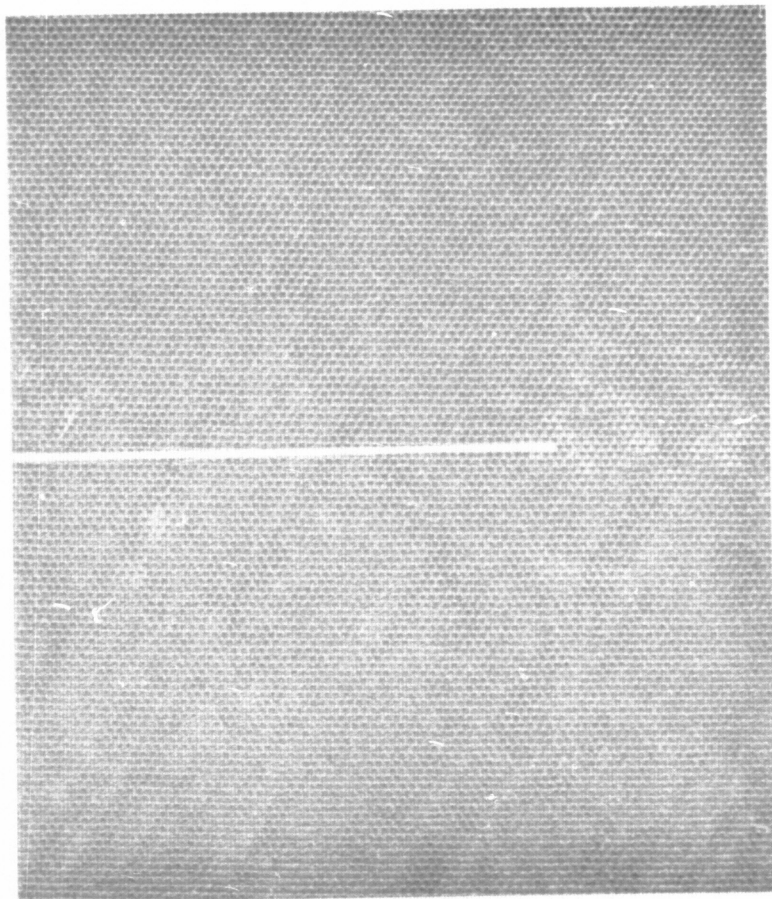


Figure 19. Geometry of Typical Edge Notch.
a) Left; $\sim 7X$ b) Right; $\sim 85X$

ORIGINAL PAGE IS
OF POOR QUALITY

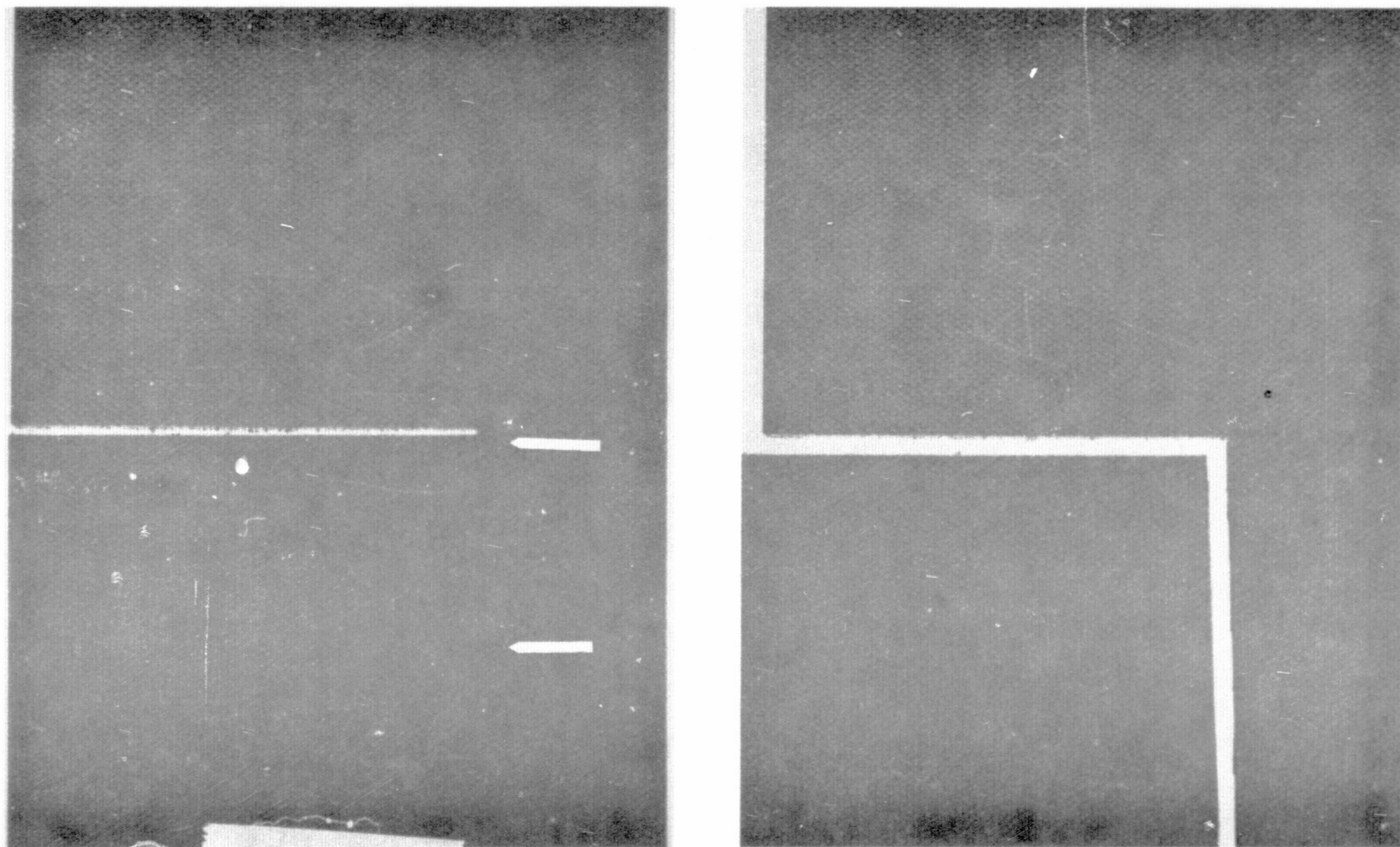


Figure 20. Fracture Planes of $[0]_{8S}$ SEN Specimens Showing Axial Splitting.
(Arrows indicate extent of crack growth.)

ORIGINAL PAGE IS
OF POOR QUALITY

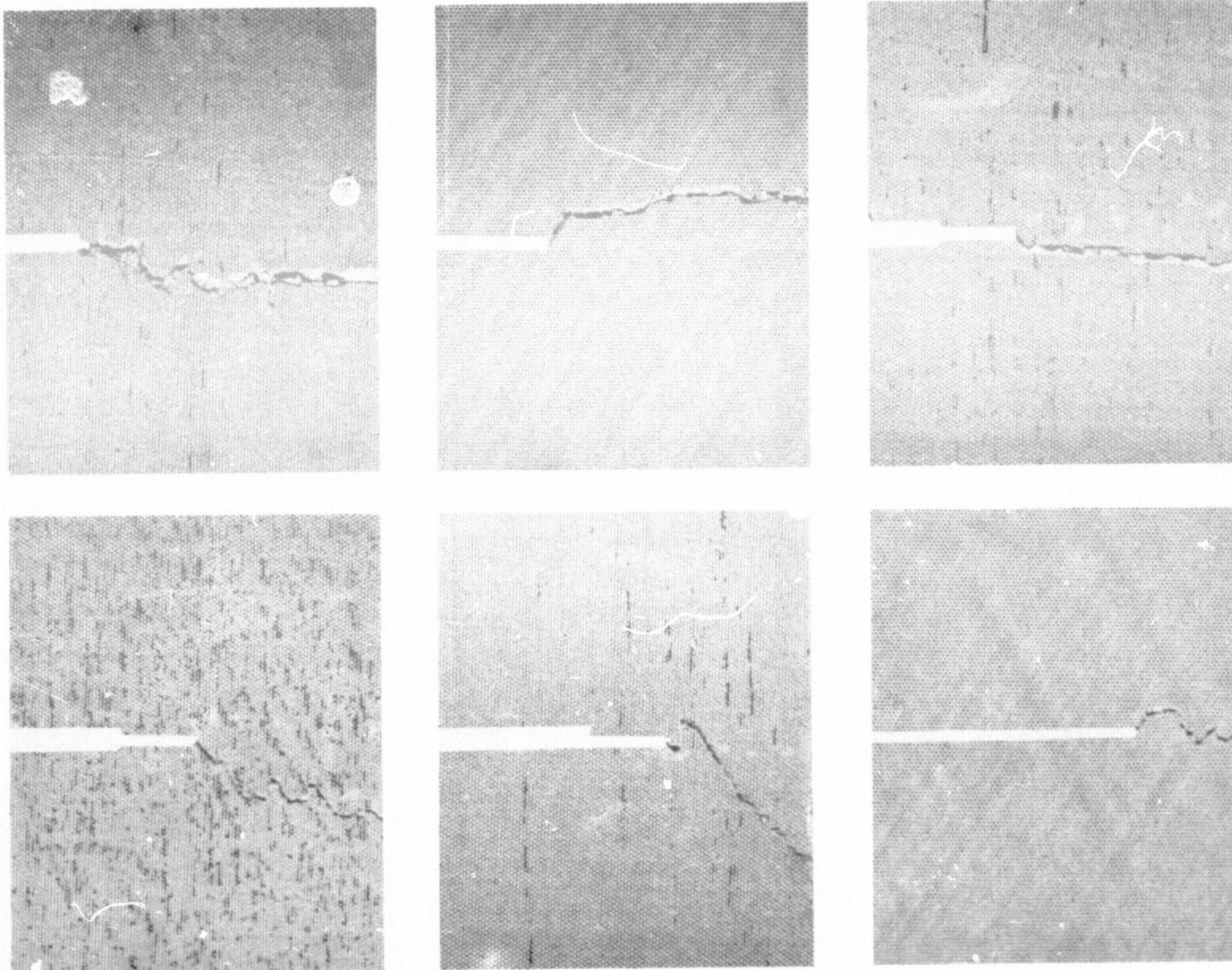


Figure 21. Fracture Planes of $[0/\pm 30/0]_{2S}$ Specimens.

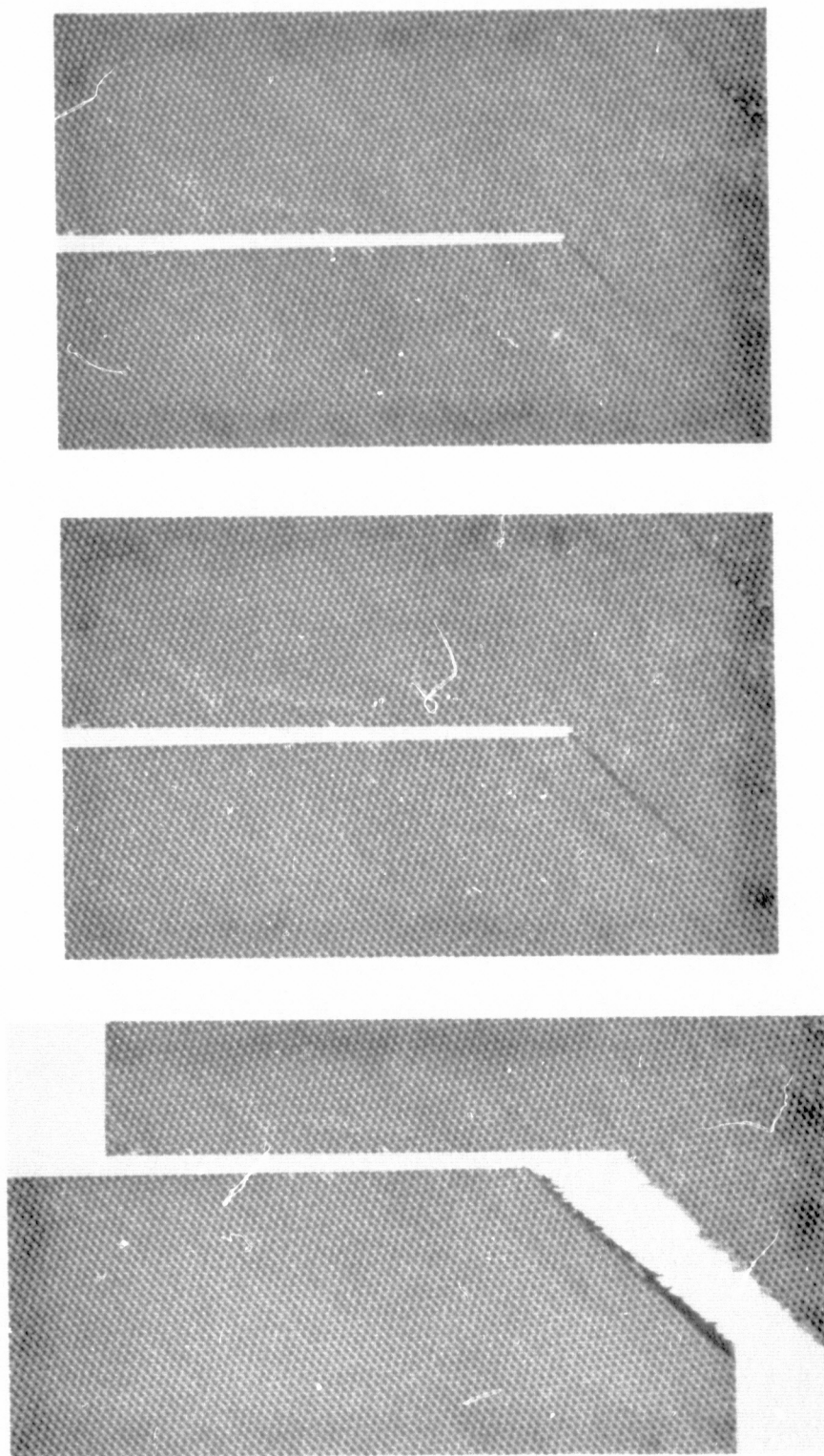


Figure 22. Stable Crack Growth for $[45]_{8S}$ Specimen.

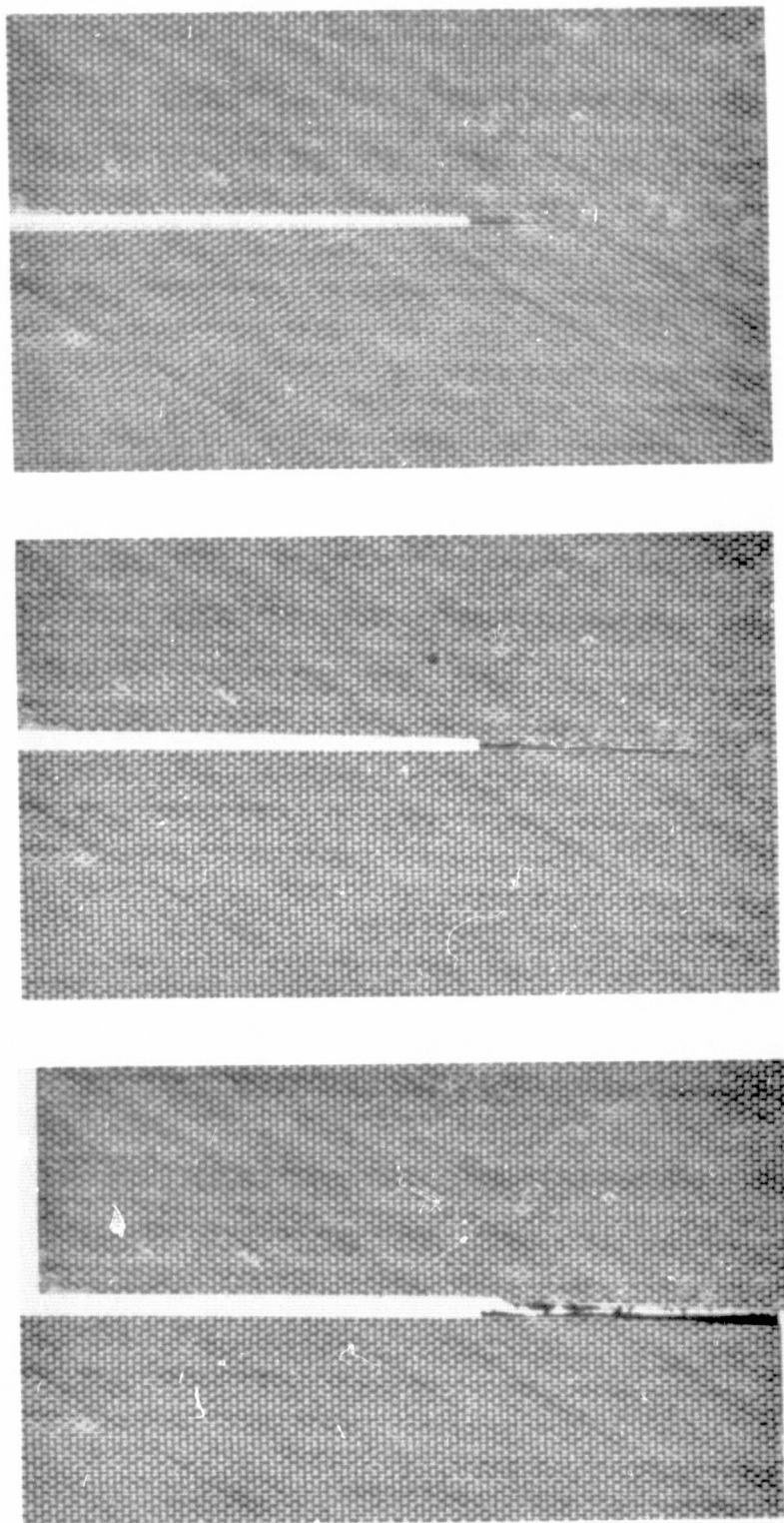


Figure 23. Stable Crack Growth for $[90/\pm 60/90]_{2S}$ Specimen.

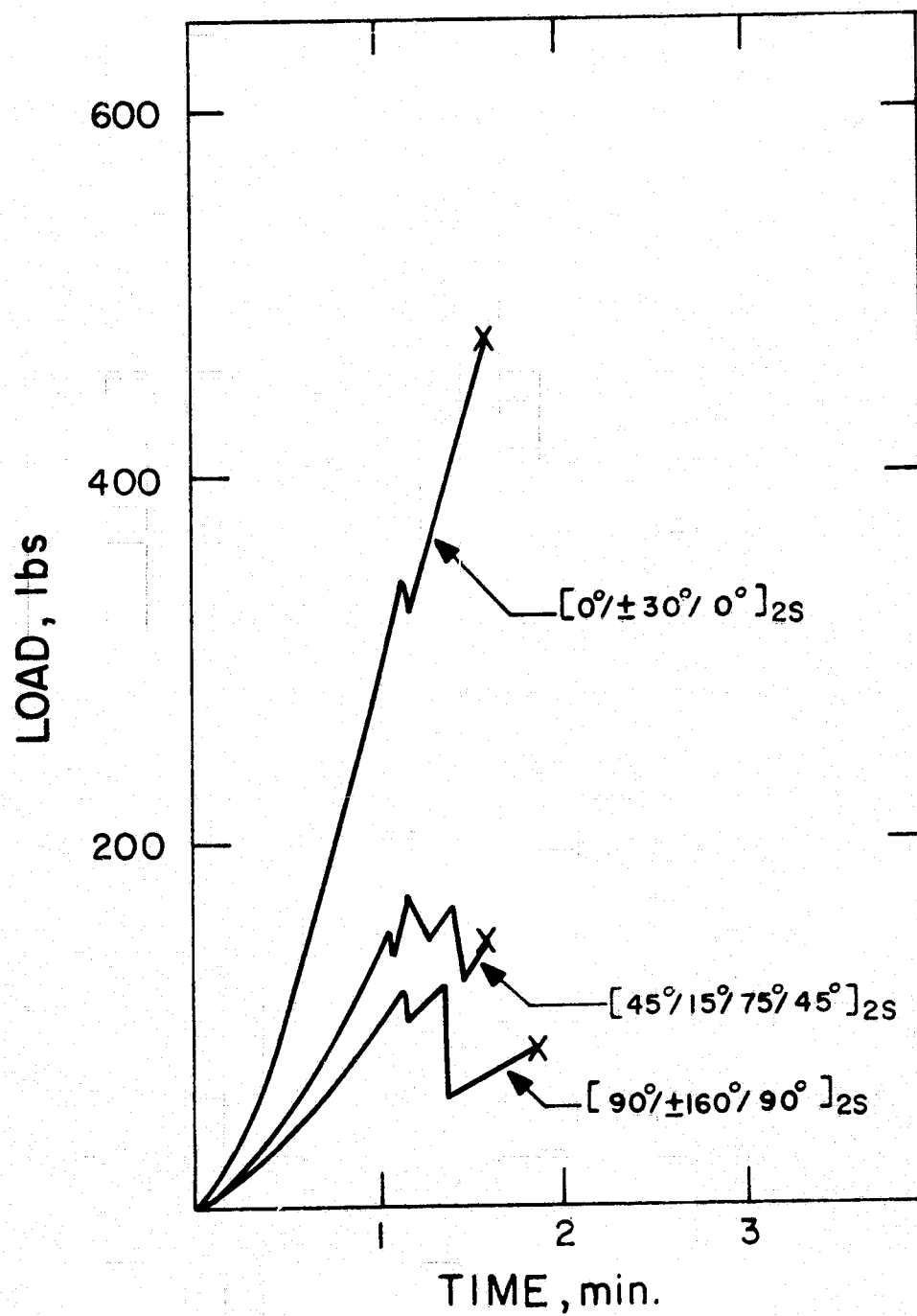


FIG. 24 TYPICAL LOAD-TIME TRACES SHOWING LOAD REDUCTION (SEN)

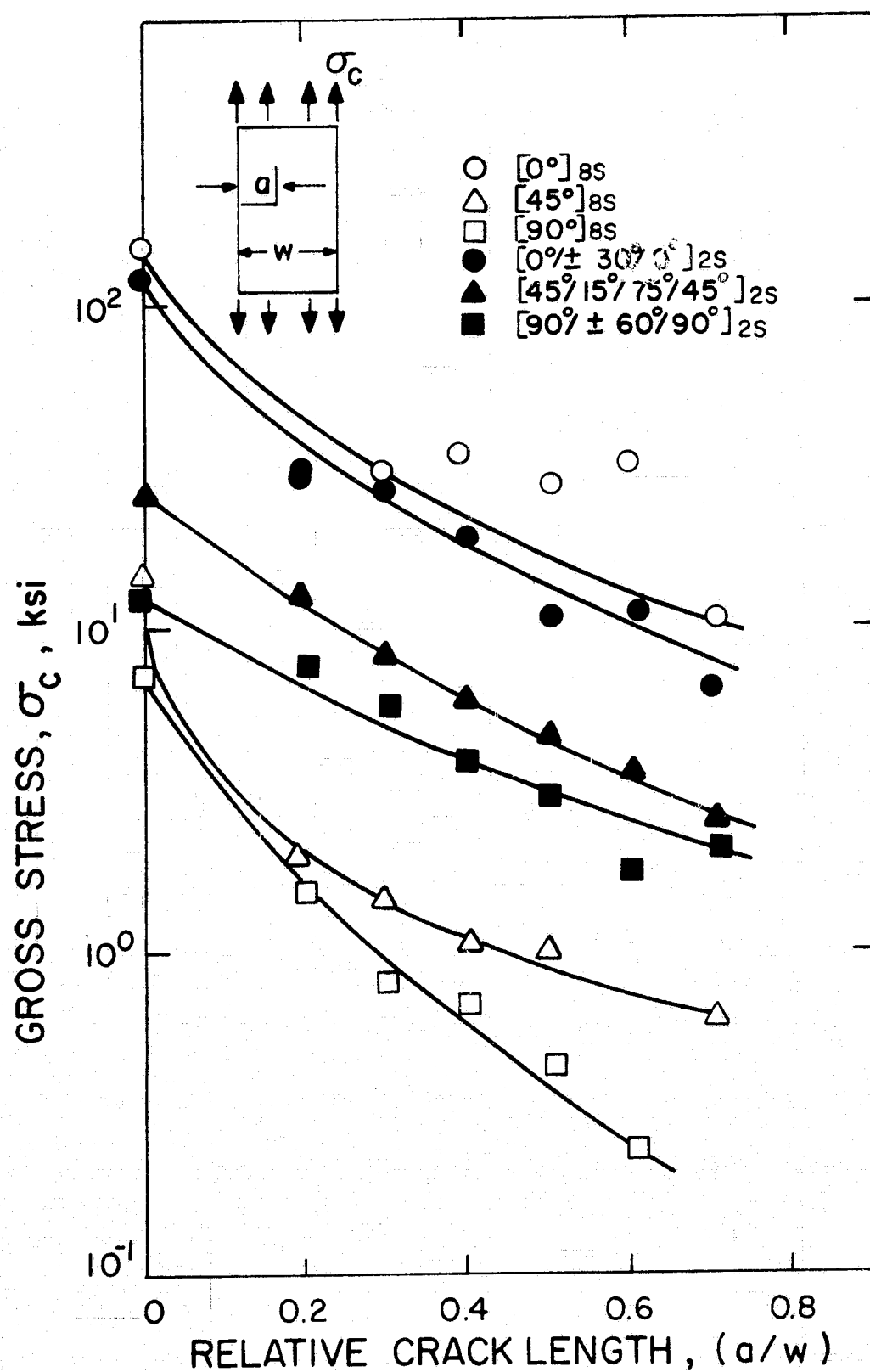


FIG. 25 SINGLE EDGE NOTCH FRACTURE DATA FOR HERCULES GRAPHITE/EPOXY LAMINATES.

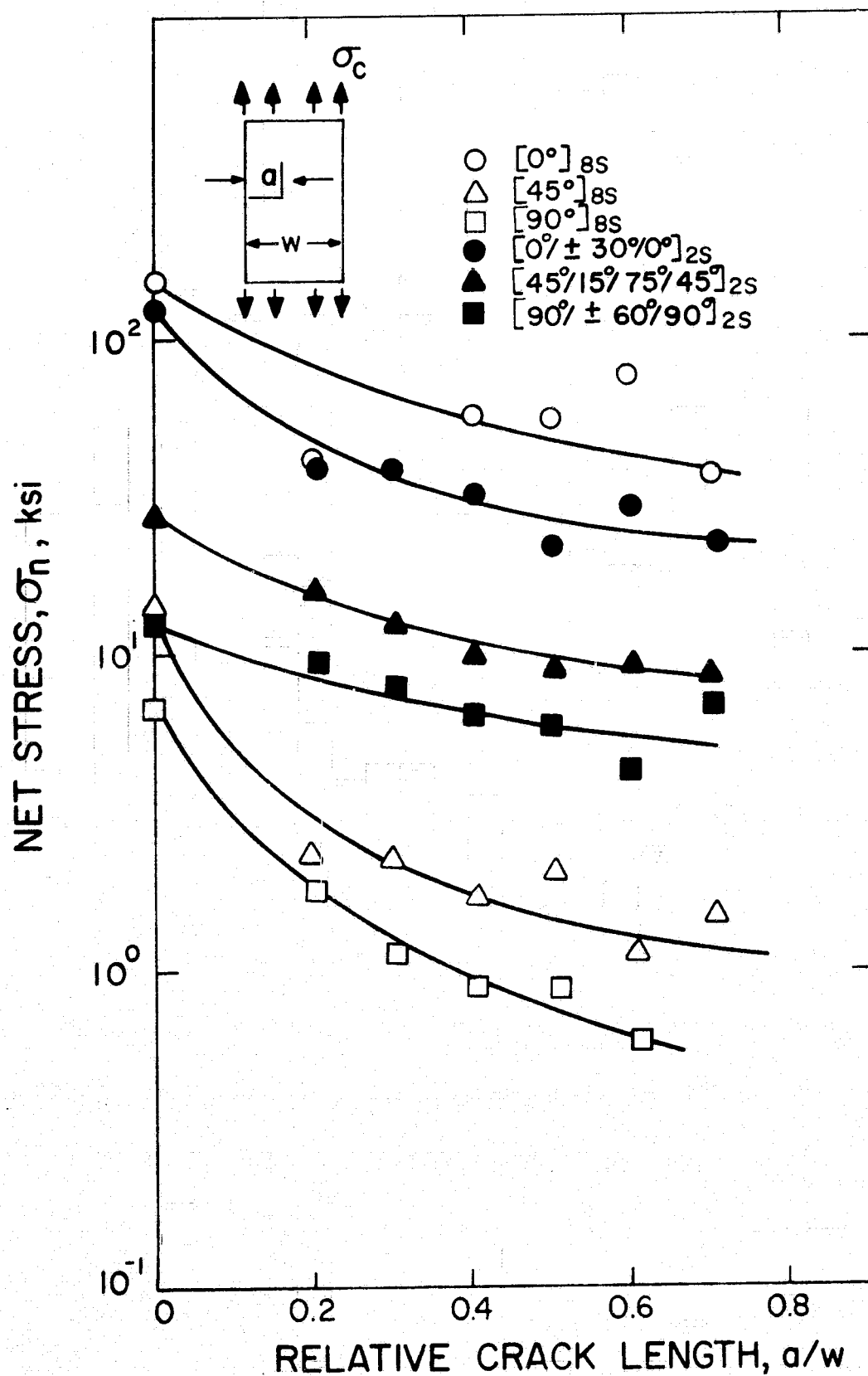


FIG. 26 SINGLE EDGE NOTCH FRACTURE DATA FOR HERCULES GRAPHITE / EPOXY LAMINATES.

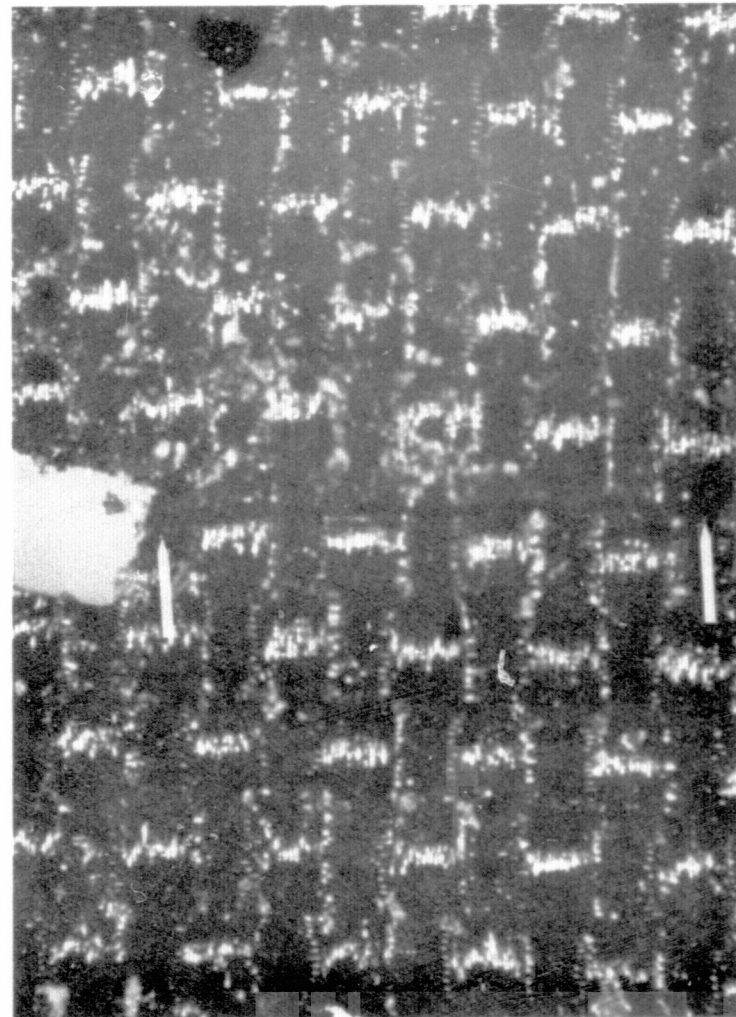
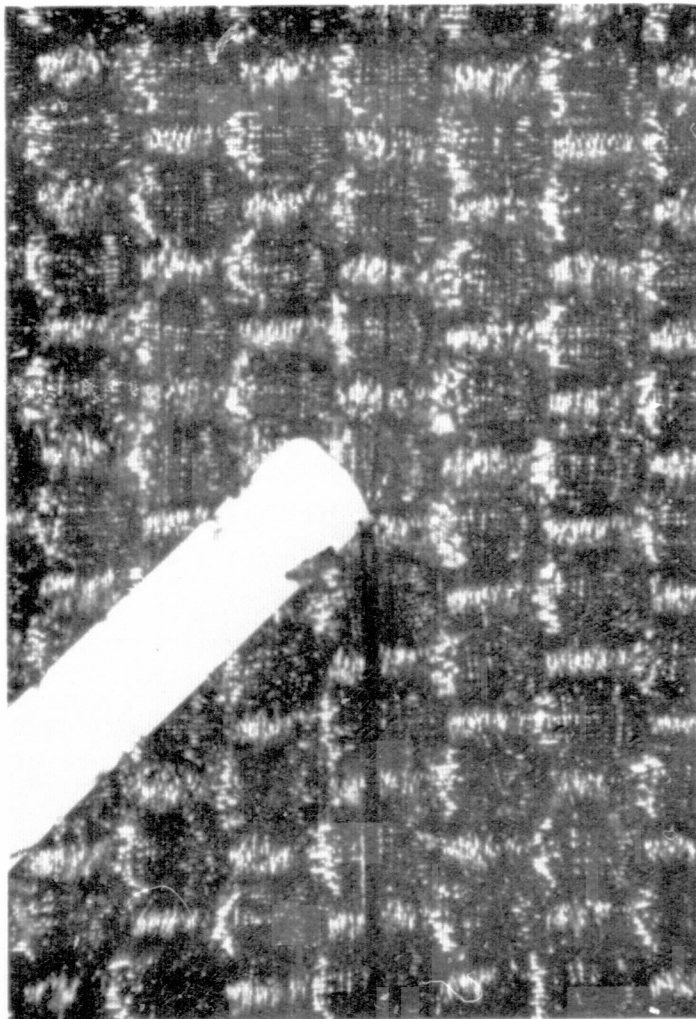
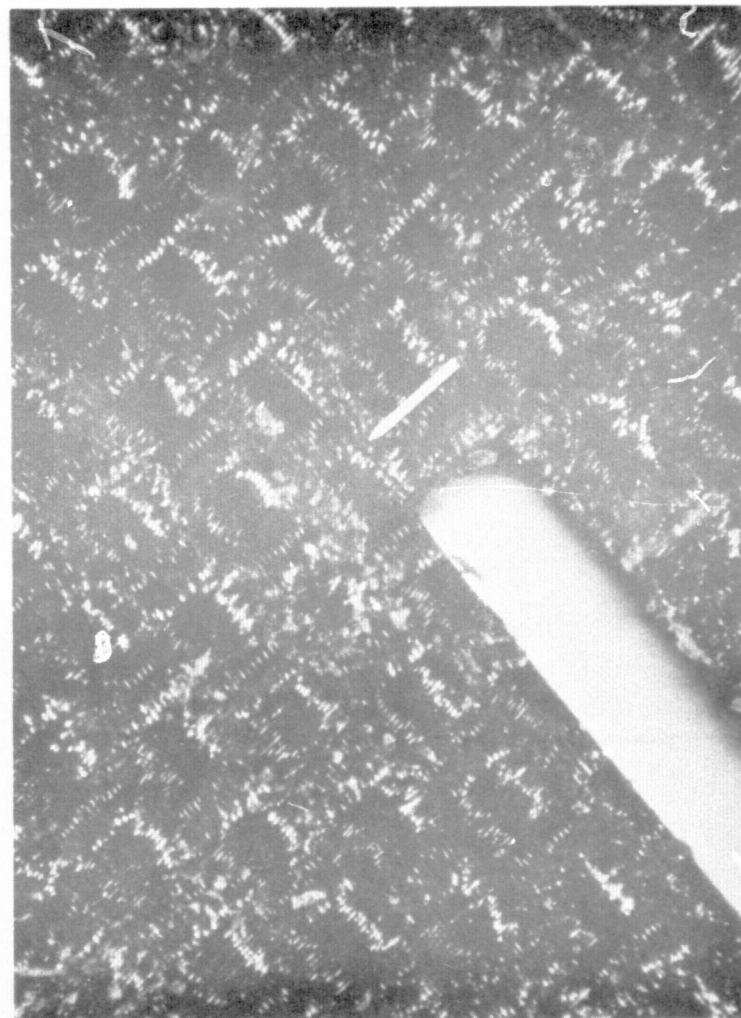


Figure 27. ISEN Fracture Planes for $[0]_{8S}$ and $[90/\pm 60/90]_{2S}$ Specimens.
a) Left; $[0]_{8S}$ specimen b) Right; $[90/\pm 60/90]_{2S}$ specimen.
(Arrows indicate extent of crack growth.)

C. 2



100



Figure 28 (cont.) ISEN Fracture Plane for $[45/15/75/45]_{2S}$ Specimen.
 c) Left; loaded d) Right; fractured
 (Arrow indicates extent of crack growth.)

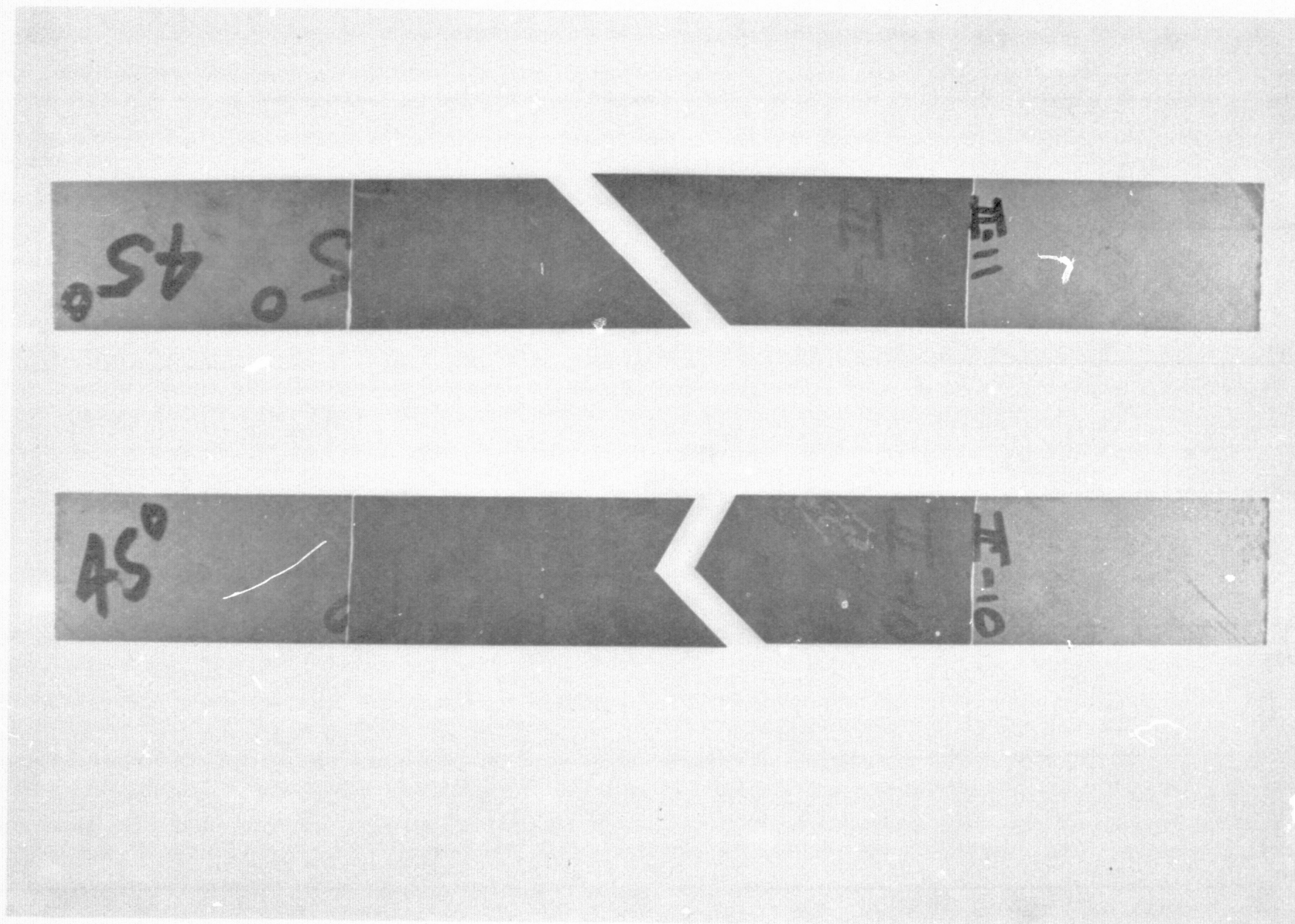


Figure 29. ISEN Fracture Planes for $[45]_{8S}$ Specimens.

ORIGINAL PAGE IS
OF POOR QUALITY

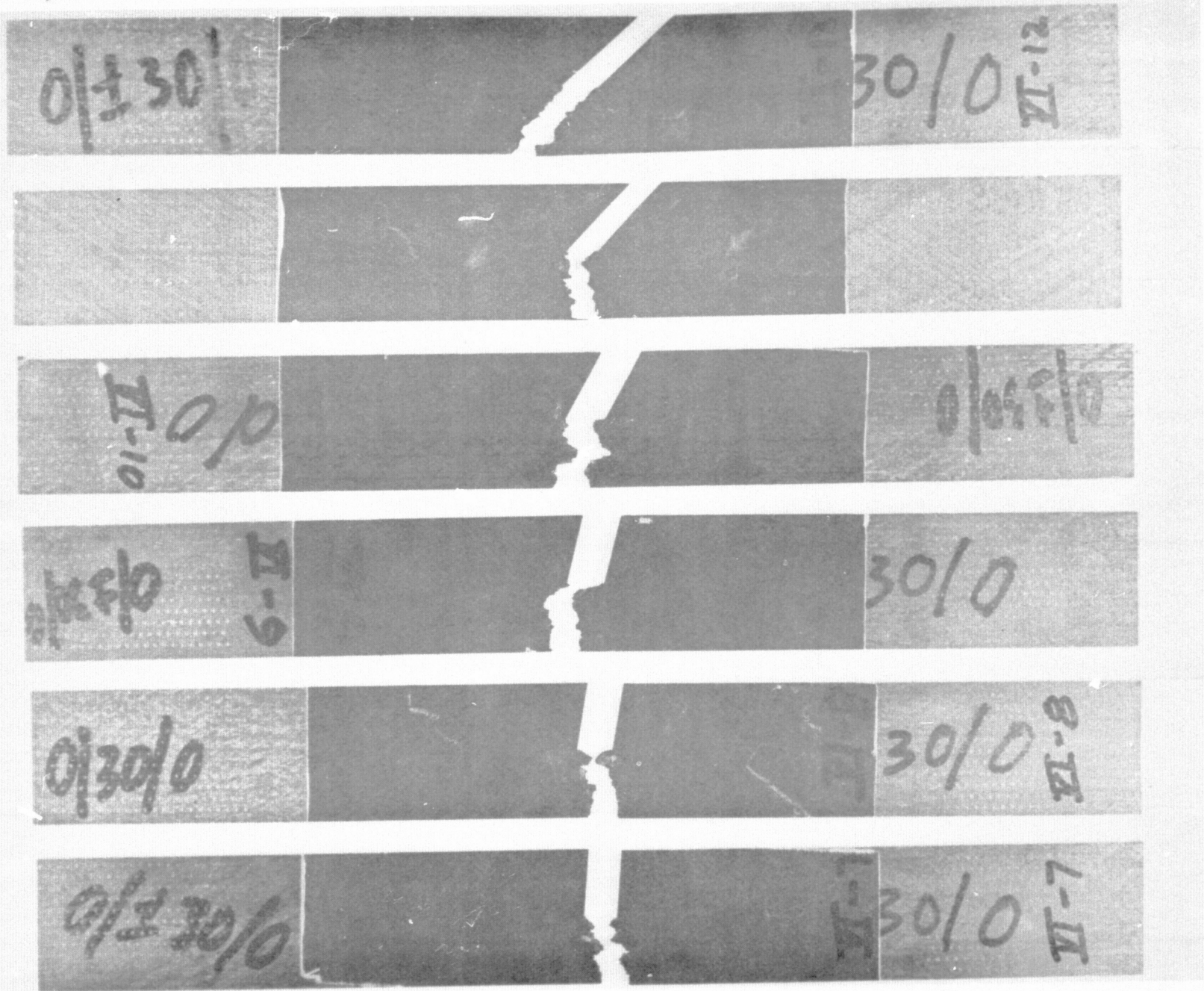


Figure 30. ISEN Fracture Planes for $[0/\pm 30/0]_{2S}$ Specimens.

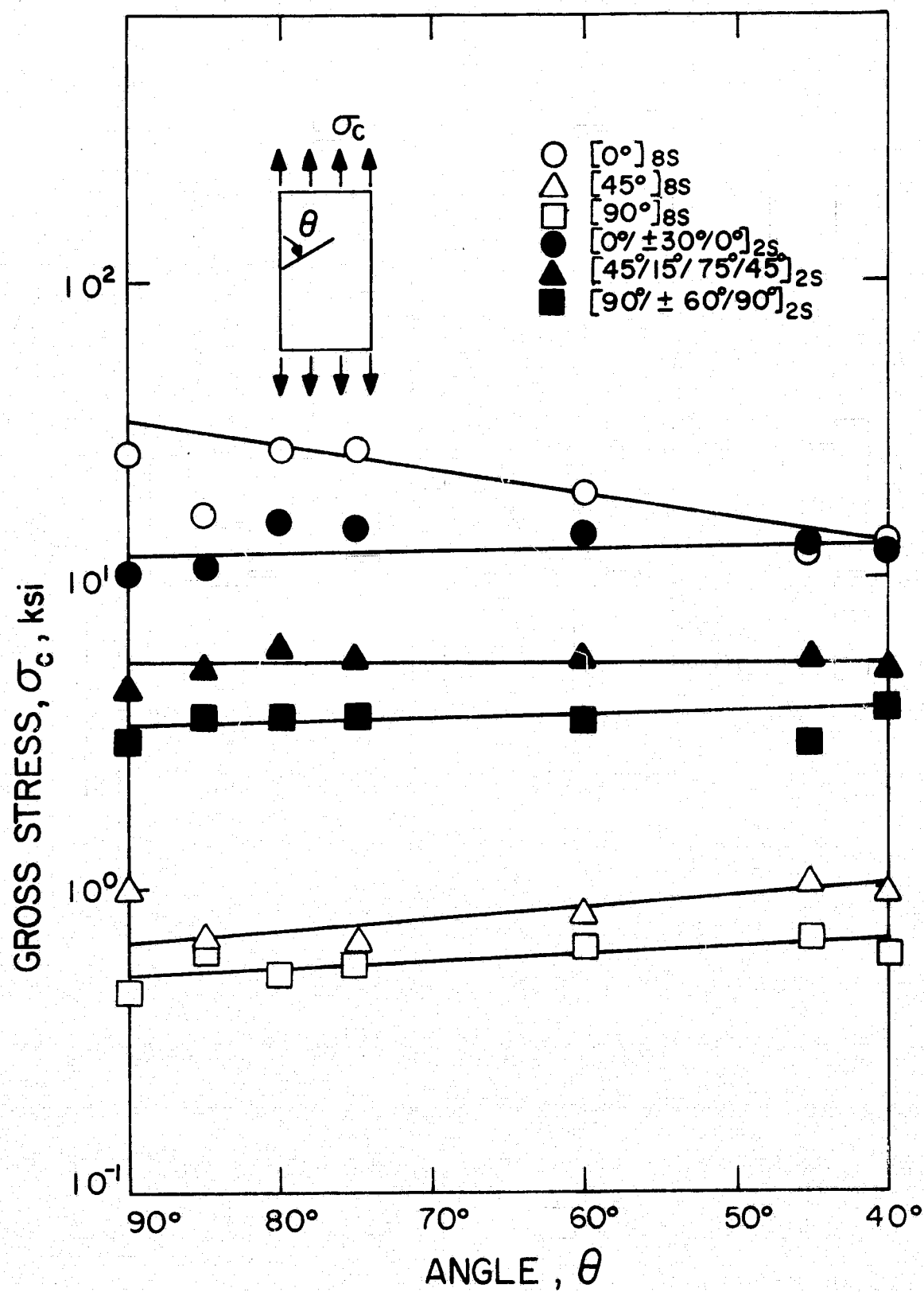


FIG. 31 INCLINED SINGLE EDGE NOTCH (ISEN) GROSS FRACTURE STRESSES

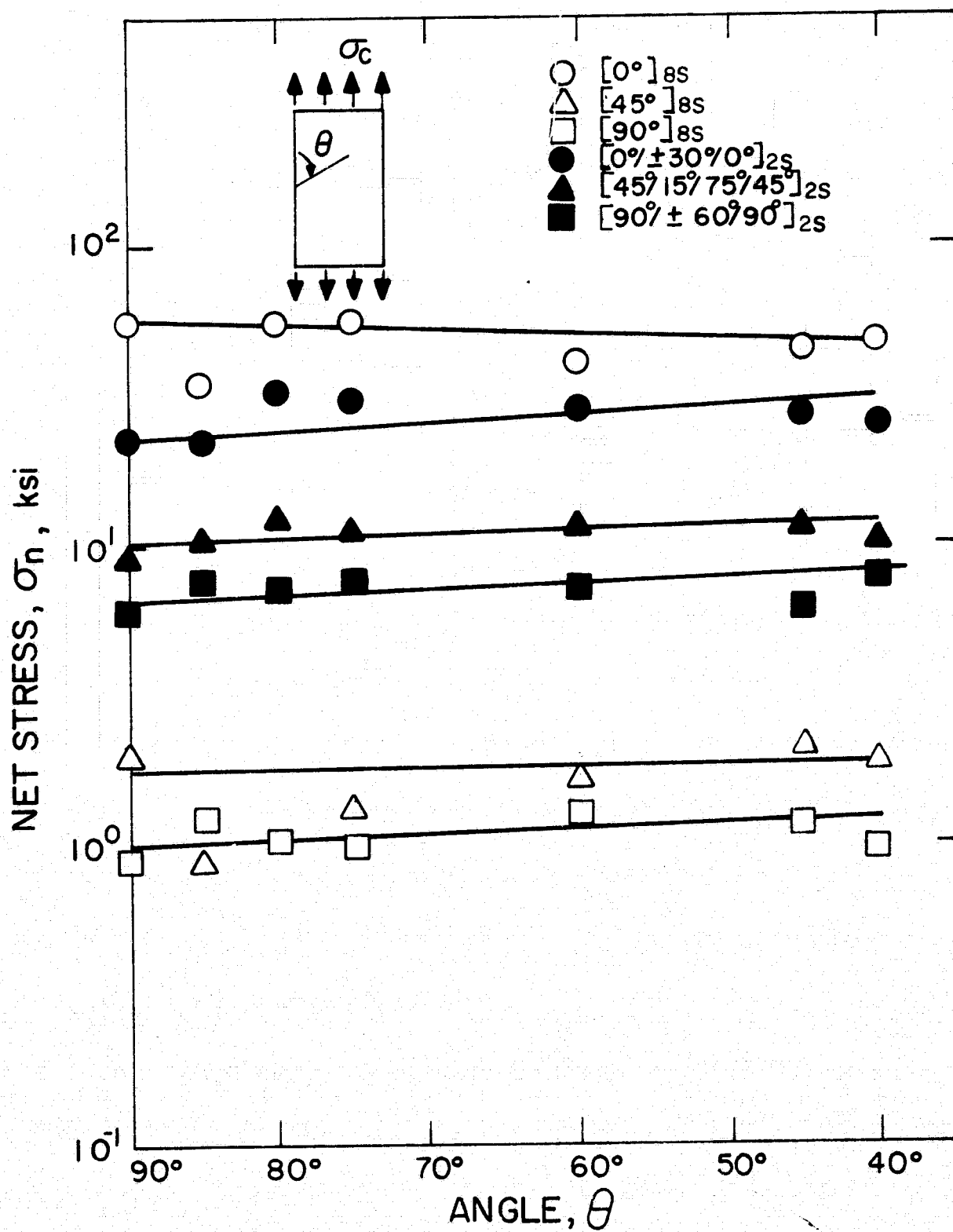


FIG. 32 INCLINED SINGLE EDGE NOTCH (ISEN) NET FRACTURE STRESSES

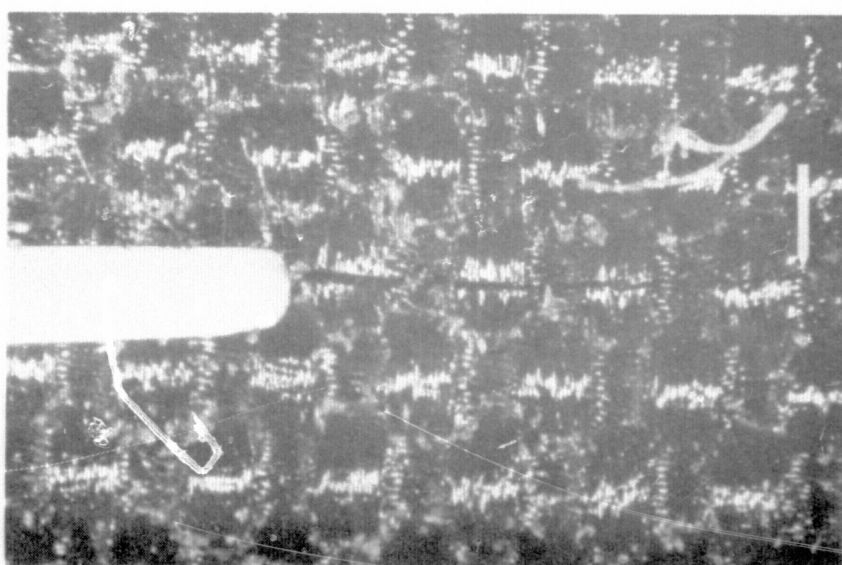
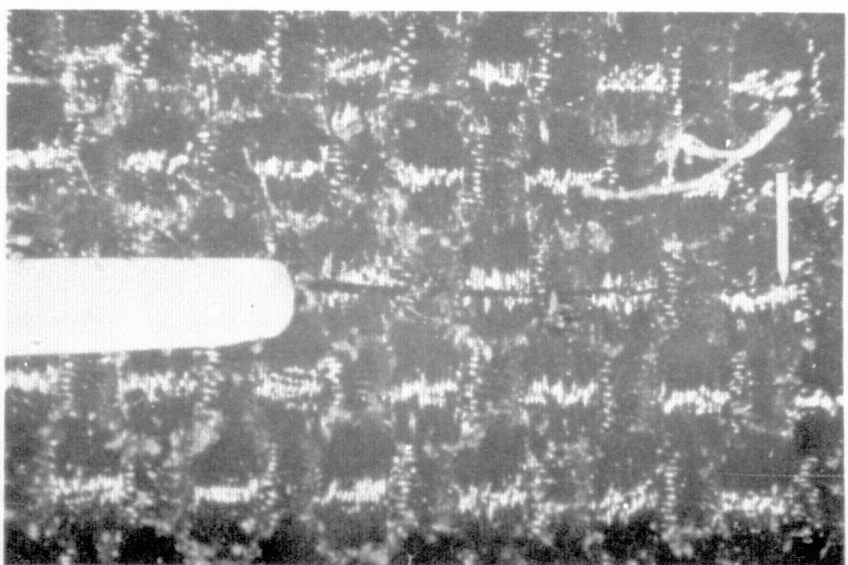
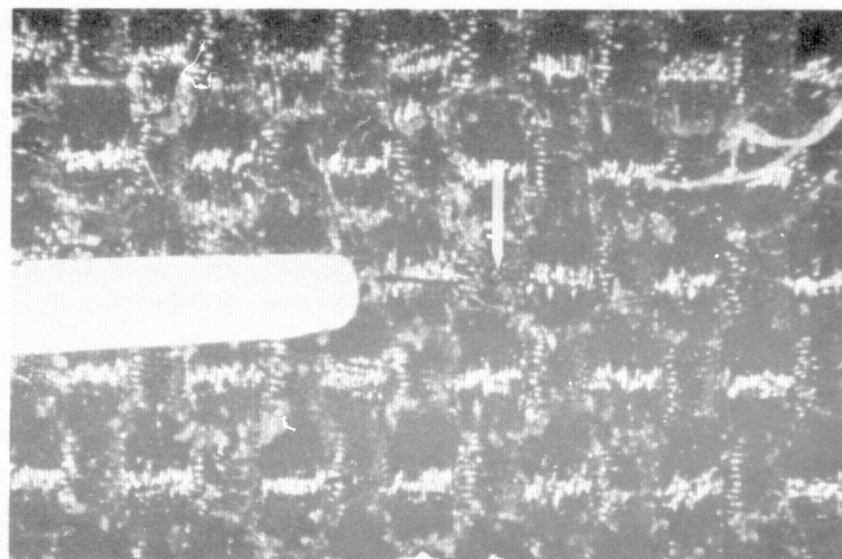
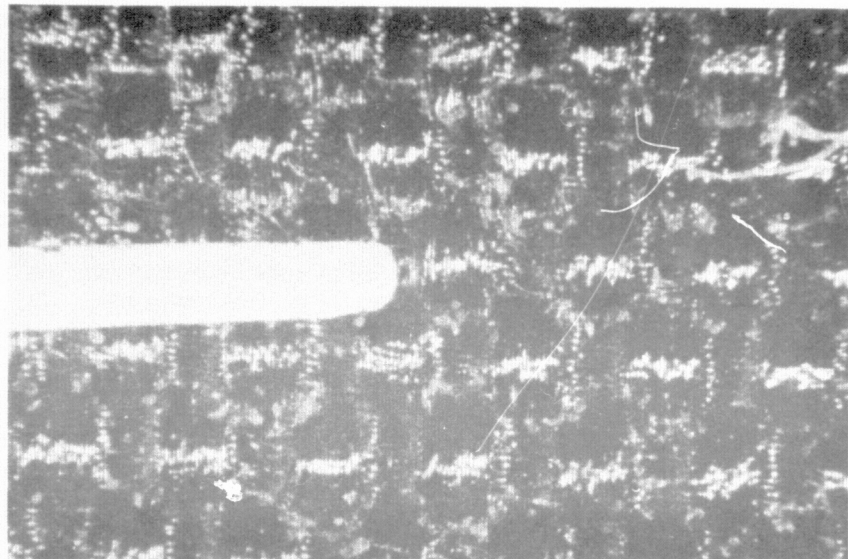


Figure 33. Stable Crack Growth for $[0/\pm 30/0]_{2S}$ DEN Specimen.
(Arrows indicate extent of crack growth.)

ORIGINAL PAGE IS
OF POOR QUALITY

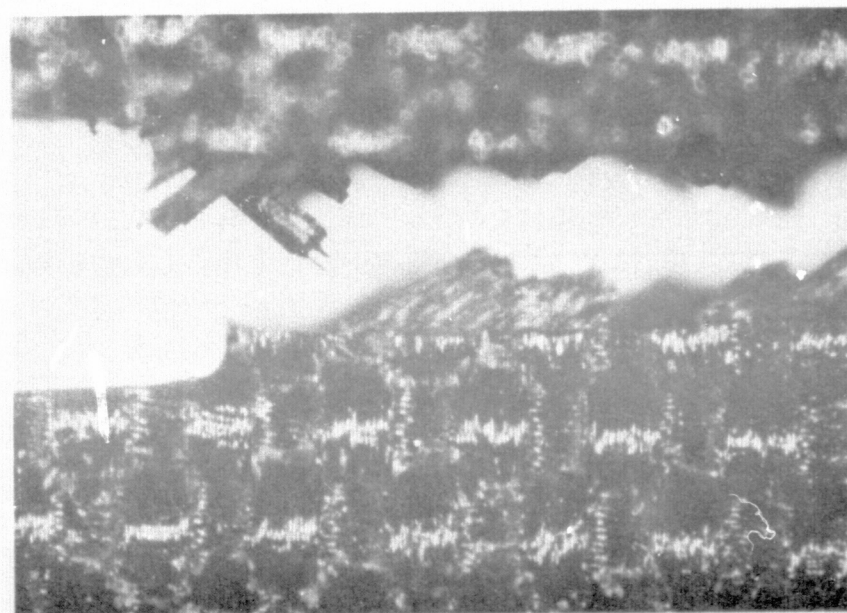
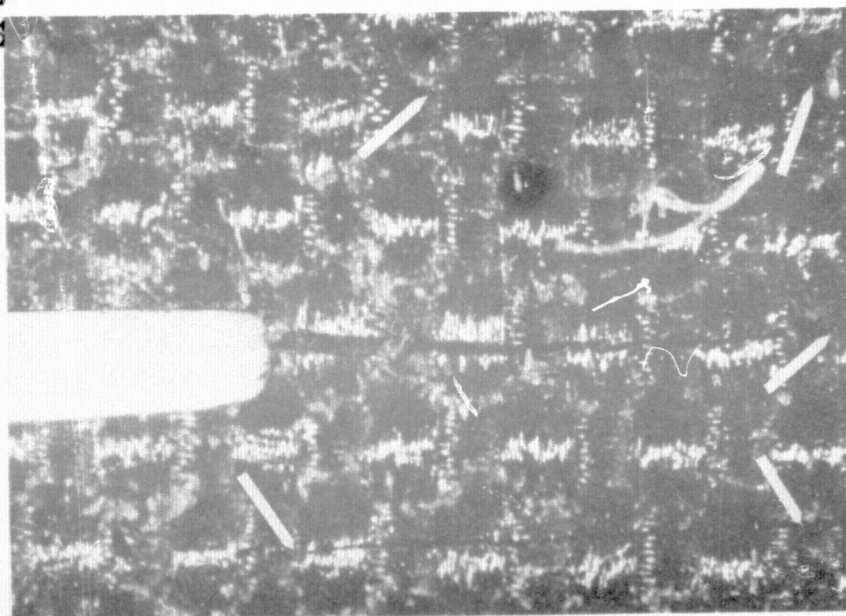
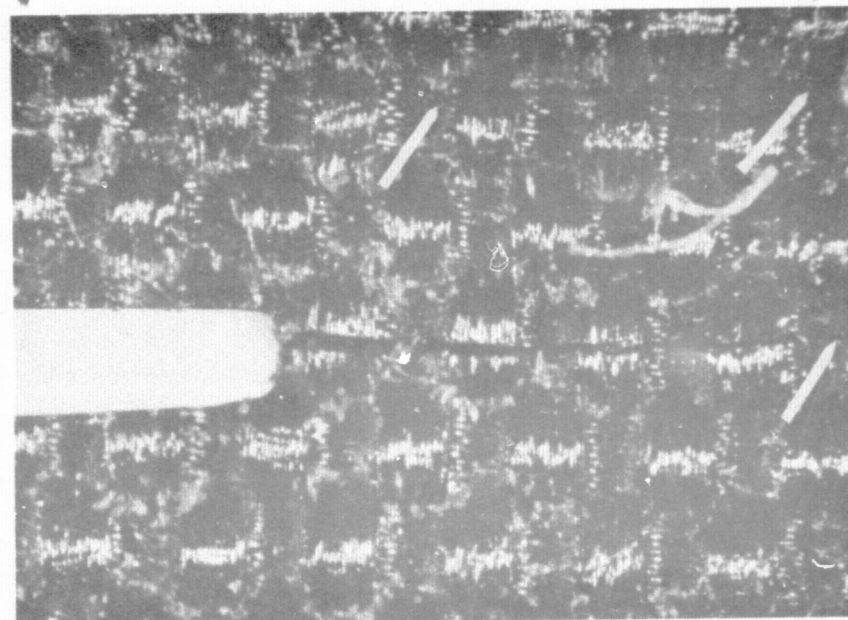
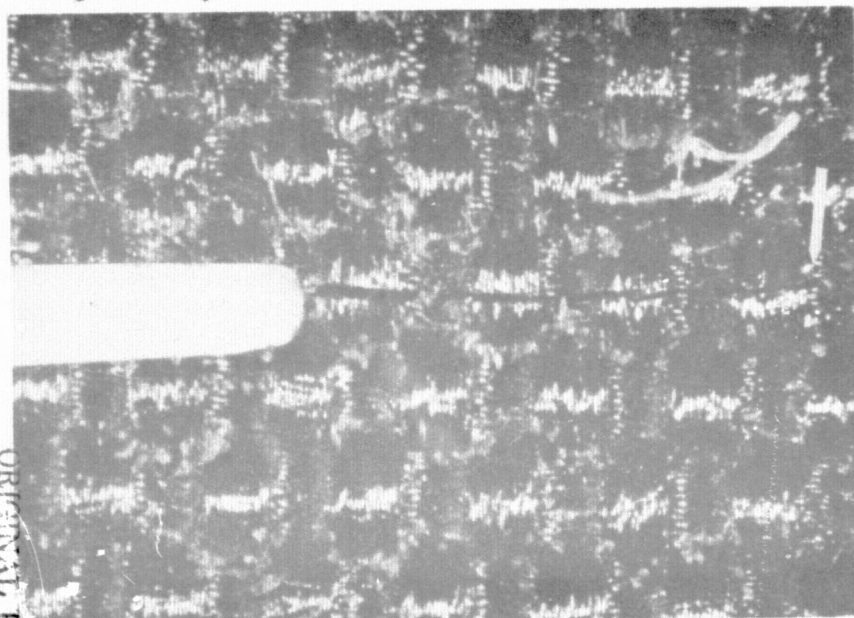


Figure 33 (cont.) Stable Crack Growth for $[0/\pm 30/0]_{2S}$ DEN Specimen.
(Arrows indicate extent of crack growth. Note additional cracks above and below the notch plane.)

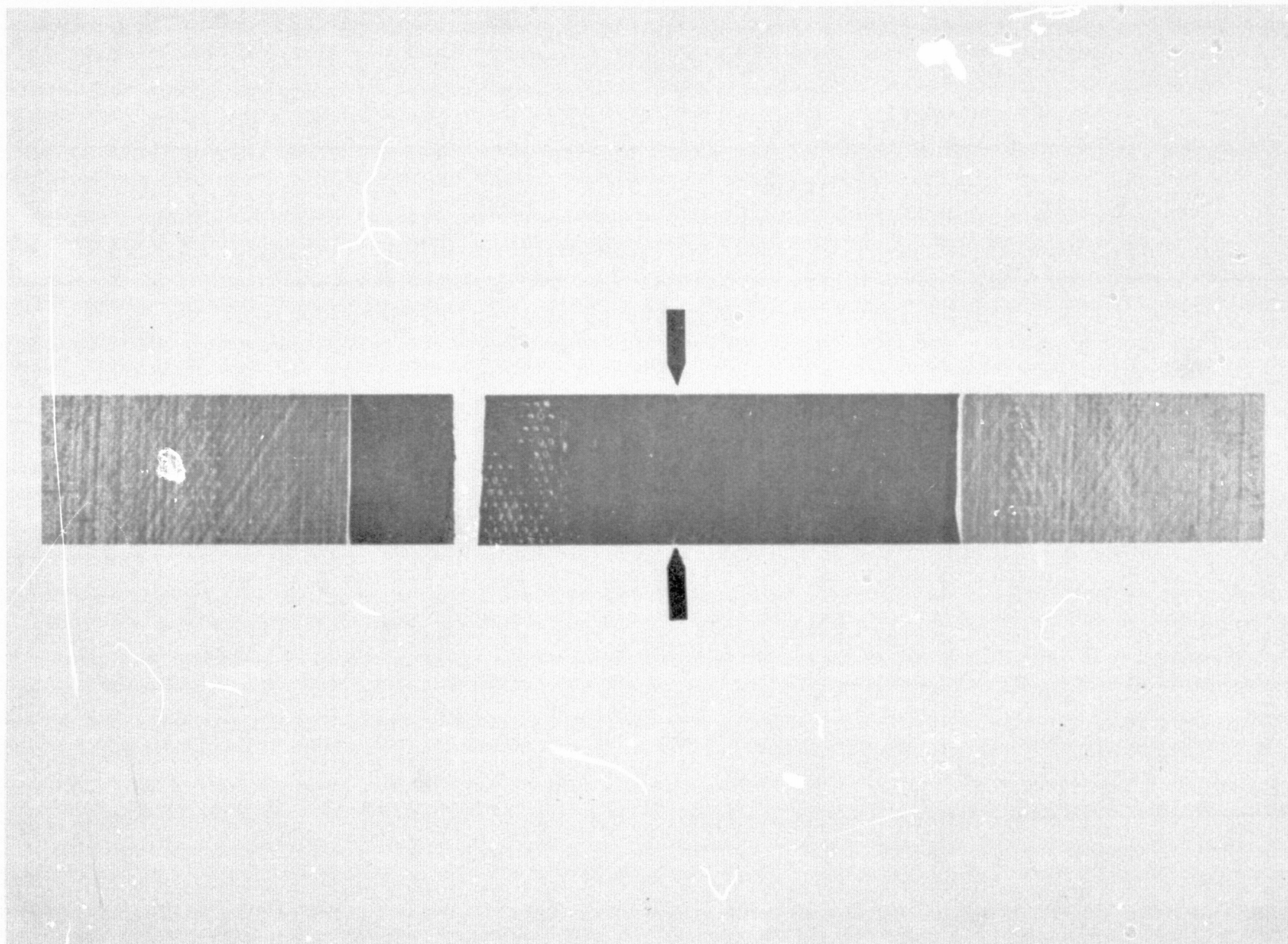


Figure 34. Fracture Plane for $[90/\pm 60/90]_{2S}$ DEN Specimen.
(Note location of plane relative to notch.)
(Arrows indicate notches.)

ORIGINAL PAGE IS
OF POOR QUALITY

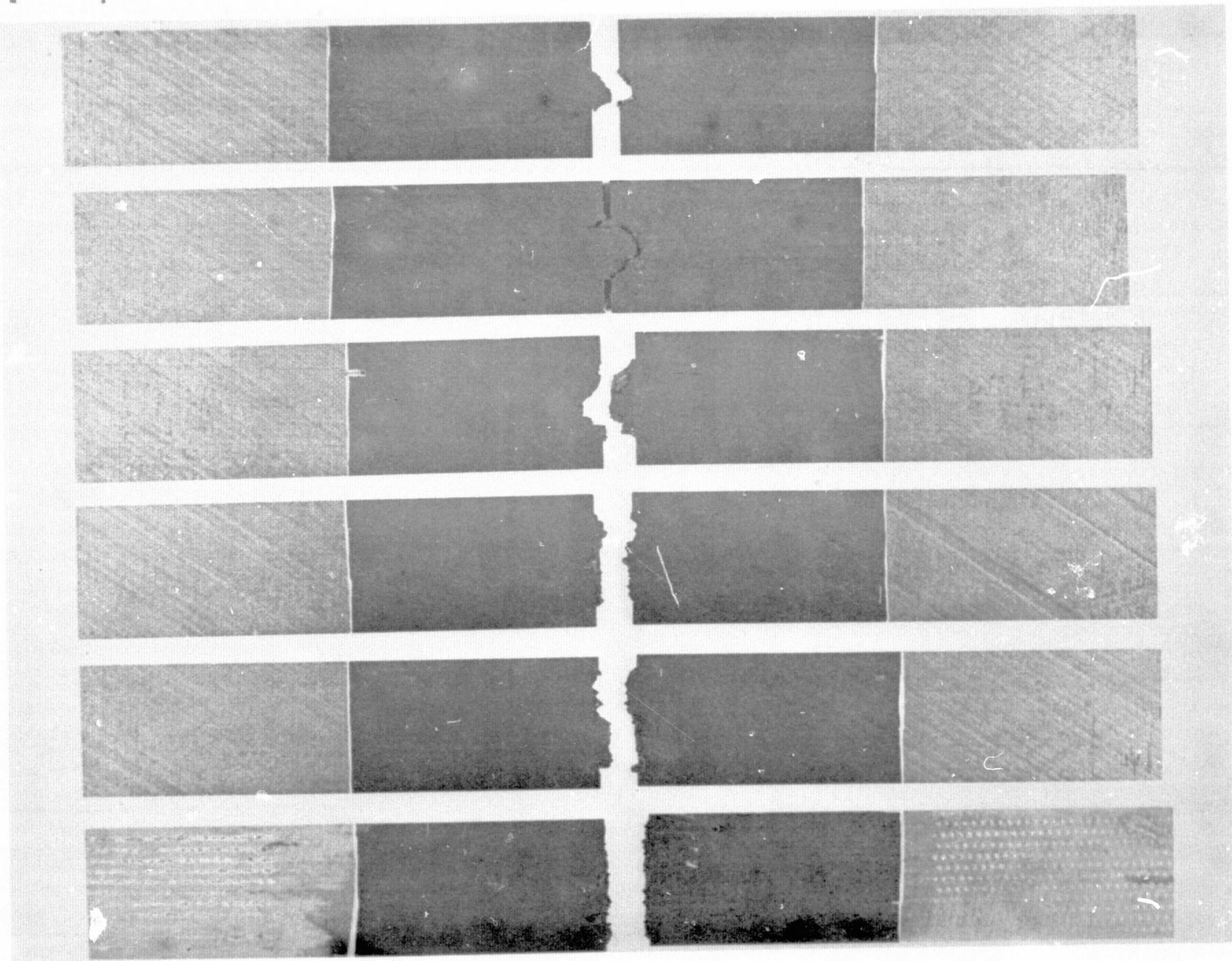


Figure 35. Fracture Planes for $[0/\pm 30/0]_{2S}$ DEN Specimens.

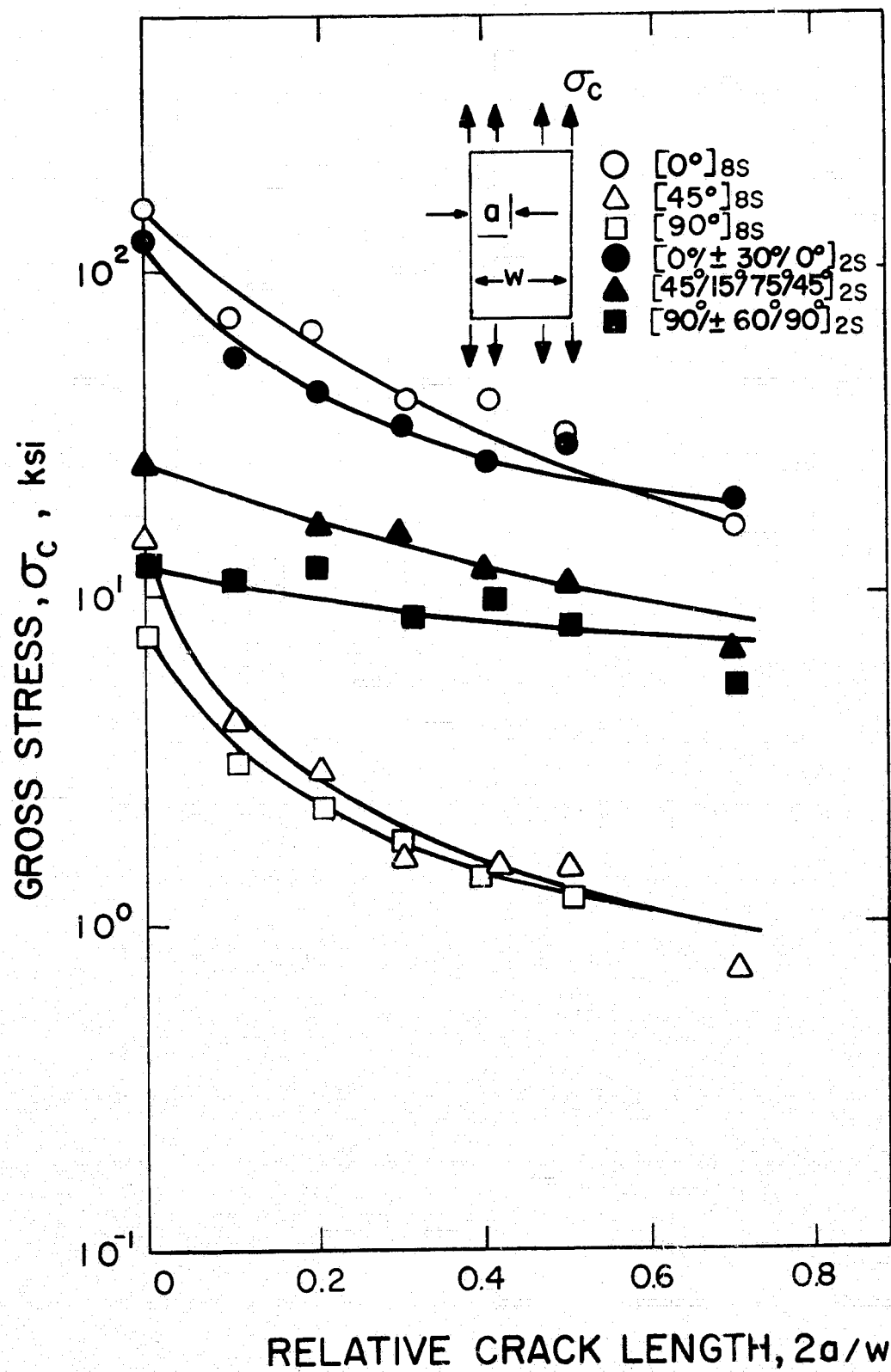


FIG. 36 DOUBLE EDGE NOTCH (DEN) GROSS FRACTURE STRESSES

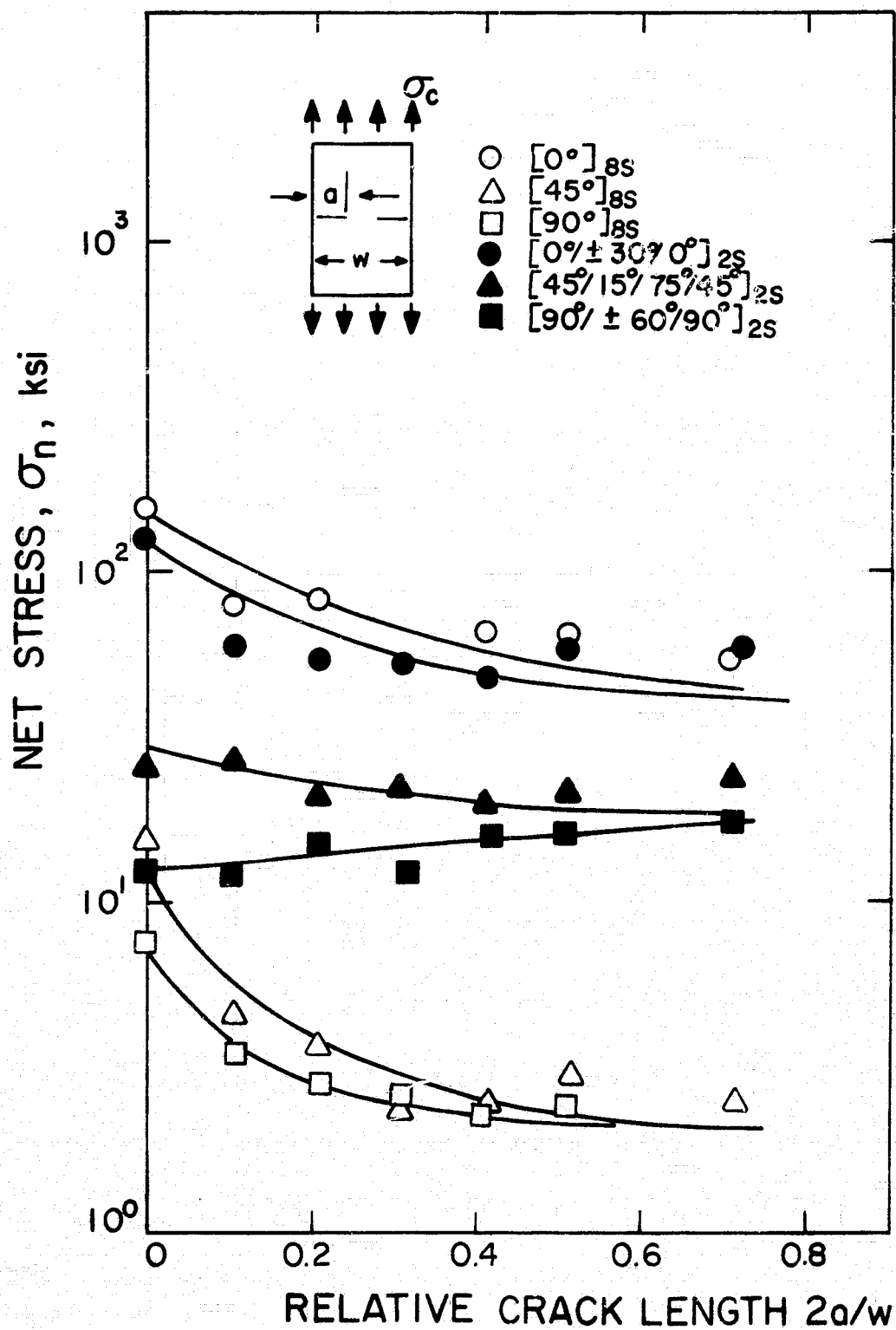


FIG. 37 DOUBLE EDGE NOTCH (DEN) NET FRACTURE STRESSES

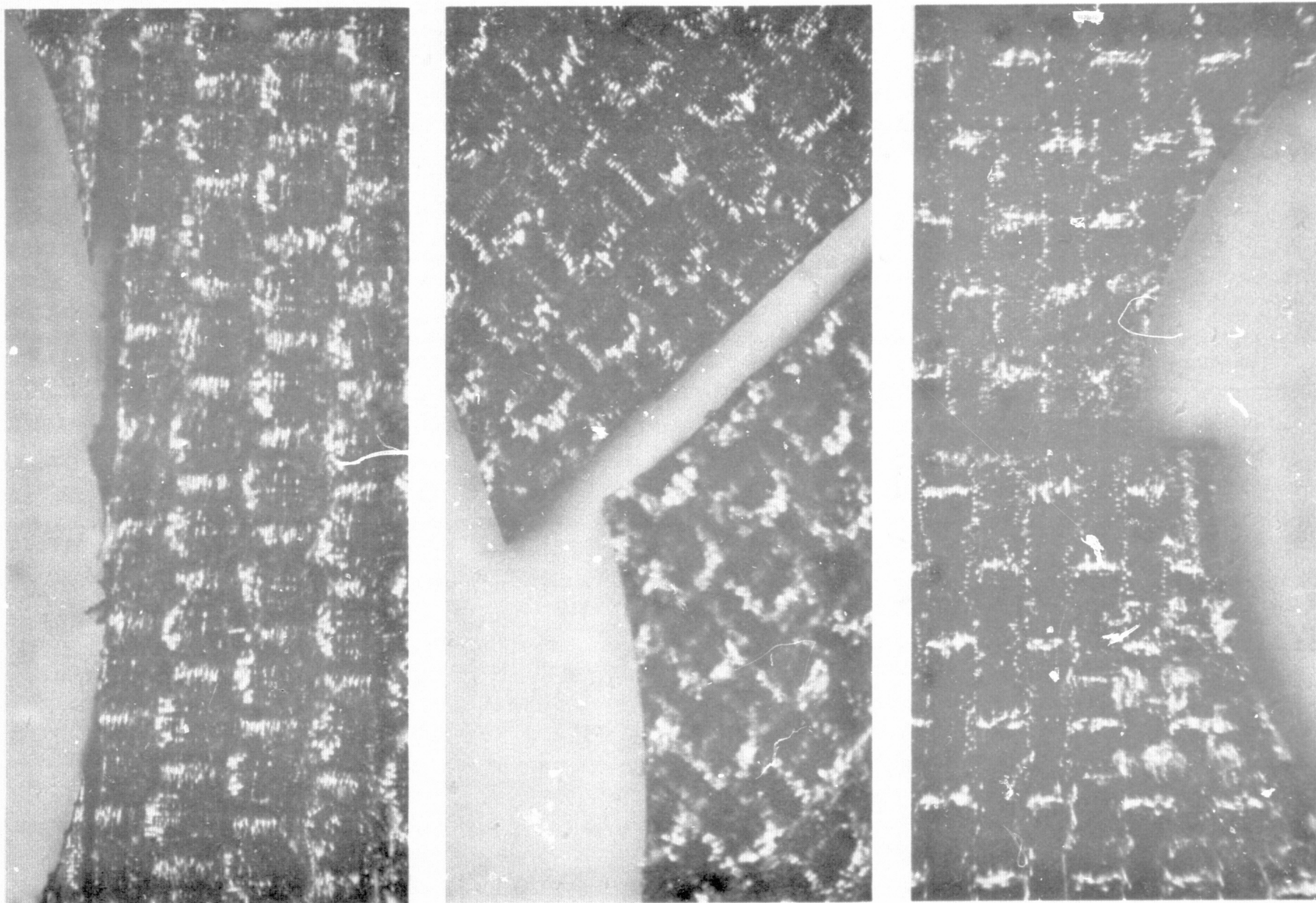


Figure 38. Fracture Planes for Specimen Containing a Circular Hole.
a) - c) Left to right; $[0]_{GS}$, $[45]_{GS}$ and $[90]_{GS}$.

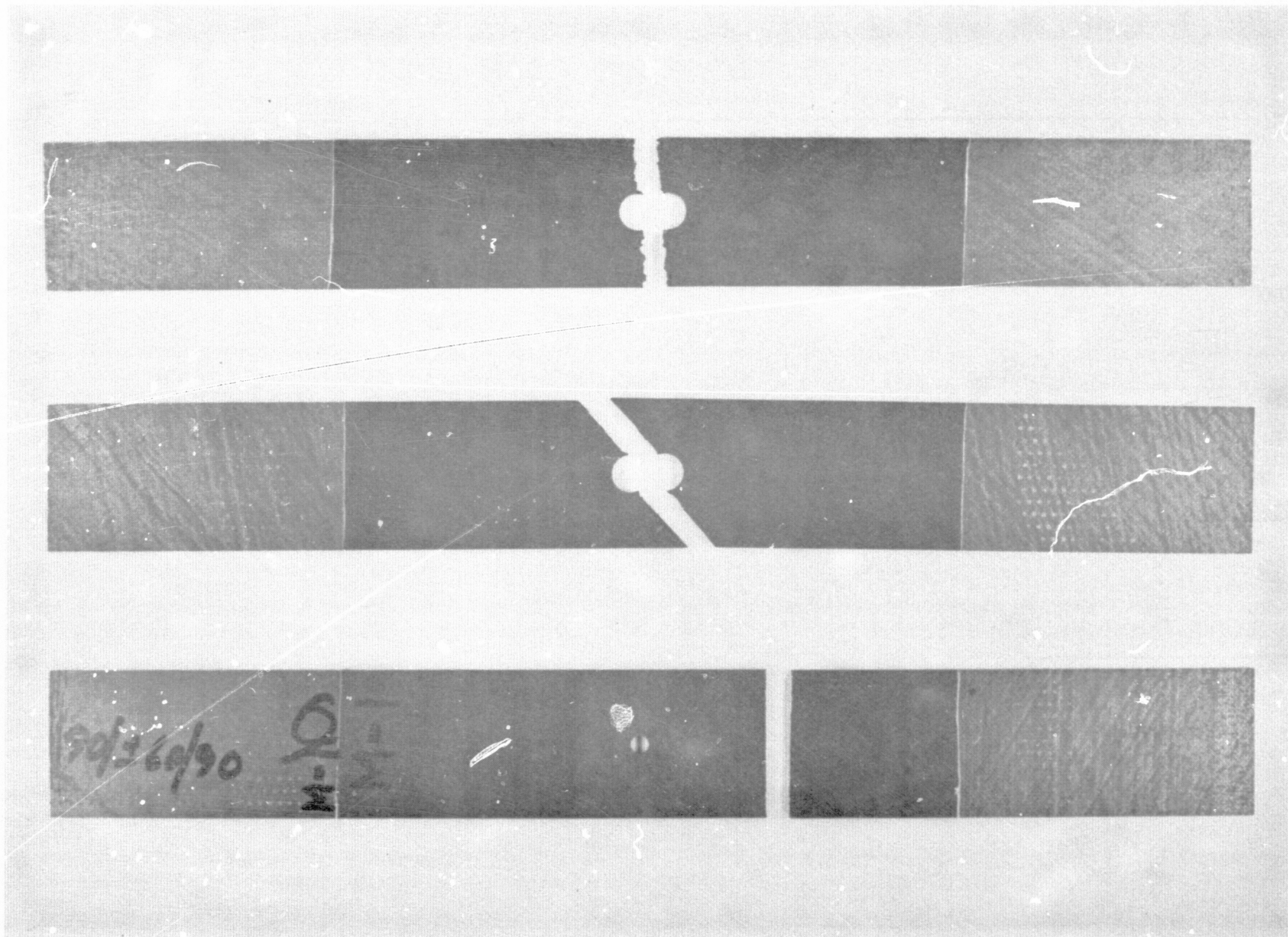


Figure 39. Fracture Planes for Specimen Containing a Circular Hole.
a) - c) Top to Bottom ; $[0/\pm 30/0]_{2S}$, $[45/15/75/45]_{2S}$ and $[90/\pm 60/90]_{2S}$.

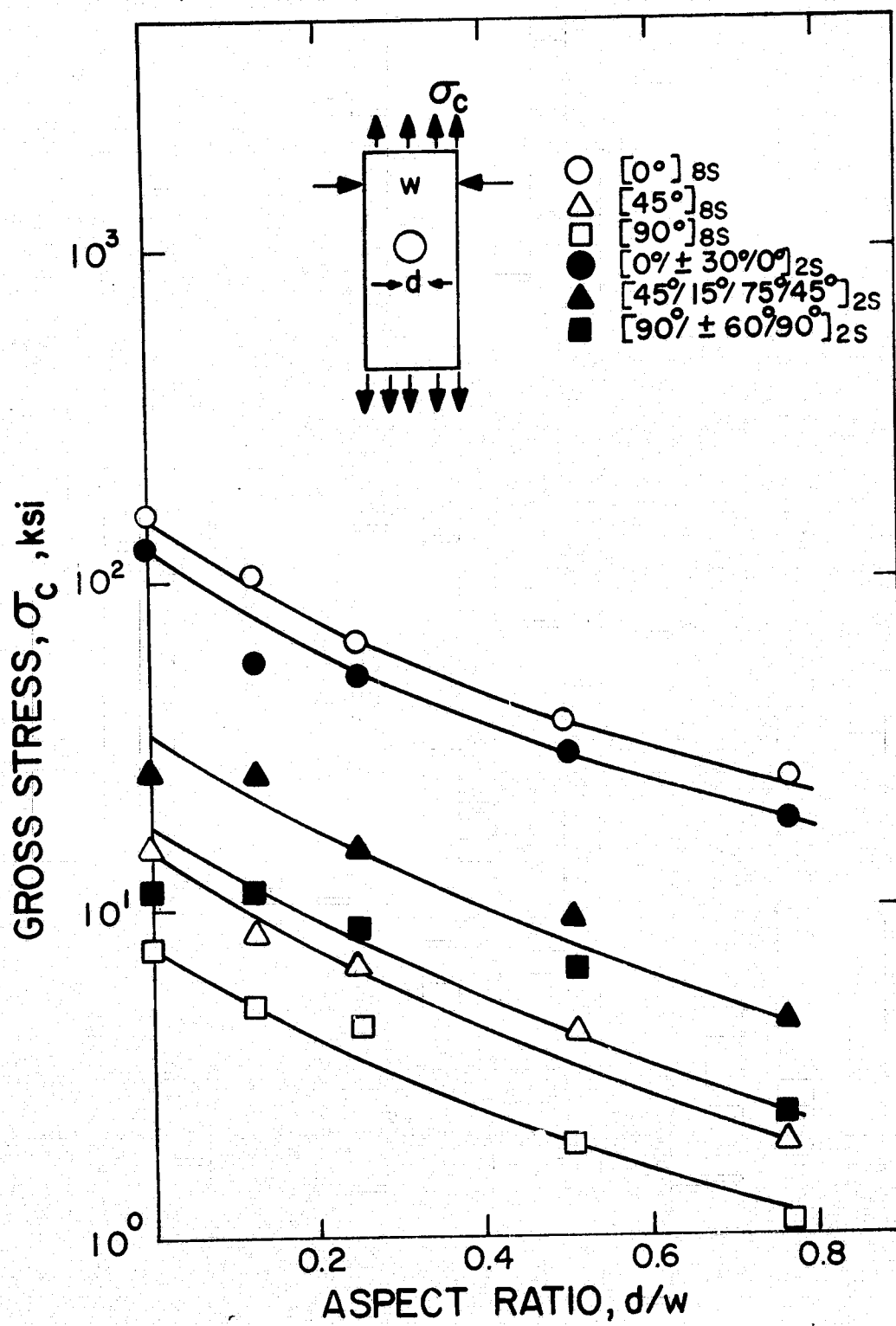


FIG. 40 CIRCULAR HOLE GROSS FRACTURE STRESSES

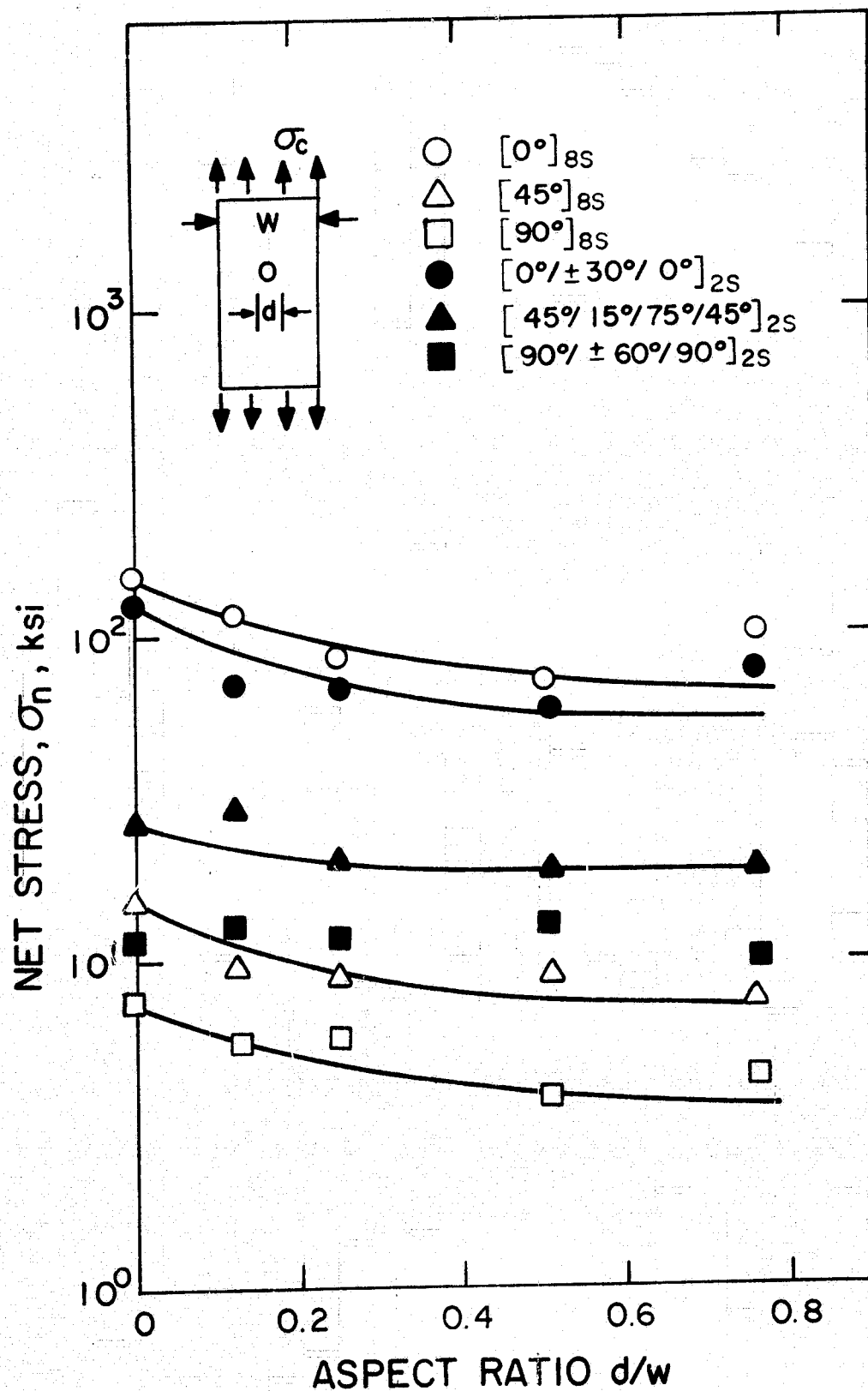


FIG. 41 CIRCULAR HOLE NET FRACTURE STRESSES

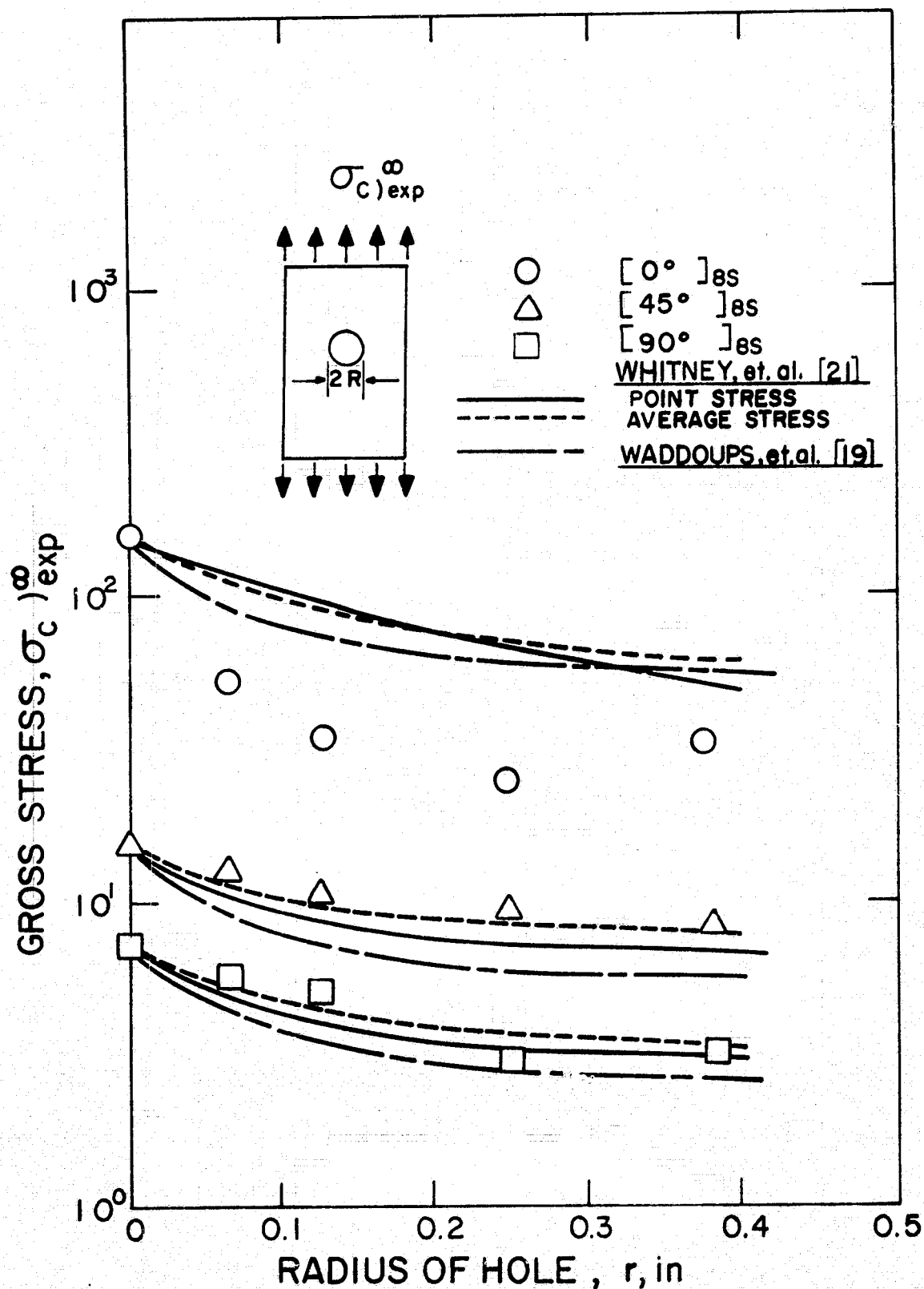


FIG. 42 COMPARISON OF EXPERIMENTAL AND THEORETICAL FRACTURE STRENGTHS (RESULTS CORRECTED TO INFINITE WIDTH USING ORTHOTROPIC STRESS CONCENTRATION FACTOR)

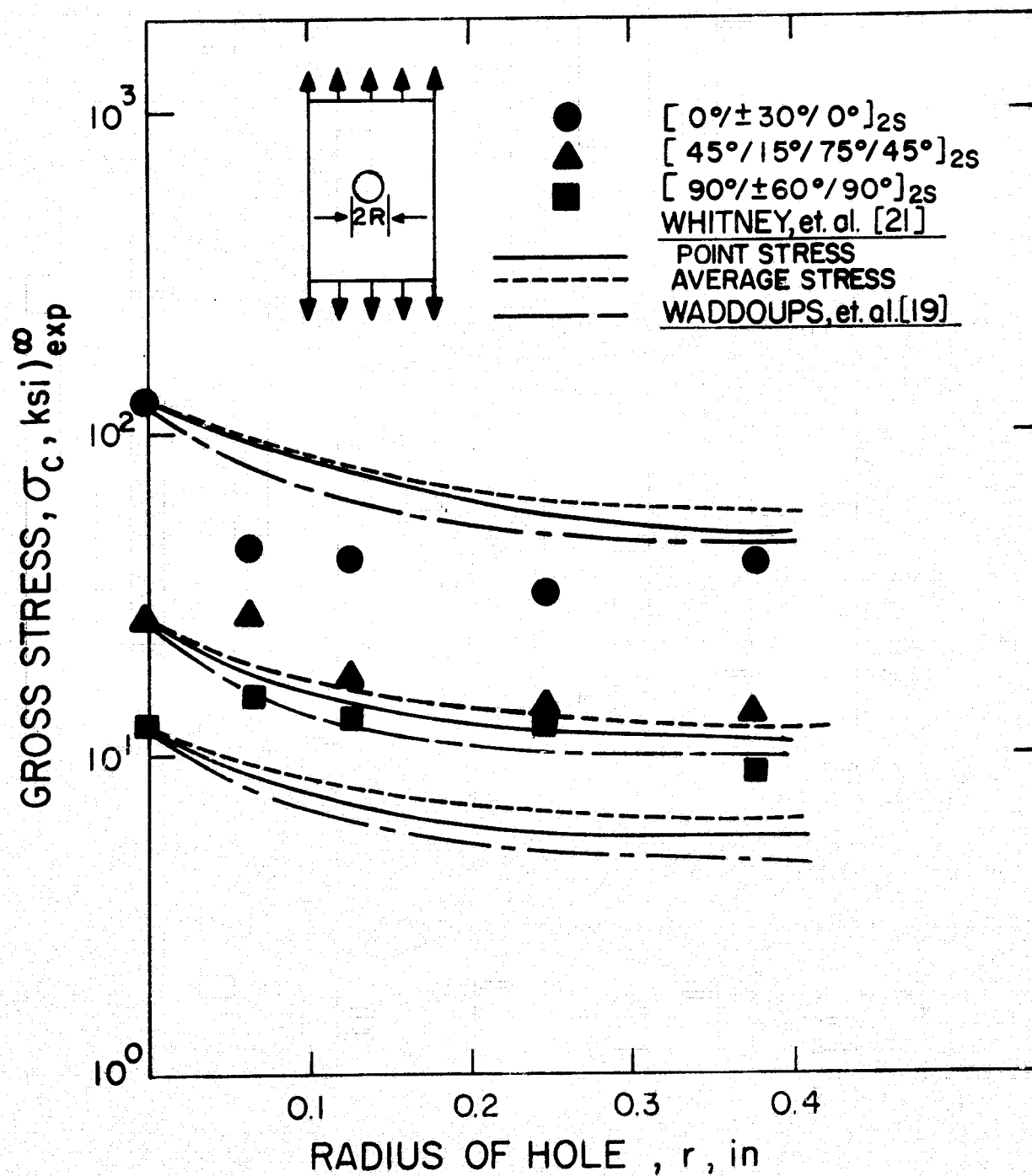


FIG. 43

COMPARISON OF EXPERIMENTAL AND THEORETICAL FRACTURE STRENGTHS (RESULTS CORRECTED TO INFINITE WIDTH USING ORTHOTROPIC STRESS CONCENTRATION FACTOR)

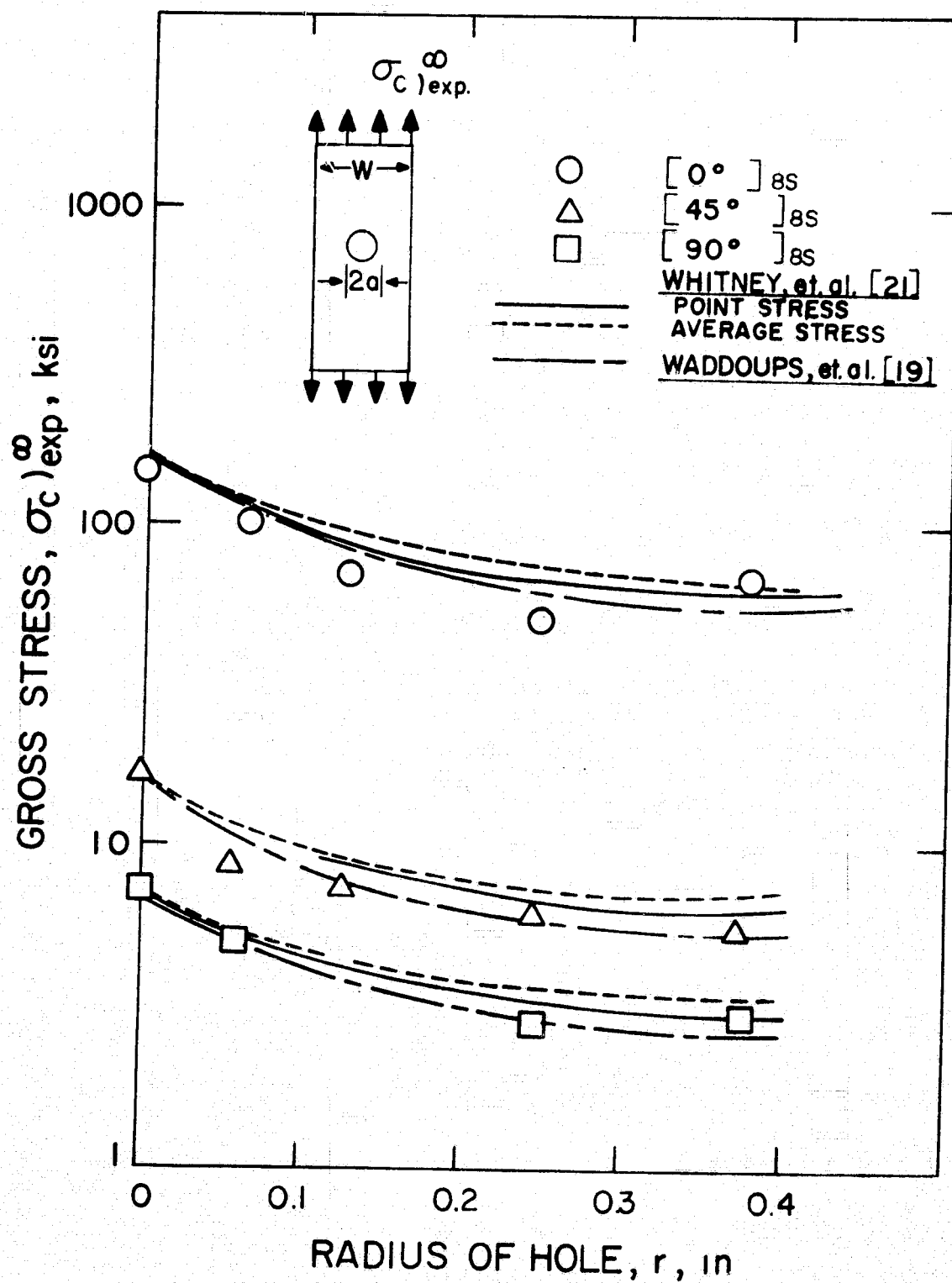


FIG. 44 COMPARISON OF EXPERIMENTAL AND THEORETICAL FRACTURE STRENGTHS (RESULTS CORRECTED TO INFINITE WIDTH USING ISOTROPIC STRESS CONCENTRATION FACTOR)

